Rare earth- and Si nanostructure-based light emitting devices for integrated photonics

Yonder Antonio Berencén Ramírez

ADVERTIMENT. La consulta d'aquesta tesi queda condicionada a l'acceptació de les següents condicions d'ús: La difusió d'aquesta tesi per mitjà del servei TDX (**www.tdx.cat**) i a través del Dipòsit Digital de la UB (**diposit.ub.edu**) ha estat autoritzada pels titulars dels drets de propietat intel·lectual únicament per a usos privats emmarcats en activitats d'investigació i docència. No s'autoritza la seva reproducció amb finalitats de lucre ni la seva difusió i posada a disposició des d'un lloc aliè al servei TDX ni al Dipòsit Digital de la UB. No s'autoritza la presentació del seu contingut en una finestra o marc aliè a TDX o al Dipòsit Digital de la UB (framing). Aquesta reserva de drets afecta tant al resum de presentació de la tesi com als seus continguts. En la utilització o cita de parts de la tesi és obligat indicar el nom de la persona autora.

ADVERTENCIA. La consulta de esta tesis queda condicionada a la aceptación de las siguientes condiciones de uso: La difusión de esta tesis por medio del servicio TDR (**www.tdx.cat**) y a través del Repositorio Digital de la UB (**diposit.ub.edu**) ha sido autorizada por los titulares de los derechos de propiedad intelectual únicamente para usos privados enmarcados en actividades de investigación y docencia. No se autoriza su reproducción con finalidades de lucro ni su difusión y puesta a disposición desde un sitio ajeno al servicio TDR o al Repositorio Digital de la UB. No se autoriza la presentación de su contenido en una ventana o marco ajeno a TDR o al Repositorio Digital de la UB (framing). Esta reserva de derechos afecta tanto al resumen de presentación de la tesis como a sus contenidos. En la utilización o cita de partes de la tesis es obligado indicar el nombre de la persona autora.

WARNING. On having consulted this thesis you're accepting the following use conditions: Spreading this thesis by the TDX (**www.tdx.cat**) service and by the UB Digital Repository (**diposit.ub.edu**) has been authorized by the titular of the intellectual property rights only for private uses placed in investigation and teaching activities. Reproduction with lucrative aims is not authorized nor its spreading and availability from a site foreign to the TDX service or to the UB Digital Repository. Introducing its content in a window or frame foreign to the TDX service or to the UB Digital Repository is not authorized (framing). Those rights affect to the presentation summary of the thesis as well as to its contents. In the using or citation of parts of the thesis it's obliged to indicate the name of the author.

Rare earth- and Si nanostructure-based light emitting devices for integrated photonics

Ph.D. Thesis by

Yonder Antonio Berencén Ramírez

In partial fulfillment of the requirements

for the degree of Doctor en Física por

la Universidad de Barcelona

"International Mention Program"

Departament d'Electrònica

Programa de doctorado: Física

2014

Tutor: Prof. Dr. Blas Garrido Fernández

Director: Prof. Dr. Blas Garrido Fernández

Director: Prof. Dr. José Antonio Rodríguez Pérez

This page intentionally left in blank

Signatures of author and directors:

Author:

Yonder Antonio Berencén Ramírez

Director:

Prof. Dr. Blas Garrido Fernández

Director: 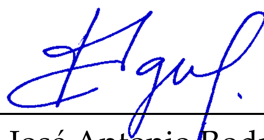

Prof. Dr. José Antonio Rodríguez Pérez

Declaration:

I hereby declare that none of the presented articles in this thesis has been previously accepted for the award of any other degree or diploma in any university or equivalent institution.

To my family, but especially to my

grandfather who anticipated

my PhD from birth.

Abstract

Nowadays, a Si-based light source is the paramount component required to achieve a complete integration of Si photonics. Nevertheless, the physical limitations of the bulk silicon as light emitter and the limited knowledge on the most suitable environment to efficiently excite rare-earth ions prevents the evolution of the research activities in this area. Among several dielectric media, silicon-rich silicon oxide and silicon-rich silicon nitride materials have been the most investigated so far. These materials have many advantages over other dielectric material systems. These advantages include a high compatibility with mainstream Si technology, a favorable environment for the segregation of Si nanostructures after relatively low temperature annealing, a high contrast refractive index suitable for strong photon confinement, for instance, for making high quality optical cavities; and excellent hosts for rare-earth ions from the viewpoint of optical and electrical pumping. Therefore, this thesis presents experimental work on developing rare-earth ions and Si nanostructures as a material platform for light emitting devices in the visible and near-infrared range. The realization of the different electroluminescent devices, based on a single, bi- or tri-layer approach of silicon oxide and/or silicon nitride co-doped or not with rare earth ions, is successfully performed. Several complementary metal oxide semiconductor (CMOS) compatible fabrication techniques such as co-magnetron sputtering, plasma-enhanced chemical vapor deposition (PECVD), low-pressure chemical vapor deposition (LPCVD) and ion implantation are used. By using characterization techniques such as time of flight secondary ion mass spectrometry (TOF-SIMS), secondary ion mass spectrometry (SIMS), X-ray photoelectron spectroscopy (XPS), energy-filtered transmission electron microscopy (EFTEM), focused ion beam (FIB) and ellipsometry, the structural and compositional properties of the studied active layers are determined. In addition, electro-optical properties at room and at high temperatures (25 ^{0}C – 300 ^{0}C) under quasi-static and dynamic regimes are studied in both visible and near-infrared spectral region. Typically, the used electro-optical techniques have been current-voltage, capacitance-voltage, charge to breakdown, electroluminescence (EL)-current, EL-voltage and time-resolved EL.

On the one hand, in regard of light emitting devices at 1.54 μm, the presence of Si nanostructures leads to an increase in the current of four to five orders of magnitude, in Er-doped silicon-rich silicon oxide layers with different Si excesses and made by co-magnetron sputtering. In addition, electrical conduction mechanism is dominated by field-assisted thermal ionization (Poole-Frenkel)

from Si nanostructure to Si nanostructure. Moreover, in these active layers the main electroluminescence mechanism takes place by energy transfer between Er ions and Si nanostructures. On the contrary, in the layers fabricated by low-pressure chemical vapor deposition, the conduction mechanism of either Er-doped SiO_2 or Er-doped silicon-rich silicon oxide is governed by Fowler-Nordheim tunneling. Whereas, the Poole-Frenkel mechanism dominates the electrical conduction in Er-doped Si_3N_4 or Er-doped silicon-rich silicon nitride. In addition, Er-doped SiO_2 is a more efficient material for the 1.54 μm EL emission than its Er-doped Si_3N_4 counterpart. However, the high power efficiency that offers Er-doped SiO_2 layers is paid by the short device operation lifetime and vice versa for the case of Er-doped Si_3N_4 layers. Also, direct impact excitation by hot electrons (viz. defined as electrons which are not in thermal equilibrium with the lattice; typically at high electric fields, carriers can gain sufficient kinetic energy in the conduction band greater than the Fermi level) is the most efficient EL excitation mechanism in all the studied Er-doped LED materials. A power efficiency value at 1.54 μm as high as 0.01% is obtained.

On the other hand, with respect to the visible light emitting devices, by combining low-pressure chemical vapor deposition and ion implantation, silicon nitride (N) and silicon oxide (O) layers are obtained forming bi- (NO) and tri-layer (ONO) gate stacks. A Si Gaussian-like profile centered at the bottom interface between silicon nitride and silicon oxide (NO) layers, which gives rise of a silicon excess of around 19%, is introduced by ion implantation. The electrical conduction is mostly bulk-limited, which is a combination of Poole-Frenkel and space charge-limited current mechanisms depending on the applied voltage value. At moderate voltages, the Poole-Frenkel mechanism takes place, whereas at high voltages the space charge-limited current mechanism occurs. Nonetheless, electrical measurements at high temperatures revealed a more complex electrical conduction mechanism in the studied multidielectric layers, which is unambiguously detected in whole range of voltages. In particular, a hybrid conduction mechanism formed by variable range hopping and space charge-limited enhanced by Poole-Frenkel is identified. In addition, two well-defined emission bands (red and blue-green) in both bi- and tri-layers are observed. The red emission is related to an electron-hole recombination in the Si nanostructures embedded in SiO_2, whose measured EL decay time is around 8 μs. Whereas, the blue-green band is ascribed to PF ionization of the Si-related traps in Si_3N_4, where a very fast EL decay time of hundreds of nanoseconds (around 290 ns) is measured. Moreover, by a detailed photometric study and

certain conditions of alternate current excitation regime, a color rendering index of 93, correlated color temperature of 4800 K and luminous efficacy of radiation of 112 lm/W are obtained. This result shows the potential of silicon nitride-based light sources for large-area lighting devices. Additionally, by changing the DC voltage sign applied to the gate electrode, a switchable EL from a blue-green spectrum at positive DC voltage to a near-IR spectrum at negative DC voltage is demonstrated in the bilayer (NO) structure. Also, the advantage of using MNOS capacitors instead of MNOS transistors for light emitting purposes is established.

Finally, a complementary set of devices formed by Tb-implanted silicon-rich silicon nitride/oxide light emitting devices are fabricated. Atomic terbium concentration of 1.5%, centered at the middle of silicon nitride layer is introduced by ion implantation. Whereas, the silicon-rich silicon nitride with 12% of Si excess and silicon oxide layers are fabricated by plasma-enhanced chemical vapor deposition. A 30-nm-thick silicon oxide layer is intentionally introduced, which is thicker than previous gate stack designs (typically between 3-10 nm). This fact makes possible to change the electrical conduction from bulk-limited mechanism (typically associated to silicon nitride layers) to electrode-limited one. In particular, in contrast to the previous non-terbium implanted devices, the electrical conduction mechanism is trap-assisted-tunneling at high voltages. This gate stack has two main advantages that make possible the efficient excitation of luminescent centers by direct impact of hot electrons. These are i) SiO_2 layer introduces a potential energy step of 1.3 eV at the interface between the SiO_2 and the Si_3N_4 due to the difference in electron affinities and ii) a trade-off between EL efficiency and electrical stability is achieved. In addition, this gate stack guarantees that the excitation process of terbium ions takes place via direct impact excitation, instead of by energy transfer from Si nanostructures to terbium ions. At the main EL peak of 540 nm an optical power density and external quantum efficiency as high as 0.5 mW/cm^2 and 0.1%, respectively, have been ever reported. Also, a terbium-excitation cross section of 8.2×10^{-14} cm^2 in silicon-rich silicon nitride is experimentally obtained as well as a fraction of excited terbium ions of around 7%. A suitable gate stack for efficient excitation of terbium ions by direct impact excitation by hot electrons is demonstrated. Moreover, this gate stack might be extended to another rare-earth elements such as erbium ions, which require lower excitation energies (viz. 0.8 eV) than terbium ions. In summary, the suitability of this materials platform for the realization of integrated Si-based light emitters fully compatible with CMOS technology is established.

Acknowledgements

This PhD work was possible thanks to the financial support from the scholarship grant: Subprograma de Formación de Personal Investigador FPI-MICINN (BES-2010-030479), which is associated to the Spanish project LASSI (TEC2009-08359). The European project HELIOS (FP7-ICT 224312) is also acknowledged.

I would like to acknowledge my family. All the important goals I have reached in my life would not have been possible without their unconditional support and wonderful advices. Special thanks to my mom for being an extraordinary person. This work probably would not have culminated without her incalculable support, physical and mental strength as well as emotional intelligence. Many thanks to my wife, who appeared in my life for giving me happiness, support, comprehension and so many nice moments.

I would like to especially thank to my directors: Prof. Blas Garrido Fernández, who gives me possibility of working in his research group, and for giving me freedom to carry out my scientific ideas. Prof. José Antonio Rodríguez Pérez, who introduced me in the world of scientific research. He also taught me since very early that the nature is opposed to reveal their secrets and that is why we need to work hard.

I would like to acknowledge the people with whom I have spent most of the time in the Prof. Garrido's group. Joan Manel Ramírez (my office mate and colleague of several battles), Sergi Hernández (¿Qué pasa contigo chico? ¿*Hacemos* un café?...Once upon a man and a coffee…), Julià López-Vidrier (the gentleman of energetic saving and everything else), Paolo Pellegrino (my teaching mate), Oriol Blázquez (Pudé, Pudé…) and other colleagues that are no longer in the group, which are Olivier Jambois, Josep Carreras, Daniel Navarro, Alexander Martínez, Federico Ferrarese, Mariano Perálvarez and Bernat Mundet.

I would like to thank Prof. Albert Cornet, Head of the Departament d'Electrònica, for his kindness and support all the time.

Many thanks to the people of administration and services of the Departament d'Electrònica, which have been always willing to help me even out of their working hours. Josep Maria, Andrés, Antonio, Trini, Conchita, Rose, Martín and Montse.

Many thanks to Dr. Lars Rebohle and Dr. Wolfgang Skorupa for their hospitality, professionalism and support during my research stay at Helmholtz-Zentrum Dresden-Rossendorf in Dresden, Germany. Thanks also to Dr. Skorupa for showing me the cultural life of Saxony.

I would like to acknowledge Dr. Carlos Domínguez and Dr. Josep Montserrat of the Instituto de Microelectrónica de Barcelona (IMB-CNM, CSIC), Barcelona, Spain for the advices regarding technological aspects and their collaborative enthusiasm.

My deepest acknowledgements to my friends here in Spain, in Cuba and worldwide scattered. You are the biggest portion of my nuclear family. Therefore, this work is devoted to all of you as well. In alphabetical order: Alejandro (el tigre), Amparito, Andy, Ariela, Borja, Carlitín, Catalina, César, Chachita, Chiqui, Chong, Dayamit, Dennis, Denys (piXel), Eida, El Gaby, Elvis, Ernesto, Gerardo (Pachuco), Gladys, Harold, Irma (Mi sol), Isabel, Jesús, Julio, Laurita, Leduán, Liuba, Liván, Manolita, Marbelis, Margarita, María Elena, Maylin, Mercy, Nordis, Pepe, Pili, Rafael (el negro), Ramón, Reinerito, Reynaldo, Reynier, Roelmis, Rojas, Ruly, Santos, Yandi y María, Yandy, Yanet, Yoa, Yosmy, Yudelys, Yudenia y Yuli.

My sincere thanks to those who feel they deserve a place in this section and were not intentionally obviated.

Yonder Berencén
Barcelona, July 2014.

List of publications included as part of the thesis

I. "Current transport and electroluminescence mechanisms in thin SiO_2 films containing Si nanocluster-sensitized erbium ions" O. Jambois, Y. Berencén, K. Hijazi, M. Wojdak, A. J. Kenyon, F. Gourbilleau, R. Rizk, and B. Garrido; *Journal of Applied Physics* **106** (6), 063526 (2009). IF: 2.210

II. "Study of the electroluminescence at 1.5 μm of SiO_x:Er layers made by reactive magnetron sputtering" O. Jambois, Y. Berencén, S. Y. Seo, A. J. Kenyon, M. Wojdak, K. Hijazi, L. Khomenkova, F. Gourbilleau, R. Rizk, and B. Garrido; *in Proceedings of the 2009 Spanish Conference on Electron Devices*, pp. 69 (2009).

III. "Er-doped Si-based electroluminescent capacitors: Role of different host matrices on the electrical and luminescence properties" Y. Berencén, J. M. Ramírez, and B. Garrido; *in Proceedings of the 2013 Spanish Conference on Electron Devices*, pp. 245 (2013).

IV. "Metal-nitride-oxide-semiconductor light-emitting devices for general lighting" Y. Berencén, J. Carreras, O. Jambois, J. M. Ramírez, J. A. Rodríguez, C. Domínguez, C. E. Hunt, and B. Garrido; *Optics Express* **19** (10), A234 (2011). IF: 3.546

V. "Blue-green to near-IR switching electroluminescence from Si-rich silicon oxide/nitride bilayer structures" Y. Berencén, O. Jambois, J. M. Ramírez, J. M. Rebled, S. Estradé, F. Peiró, C. Domínguez, J. A. Rodríguez, and B. Garrido; *Optics Letters* **36** (14), 2617 (2011). IF: 3.385

VI. "Correlation between charge transport and electroluminescence properties of Si-rich oxide/nitride/oxide-based light emitting capacitors" Y. Berencén, J. M. Ramírez, O. Jambois, C. Domínguez, J. A. Rodríguez, and B. Garrido; *Journal of Applied Physics* **112** (6), 033114 (2012). IF: 2.210

VII. "Intense green-yellow electroluminescence from Tb^{+}-implanted silicon-rich silicon nitride/oxide light emitting devices" Y. Berencén, R. Wutzler, L. Rebohle, D. Hiller, J. M. Ramírez, J. A. Rodríguez, W. Skorupa, and B. Garrido; *Applied Physics Letters* **103** (11), 111102 (2013). IF: 3.794

CONTENTS

Abstract vi
Acknowledgements ix
List of publications included as part of the thesis xi
1 INTRODUCTION 14
1.1 The need of a silicon photonics 14
1.2 Rare earth- and Si nanostructure-based light emitting devices 17
1.3 Outline of this thesis 21
2 ELECTRICAL CONDUCTION MECHANISMS IN INSULATING FILMS 23
2.1 Introduction 23
2.2 Electrode-limited conduction mechanisms 25
2.3 Bulk-limited conduction mechanisms 28
2.4 Conclusions 34
3 ELECTROLUMINESCENCE AND LED EFFICIENCY: BASIC CONCEPTS.. 35
3.1 Introduction 35
3.2 Energy transfer 35
3.3 Impact excitation 35
3.4 Impact ionization 36
3.5 Internal, extraction, power and external efficiencies 37
3.6 Calculation of the fraction of excited luminescence centers 38
3.7 Conclusions 43
4 RESULTS & DISCUSSION 44
4.1 Near-infrared light emitting devices 44
4.2 Visible light emitting devices 48
5 CONCLUSIONS AND FUTURE WORK 54
6 RESUMEN EN CASTELLANO 57
7 VITA 61
7.1 List of all publications 61

7.2 Participation in congresses 66
7.3 Participation in research projects from public calls 74
7.4 Research stays abroad 77
7.5 European Materials Research Society (EMRS) Student Award 2013 78
List of tables 79
List of figures 79
List of references 80
Appendix 86
A1. Statement of contribution in the presented articles 86
A2. Copy of the published articles included as part of the thesis 86

1 INTRODUCTION

> Do something useful and you will have everything you want. Doors are shut for those who are dull and lazy; life is secure for those who obey the law of work.
>
> — José Martí —

1.1 The need of a silicon photonics

Silicon photonics is a research field devoted to study photonic systems, which makes use of silicon as optical medium. In the early nineties, this discipline emerges as result of an alternative solution to circumvent the microelectronic bottleneck predicted by Moore in 1965 through his famous law, which states that the number of transistors per chip will double every 18 months [1].

As in microelectronics, the key for the success of integration in photonics is to realize a broad palette of optical functionalities with a small set of elementary components, as well as to develop a generic wafer-scale technology for integration. The single device in a large scale of integration chip (light source, modulator, waveguide and detector) has an insignificant cost and researchers then concentrate on the way to achieve the desired functions by using as many components as needed. Thus, silicon photonics provides with feasible solutions for electro-optical conversion and interconnection (optical interconnects as a solution to the microelectronics copper interconnect bottleneck), as well as all optical processing and integrated optical sensor solutions. Additionally, by integrating optics and electronics on the same chip, high functionality, high performance and highly integrated devices can be fabricated with well-mastered complementary metal-oxide-semiconductor (CMOS) fabrication. As an example, Figure 1 shows a conceptual image of the high-density chip-to-chip optical interconnect system, or ultra-compact interposer based on Si photonics.

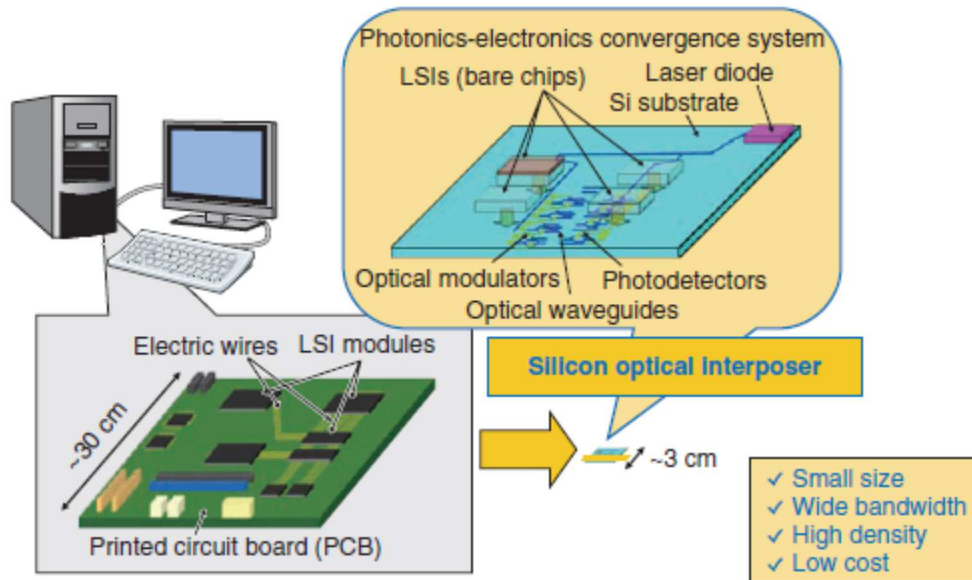

Figure 1. Concept of chip-to-chip optical interconnection based on Si photonics technology [2].

One example of the high versatility of silicon technologies is the field of photovoltaics, where a high percentage (>90%) of modules are entirely fabricated with silicon technologies. Another application of silicon photonics is the field of silicon solid-state lighting, where luminescent species (either rare earth (RE) ions or Si nanostructures (Si-nc), for instance) are introduced into silicon-based materials and then electroluminescent emission is achieved. In this respect, adding intelligence and control to the light emission in the form of integrated lighting systems is a benefit for silicon solid-state lighting in comparison with other technologies. In general, silicon-based devices are of high interest for future components in which photonic and electronic functions are integrated together.

In the rapidly developing field of optical interconnects, there are potential solutions to the interconnect bottleneck in microelectronics which is caused by the poor performance of metal interconnects at high frequencies (RC delays). Optical technologies are enabling the evolution towards ultra-broadband communication and enhanced connectivity. Optical technologies are also nowadays moving to data centres to meet the large bandwidth demands of high-performance computing systems. As it already happened in long-haul communications several years ago when optical fibres replaced copper cables, the copper cables that connect racks in the data centres are starting to be replaced by optical fibres. Following the same trend, it is foreseen that optics will become competitive with copper at shorter and shorter distances leading to optical on-

board and eventually to on-chip optical communications. In particular, Figure 2 shows the relation between the interconnect bandwidth and the footprint of interconnect modules.

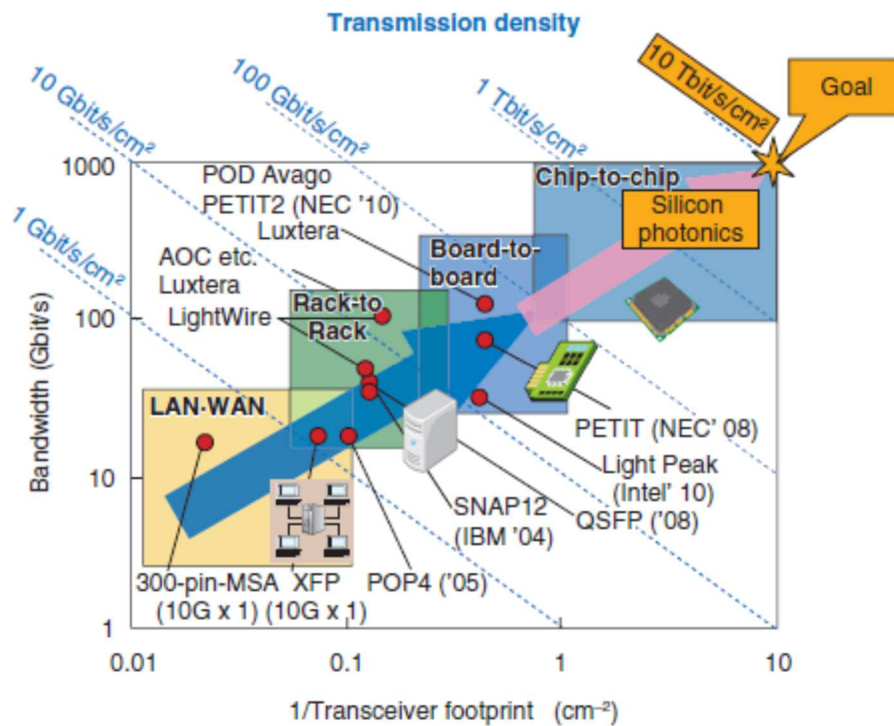

Figure 2. Trends in optical interconnection technology. Active optical cable (AOC), post office protocol version 4 (POP4), multi-source agreement (MSA) and quad small form-factor pluggable (QSFP) [2].

High performance computing also requires integrated novel photonic components and architectures supporting bandwidth growth of 100-1000 times at a reduction in cost of a factor of 100-1000 compared to the current state of the art.

Silicon CMOS photonics is accepted as the key technology platform for boosting photonic integration and hence enabling the required electronic-photonic convergence for on-chip optical interconnects. There have been significant advances in the development of active devices based on silicon photonics during the last few years [3]-[10]. However, the main drawback nowadays to attain monolithically integrated both photonic and electronic components on the same chip has been the lack of an efficient Si-based light emitting device, LED (hereafter D will be referred to device in lieu of diode, unless otherwise stated), electrically driven, or even a Si-based laser. In fact, most of the basic components required for the building block of silicon photonics have

been demonstrated, but the missing link is a silicon-based light source. Mostly, because silicon is a very inefficient light emitter, due to its indirect band gap. Therefore, the general objective of this thesis focuses on helping to fill this gap by contributing to the development of efficient light emitters, electrically driven, based on rare-earth ions and Si nanostructures in dielectric matrices by using technological processes fully compatible with CMOS technology.

1.2 Rare earth- and Si nanostructure-based light emitting devices

Generally, most of the developed LEDs resemble an architecture metal-insulator-semiconductor (MIS) capacitors, where luminescent centers are located inside the insulator material. Top electrodes of indium-tin-oxide or highly-doped *n*-type polycrystalline silicon and back electrodes of aluminum or gold are commonly used. In particular, Figure 3 shows a sketch of the MIS capacitor-based LEDs.

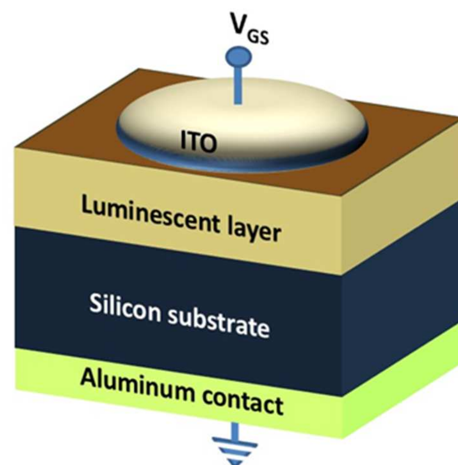

Figure 3. Sketch of typical LEDs architecture based on MIS capacitor.

Si-based integrated light sources were first reported in the early nineties [11], after the discovery of strong visible photoluminescence emission from porous silicon [12]. Since then, several strategies aimed at obtaining an efficient Si-based LED have been proposed. These strategies can be roughly divided into two groups: those that concentrate their study on the intrinsic emission from matrix (viz. emission coming from Si-nc or/and emission ascribed to defects related to Si excess) and those that focus on the extrinsic emission, which is produced by optical doping, for instance, by using rare earth ions.

One common way to obtain intrinsic emission is nanostructuring silicon, which produces a dramatic increase in the luminescent emission because of

quantum confinement of excitons in Si-nc. Confinement brings about relaxation of the selection rules for radiative transitions in the indirect band gap of silicon. Furthermore, band gap modulation-dependency on Si-nc size makes possible the tuning of the emission in the red-near infrared part of the electromagnetic spectrum [13]. Several works have reported either red or near-infrared electroluminescence (EL) from silicon-rich silicon oxide (SiO_x), which is mostly ascribed to exciton recombination in Si-ncs [14]-[22]. In addition, green or blue EL is commonly attributed to the defects associated to Si excess [23]-[28]. Although, some studies have reported red EL emission coming from defects, whose origin is corroborated thanks to the fact that peak positions do not change with the fabrication conditions [29]. In respect to the structure and size of Si-ncs, it has been also reported that amorphous Si-ncs require lower voltages, but higher currents, to achieve the same EL intensity than its crystalline form [30]. Likewise, larger Si-ncs are much less efficient than smaller ones [18]. Another specific approach to obtain intrinsic emission is ordering the Si-ncs in one preferential direction by means of a superlattice formed by alternating SiO_x and SiO_2 thin-film layers. Red or near-infrared EL emission from such structures has been observed [31]-[42] and explained by either excitonic recombination taking place in the confined states within the Si-ncs [42] or hot electron relaxation [34]. Additionally, intrinsic emission from silicon-rich silicon nitride (SiN_x) has been observed [43]-[47], but lesser works than for SiO_x have been published owing to its recent appearance as suitable electroluminescent material. For example, orange EL peaking at 600 nm has been observed at room temperature from Si-ncs embedded in silicon nitride matrix [43] and the orange emission was ascribed to electron-hole pair recombination within the Si-ncs. Also, green EL from N-rich oxidized amorphous silicon nitride has been reported [44]. The origin of the green emission was attributed to radiative recombination in the localized states related to the Si-O bonds. Later on, same authors also demonstrated a remarkable enhancement on green EL intensity by employing Si-rich oxidized amorphous silicon nitride layers instead of N-rich oxidized amorphous silicon nitride ones [45]. By Si implantation into silicon nitride, a violet and a green-yellow bands have been also observed [46]. The two bands give rise to a strong white-color EL at high injection currents. The violet band was associated to the radiative recombination between the defect state related to the Si dangling bond ($\equiv Si^0$) located in the middle of the silicon nitride band gap and the bonding state of the Si-Si≡ unit that is close to the valence band edge. Likewise, the green-yellow band

was attributed to the transition from $\equiv Si^0$ state to the state related to the nitrogen dangling bonds ($=N^-$) in the valence band tail. In addition, red or near-infrared EL has been reported from SiN_x/SiO_2 superlattice structures [47]. The observed EL intensity at 800 nm was explained by bipolar recombination of electron-hole pairs at Si-ncs.

Nevertheless, despite numerous published works on the intrinsic emission from Si-based matrices [14]-[47], it is difficult to obtain a precise control over the emission energy throughout the visible spectrum. This is because surface states of Si-ncs and defects limit the tunability range of these systems. Light emission from Si nanostructures strongly depends on composition and processing parameters, and slight variations in the processing can lead to changes in the emission spectra. One method of obtaining specific emission energies is through the incorporation of RE dopants into these materials that leads to luminescence characteristic of the electronic energy levels of the RE [48]. The use of RE dopants to achieve specific color emissions for lighting has been traditionally applied to phosphor-based systems [49]. However, during the last decade, the emissions arising from the RE ions themselves and not specifically in the use of RE ions as color converters have been seriously considered [50]-[64]. Different Si-based materials and optical dopants for the extrinsic emission have been proposed [56]-[64]. For instance, the use of erbium ions is of particular interest for telecoms applications, as its main emission line at 1.54 μm fits well with the global absorption minimum of silica, the basic material of most optical fibers. In the late nineties, 1.54 μm EL from Er-doped silicon oxide [50] and Er-doped silicon-rich silicon oxide LEDs [51] was simultaneously reported. After these precursor works, there were a myriad of publications [52]-[62] which have been basically focused on how to improve the 1.54 μm power efficiency. Additionally, EL emission at 1.54 μm from Er-doped SiN_x LEDs has been reported [63]. More recently, 1.54 μm EL from Er-doped Si_3N_4 has been also published [64]. Moreover, other RE-based LEDs with emission wavelength in the visible range have been reported. The most relevant ones, from my humble opinion, span from those with bright green emission from Tb-implanted SiO_2 layers [65]-[68] to those with ultraviolet emission from Gd- [69], blue emission from Ce- [70], [71], blue emission thanks to co-operative upconversion from Yb- [72]-[74] and both blue and green emission bands from Tm-implanted SiO_2 LEDs [75], [76]. For the particular case of Eu-implanted SiO_2, it has been found that the EL spectrum can radically change the color from red to blue and vice versa, depending on the

oxidation state of Eu and the injection current value [77]. However, despite several works report on different RE-implanted SiO_2 emitting in the visible range, none has studied the effect, from the electroluminescent viewpoint, of introducing these RE ions into SiN_x or Si_3N_4 matrices. Actually, intense green-yellow EL from Tb-implanted SiN_x LEDs has been recently reported [78], which has been one of the most important results presented in this thesis. Therefore, there is room for researching in this platform of materials based on RE-doped silicon nitride LEDs.

Table 1 summaries the main wavelength associated to either intrinsic or extrinsic emission and power efficiency (defined as the ratio between the optical output power of the device and the electrical input power, both in watt) of the different LED materials developed since last decade. Particularly, Table 1 shows that porous Si material gives the highest power efficiency value so far. However, its fabrication procedure is not compatible with the mainstream Si technology [79] and also porous Si material shows low mechanical and chemical stability [80]. Likewise, modest improvements on the power efficiency for Si technology-based LEDs have been achieved. Therefore, the development of a fully Si-technology compatible RE- and Si nanostructure-based materials platform for LEDs in the visible and near-infrared range is required. Thus, the general objective can be broken down into the following specific objectives that would together achieve the overall goal of the thesis:

- To explore the most suitable CMOS-compatible fabrication technique for obtaining the best electroluminescent thin-film material.
- To study the effect of the different used fabrication techniques on the electrical and EL mechanisms at a given electroluminescent material composition.
- To study the influence of the Si nanostructures excess and RE ion concentration on the electrical and EL properties of the fabricated LEDs.
- To identify the electrical conduction mechanisms and EL excitation processes of RE ions and Si nanostructures in different silicon oxide and silicon nitride environments.
- To study the influence of combining silicon oxide and silicon nitride thin-film layers in the form of NO or ONO on the electrical and EL properties.
- To identify advantages between MNOS capacitor-like devices and MNOS field-effect transistor ones as optimum architecture for the LEDs.

- To tailor an optimum gate stack for boosting the power efficiency of the studied LEDs in both visible and near-infrared ranges.

Year	Material	λ(μm)	Power efficiency (%)	Reference
2000	Porous Si	0.68	0.37	[79]
2003	Yb:SiO_2	0.98	0.01	[72]
2004	Gd:SiO_2	0.31	5×10^{-4}	[69]
2005	Tb:SiO_2	0.54	0.3	[68]
2005	Si-nc:Si_3N_4	0.60	5×10^{-3}	[43]
2006	Ce:SiO_2	0.44	0.01	[71]
2006	Si-nc:SiO_2	0.78	0.01	[22]
2009	Si-nc/SiO_2 ML	0.85	0.17	[41]
2010	Er:SiO_x	1.54	0.01	[60]
2012	Er:SiO_2	1.54	0.01	[61]
2013	Si-nc:SiO_2	0.48	10^{-4}	[81]
2013	Er:Si-nc/SiO_2 ML	1.54	3×10^{-5}	[62]
2013	Tb:SiN_x	0.54	0.01	[78]
2013	Er:Si_3N_4	1.54	1.3×10^{-5}	[64]
2013	Er:SiN_x	1.54	8×10^{-5}	[64]
2013	Er:SiO_2	1.54	0.03	[64]

Table 1. Power efficiency of different RE- and Si-based materials for light emitting devices

1.3 Outline of this thesis

This thesis presents experimental work on developing rare-earth ions and Si nanostructures as a material platform for LEDs in the visible and near-infrared range, which are aimed to integrated Si photonics applications. The chapters are structured as follows:

In chapter 1, an introduction related to the need of a Si photonics is presented. In addition, the state of the art of RE ion- and Si nanostructure-based light emitters is outlined. Chapter 2 reviews the most common electrical conduction mechanisms that take place in insulating materials. For the sake of a better understanding, the electrical mechanisms have been divided into electrode-limited and bulk-limited conduction. Likewise, chapter 3 introduces the different mechanisms of electroluminescence excitation and basic concepts on LED efficiency. Additionally, the procedure for calculation of the fraction of excited luminescence centers in RE- and Si-based light emitting devices with planar

surface is established. Chapter 4 is dedicated to summarize the most important results of the published papers related to the aims of this thesis. As part of conclusions, some future perspectives for this line of research are also tackled.

2 ELECTRICAL CONDUCTION MECHANISMS IN INSULATING FILMS

> The most startling result of Faraday's Law is perhaps this. If we accept the hypothesis that the elementary substances are composed of atoms, we cannot avoid concluding that electricity also, positive as well as negative, is divided into definite elementary portions, which behave like atoms of electricity.
>
> — Hermann von Helmholtz —

2.1 Introduction

This chapter is devoted to introduce in a compact and simple way the different electrical conduction mechanisms that take place in a metal-insulator-metal (MIM) structure, where the insulating film is generally thinner than 1 μm thick. For many practical applications, it is essential to be aware of the basic electrical properties of insulating materials in the correct perspective. For methodological reasons, we have divided this chapter into two mechanism groups: (i) electrode-limited conduction (viz. tunneling and Schottky processes) and (ii) bulk-limited conduction (viz. Poole-Frenkel, hopping and space-charge-limited) [82]. Generally speaking, we understand as electrode-limited conduction those mechanisms where the electrode is not able to supply all carriers needed for the bulk conduction and thus the charge transport is limited by the rate at which carriers are injected into the insulator from the electrode. On the contrary, the bulk-limited mechanisms are usually identified when current is limited by the rate at which carriers can flow through the insulator. Normally, electric fields of the order 10^4 to 10^5 V cm^{-1} are enough to obtain observable current flow through the films.

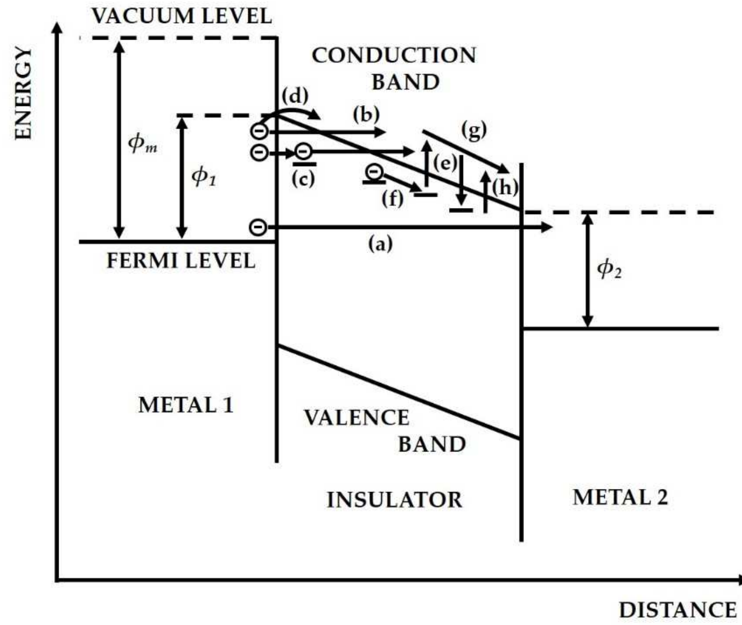

Figure 4. Schema of different conduction mechanisms and electrical processes in MIM structures. (a) Direct tunneling, (b) Fowler-Nordheim tunneling, (c) trap-assisted tunneling, (d) Schottky emission, (e) Poole-Frenkel, (f) hopping of carriers from trap to trap, (g) carrier scattering in the conduction band, and (h) carrier trapping at impurities and/or imperfections

We consider the current flow through a thin insulating film equipped with metal electrodes in a metal-insulator-metal sandwich form. The carrier transport takes place via a number of different mechanisms as shown in Figure 4. Direct tunneling (DT) of carriers from one metal to the other is the simplest process as it is less strongly dependent on the actual microscopic structure of the insulator [mechanism (a)]. In addition, if bands are sufficiently bent due to the action of a strong electric field, carriers from metal or electrode will tunnel into the insulator conduction band through the triangular-shape barrier [Fowler-Nordheim tunneling, FNT, process (b)]. In other words, carriers will cross an effective tunnel thickness smaller than the one associated to the direct tunneling process. Likewise, if the dielectric barrier has traps, the tunnel injection can be assisted by the traps close to the electrode and consequently an effective reduction of the injection barrier height occurs. This tunneling mechanism is known as trap-assisted tunneling (TAT) and basically consists of a two-step sequential process in which injected electrons tunnel first to the traps inside the insulator band gap and afterwards to the insulator conduction band [mechanism (c)]. Injection of carriers into the conduction (or valence) band of the insulator can also take place by thermionic (or Schottky) emission over the contact barrier [mechanism (d)].

This latter process is analogous to carrier emission from a metal into vacuum. Additionally, scattering mechanisms in the conduction band can affect the current flow [(g)]. Owing to the very small distances involved such effects can be expected to be small. Amorphous materials, for instance silicon nitrides and oxynitrides, usually contain large densities of trapping sites or defects, which can be associated to dangling bonds, vacancies or impurities; such as oxygen, hydrogen or nitrogen. Consequently, carrier trapping at impurities and imperfections [(h)] should be expected to be important. Carrier trapping changes the space-charge distribution in the insulator. Any trapping effect depends on the ratio of free-to-trapped carrier and is therefore strongly temperature-dependent. The tunneling of carriers from the metals directly into the traps and vice versa [mechanisms (b), (c)], thermally active carriers [Poole-Frenkel mechanism (e)] and hopping of carriers from trap to trap [(f)], also constitute some other possible modes of carrier transport.

2.2 Electrode-limited conduction mechanisms

2.2.1 Tunneling

The penetration probability of an electron from one electrode to the other through the insulator is strongly dependent on the applied electric field. The effects of temperature, electron effective mass in the conduction band, dielectric constant, charge image forces and shape of the potential barrier must all be taken into account when calculating the tunnel currents.

Therefore, from a generalized energy band diagram like in Figure 4, we can obtain the expressions for the current density associated to the different tunneling processes. In particular, depending on the applied electric field, electrons (holes) have essentially three ways of tunneling the potential barrier according to their energy: (i) through the trapezoidal part (DT), (ii) the triangular part (FNT), or the traps located in the insulator band gap (TAT) [see Figure 4, processes (a), (b) and (c), respectively]. Thus, using the well-known Wentzel-Kramers-Brillouin (WKB) approximation and the Tsu-Esaki formula, the particular expressions for the current density corresponding to each mentioned processes are respectively given by [83]-[85]:

$$J_{DT} \propto F^2 exp\left\{-\left[\frac{4\sqrt{2m^*}}{3\hbar qF}\left(\phi_1^{3/2} - \left(\phi_2 - qFd\right)^{3/2}\right)\right]\right\} \tag{2.2.1}$$

$$J_{FN} \propto F^2 exp\left(-\frac{4\sqrt{2m^*}}{3\hbar qF}\phi_1^{3/2}\right) \tag{2.2.2}$$

$$J_{TAT} \propto exp\left(-\frac{4\sqrt{2m^{*}}}{3\hbar qF}\phi_t^{3/2} \right) \tag{2.2.3}$$

where m^* is the effective electron mass, $\hbar$ is the reduced Planck's constant, q the elementary charge, F the applied electric field, d the insulator layer thickness, ϕ_1 the carrier barrier height, and ϕ_t the trap energy, in (eV), below the insulator conduction band edge.

These equations predict that the current density J should be independent of the temperature. In addition, a plot of Log (J/F^2) against ($1/F$) should yield a straight line, whose slope can be used to experimentally estimate the barrier height. This representation is also commonly called the Fowler-Nordheim plot.

2.2.2 Schottky-type conduction

The electrode-limited Schottky-type conduction process is highly dependent on the potential barrier at the metal-insulator interface. When an electron escapes from the metal surface, the latter becomes positively charged and exerts in turn an attractive force on the electron. Owing to the resulting image force the potential step at the metal-insulator interface changes not abruptly, but smoothly. The potential energy of the electron due to the image force is given by:

$$\phi_{image} = -\frac{q^2}{16\pi\varepsilon\varepsilon_0 x_0} \tag{2.2.4}$$

where ε and ε_0 are the relative permittivity of the material and vacuum permittivity, respectively; and x_0 is the distance of the carrier from the electrode surface. In the course of emission the escaping electrons spend only an extremely short time in the immediate vicinity of the surface. Hence ε used in equation (2.2.4) should be the high frequency dielectric constant of the insulator and ε_0 the vacuum permittivity.

In the electrode-limited conduction processes, the image force effects have a significant importance [82], [85]. The potential barrier in the presence of image force is shown by the solid line AB in the Figure 5. Schottky assumes that the image force is limited to a distance x_0 of the electron from the electrode surface [85], [86]. Under the influence of an electric field F the potential barrier is lowered due to the interaction of the field with the image force.

Referring to the Figure 5, it is observed that the potential barrier is lowered by $\Delta\varphi_s$. The dashed line AD represents the lowered potential barrier. The potential energy of the barrier under the electric field with respect to the Fermi level (FL) of the electrode is less than φ_0 by $\Delta\varphi_s$. In fact, $\Delta\varphi_s$ represents the change in the

barrier height owing to the interaction of the field with the image potential and is given by:

$$\Delta\varphi_s = \left(\frac{q^3}{4\pi\varepsilon\varepsilon_0}\right)^{1/2} F^{1/2} = \beta_s F^{1/2} \qquad (2.2.5)$$

$$\text{where } \beta_s = \left(\frac{q^3}{4\pi\varepsilon\varepsilon_0}\right)^{1/2} \qquad (2.2.6)$$

and β_s is called the Schottky constant or coefficient.

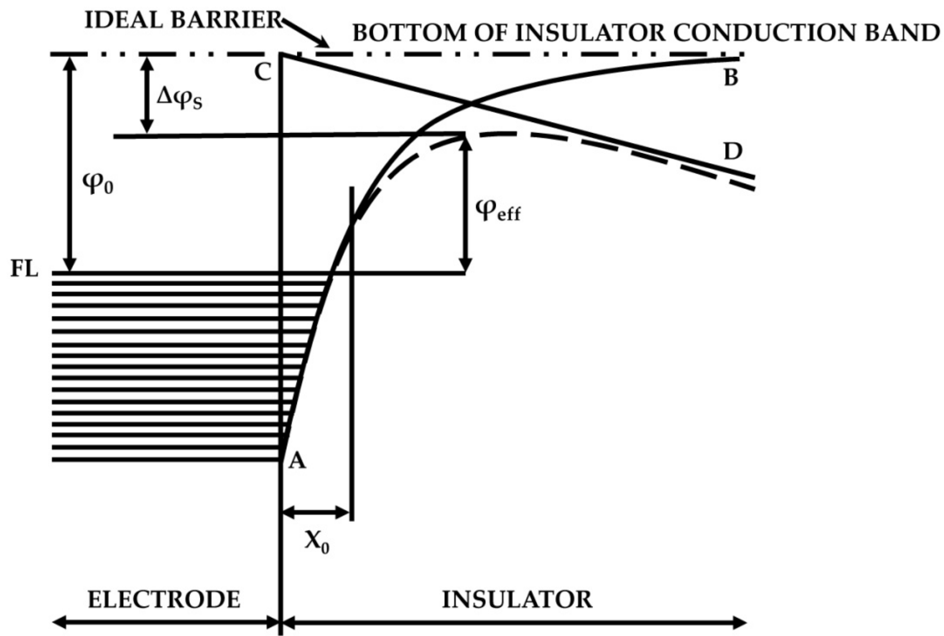

Figure 5. Potential barrier lowering due to Schottky effect

In this type of barrier lowering cases, the electrode-limited current density obeys the Richardson-Schottky law. The expression for the current density in an electrode-limited Schottky-type conduction mechanism is therefore given as follows [86]:

$$J = AT^2 exp\left[-\frac{\left(\varphi_0 - \Delta\varphi_s\right)}{kT}\right] \qquad (2.2.7)$$

or

$$J = AT^2 exp\left[\frac{\left(\beta_s F^{1/2} - \varphi_0\right)}{kT}\right] \qquad (2.2.8)$$

A being the Richarson constant, k the Boltzmann constant and T the absolute temperature. In particular, equation (2.2.8) shows that, in the Schottky mechanism, the current density (J) has an exponential dependence on the square root of the applied electric field ($F^{1/2}$). The plot of Log (J) against ($F^{1/2}$) should yield a straight line, whose slope gives the Schottky barrier height at a given temperature. This plot is known as Schottky representation.

At low temperatures, field emission dominates over thermionic emission. The electrode-limited conduction can change from Schottky to field emission as the temperature of the sample is lowered [87], [88].

2.3 Bulk-limited conduction mechanisms

2.3.1 Poole-Frenkel

The exponential dependence of the current density on the square root of the applied electric field is not a unique characteristic of the Schottky-type conduction mechanism. Such a relation holds equally well for the electric field-enhanced thermal excitation of trapped carriers from localized centers (traps) or potential wells within the bulk of the insulator. This conduction process is the so called Poole-Frenkel effect [89]. Here, similar to the lowering of the interfacial barrier in Schottky effect, the applied electric field lowers the coulombic-type potential barrier (see Figure 6). The potential energy of an electron under the action of the electric field for a trapping center is given by the common Coulomb expression as follows:

$$\phi_c = -\frac{q^2}{4\pi\varepsilon\varepsilon_0 x} \tag{2.3.1}$$

where x is the distance from the trap center.

The potential energy ϕ_c is four times higher than the image force one given by equation (2.2.4). Hence, the Poole-Frenkel lowering of a coulombic barrier will be twice the one due to Schottky effect. However, Poole-Frenkel-type conduction is a bulk-limited mechanism, in contrast to the electrode-limited Schottky mechanism. Figure 6 shows the Poole-Frenkel effect at a trapping center and also the hopping mechanism, which will be described in the next subsection.

The current density expression for this bulk-limited mechanism is given by [90]:

$$J = \sigma_0 F exp\left[\frac{\left(\beta_{PF} F^{1/2} - \phi_c\right)}{kT}\right] \tag{2.3.2}$$

where σ_0 stands for the low field conductivity and is given as follows:

$$\sigma_0 = nq\mu \tag{2.3.3}$$

n being the number of charge carriers and μ the mobility. ϕ_c represents the ionization potential of the Poole-Frenkel trapping centers.

In addition, the factor $\beta_{PF} = \left(\frac{q^3}{\pi\varepsilon\varepsilon_0}\right)^{1/2}$ factor in equation (2.3.2) is the so called Poole-Frenkel constant or coefficient. It has to be noticed that $\beta_{PF} = 2\beta_S$. From the equation (2.3.2) is observed that the current density exponentially varies as the square root of the applied electric field, which is very akin to Schottky mechanism. Consequently, a general relationship like:

$$J = J_0 exp\left[\frac{(\beta F^{1/2} - \phi_{eff})}{kT}\right] \tag{2.3.4}$$

can be equally applied to Poole-Frenkel and Schottky mechanisms where:

$$\beta = \left(\frac{q^3}{a\pi\varepsilon\varepsilon_0}\right)^{1/2} \tag{2.3.5}$$

with a=1 for Poole-Frenkel and a=4 for Schottky effect, respectively.

It has to be highlighted that in both cases the carrier movement is facilitated by the application of an external electric field, which acts lowering the potential barrier for emission. The graph representation of Log (J) versus ($F^{1/2}$) renders a straight line in which the slope gives information on the potential barrier height. This plot is also known as Poole-Frenkel plot.

On the other hand, the simplest way to differentiate between Poole-Frenkel and Schottky mechanism is to compare the experimental values of the β coefficients with the theoretical ones. The experimental β coefficients can also be extracted from the slope of the Log (J) against ($F^{1/2}$) plots. Moreover, the theoretical values can be computed knowing the permittivity values. Nevertheless, the coincidence between the experimental and theoretical coefficients is not a sufficient proof of the occurrence of either mechanism [91], [92]. The β_s and β_{PF} values experimentally obtained from the plot may not be separate enough to differentiate between them. The theoretical calculations are also highly risky if the permittivity values are not accurate. Owing to such uncertainty in establishing the conduction mechanism on the basis of β coefficient measurements solely, other methods are also used. For instance, the application of asymmetric electrodes is a most usual alternative method [93]. The Schottky mechanism being the electrode-limited type should depend on the properties of the electrode material, essentially its work function. For Schottky process, an

interchange of the field polarity should bring on a shift in the current-voltage characteristic by several orders of magnitude depending upon the difference in the work functions of the dissimilar materials for electrodes. On the contrary, Poole-Frenkel process, being a bulk-limited conduction mechanism, should not depend on the properties of the electrode material [89].

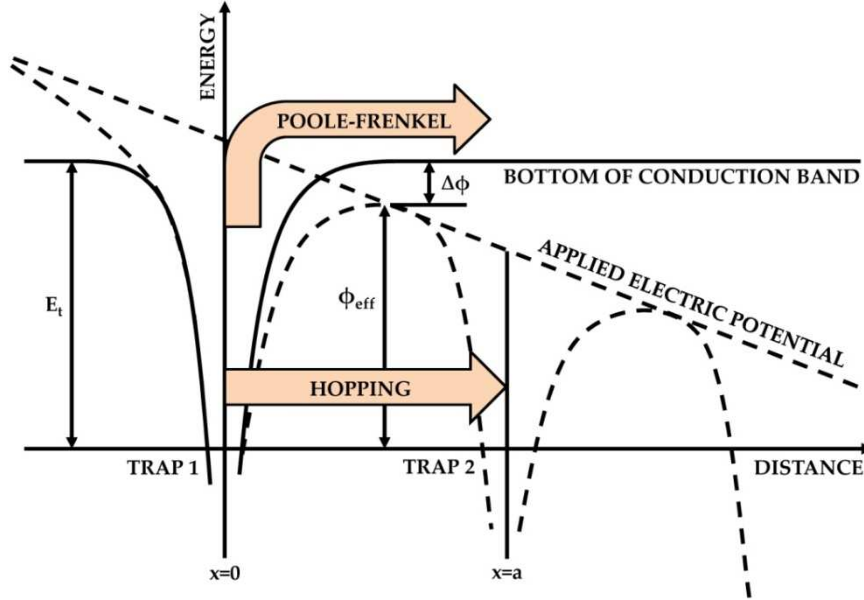

Figure 6. Potential barrier lowering at a trapping site due to Poole-Frenkel effect and hopping conduction mechanism

2.3.2 Hopping conduction

It is reasonable to assume that amorphous materials preserve their short-range order and also local binding forces are essentially the same as in crystalline forms. Thus, if the spatial fluctuations in the interatomic distances are large, the correspondingly large and random fluctuations in the depth or height of the potential wells may lead to the localization of states below a certain critical and well-defined energy. When the mean free path of carriers is comparable to the interatomic distance and the carrier mobility is low, the conduction can be expected to take place by a hopping process in the localized states [94]. In a hopping mechanism, only those carriers with a thermal energy of about kT below the Fermi level have a significant probability to take part in the conduction. Hopping conduction is due to the tunneling effect of trapped electrons, which hop from one trap site to another in insulating films. Figure 6 shows the schematic band diagram of hopping conduction process.

The relationship for the conductivity in this case reads as follows [95]:

$$\sigma = N_F q^2 \alpha v_{ph} exp(-\frac{E_A}{kT}) \qquad (2.3.6)$$

where N_F is the density of states, α^{-1} is the localization length characterizing the decay of the wave-function at a site, υ_{ph} is the phonon frequency and E_A the activation energy for hopping.

The conductivity thus shows an exponential temperature dependence. Mott has shown that for strongly localized states, the conductivity at low temperatures must follow an expression of the form [95]:

$$\sigma \propto exp(-BT^{-1/4}) \tag{2.3.7}$$

where $B = 2.06\left(\alpha^3/kN_F\right)^{1/4}$, k being the Boltzmann constant in eV·K^{-1}. At high temperatures deviations from $T^{-1/4}$ occur, which can be understood in terms of inter-chain hopping. A carrier trapped in a chain after thermally detrapping may drift along the same chain or may hop into an adjacent chain. The conduction can basically occur due to two distinct processes, a temperature dependent trap hopping (carriers hop from trap to trap, Figure 6) and a comparatively less temperature-dependent inter-chain hopping (carriers hop from chain to chain). For example, this latter process typically occurs in amorphous polymers.

In addition, the hopping distance (R) and the width of the defects band (ϖ) in the hopping conduction mechanism are respectively given by [95]:

$$R = \left(\frac{9}{8\pi\alpha N_F kT}\right)^{1/4} \tag{2.3.8}$$

$$\varpi = \frac{3}{4\pi N_F R^3} \tag{2.3.9}$$

In Poole-Frenkel conduction, carriers can overcome the trap barrier through the thermionic mechanism. However, in hopping conduction, the carrier energy is lower than the maximum energy of the potential barrier between two trapping sites. Thus, the carriers can still transit using the tunnel mechanism.

2.3.3 Space-charge-limited current

When carrier generation processes are slower than carrier transport through the film, the conduction is controlled by carrier generation and we have the Poole-Frenkel or Schottky type effects, for instance. Conversely, if transport is slower than carrier generation the theory of space-charge-limited current (SCLC) holds [96], [97]. At low applied fields, an ohmic contact to the insulator supplies carriers at a rate equal to their departure by drift at the opposite contact and the current-voltage relationship remains ohmic. At sufficiently high applied fields, more carriers are injected than what is required by ohmic current considerations.

The excess carriers mostly accumulate as space charge in the vicinity of the contacts or electrodes. The drift of this excess space charge constitutes a current higher than the ohmic current, and is termed space-charge-limited current. For a trap-free material the current density under space-charge-limited conduction regime is given by [97]:

$$J_{SCLC} = \frac{9}{8}\varepsilon\varepsilon_0\mu\frac{V^2}{d^3} \quad (2.3.10)$$

where μ is the carrier mobility in the material and V the applied voltage. This type of conduction process exhibits current-voltage characteristics having three or four distinct regions (see Figure 7). The first region corresponds to the low field conduction region, where the variation of current density with voltage is ohmic, which follows a relationship given by:

$$J_{\Omega} = \frac{9}{8}p_o\varepsilon\varepsilon_o\mu\frac{V}{d}, \text{ with } p_o = H\exp(-\frac{E_A}{kT}) \quad (2.3.11)$$

where p_o accounts for carriers thermally generated, and H is the pre-exponential factor. Therefore, as the voltage is increased, the injected carriers numerically exceed the thermally generated ones and SCLC starts. Equation (2.3.10) shows that J is directly proportional to V^2 and inversely to d^3. The region close to the ohmic one is the square law region where J varies as V^2. The transition from ohmic to square law shows the voltage onset (V_{Ω}) of SCL conduction. The presence of traps in the material considerably reduces the SCL current, since empty traps remove most of the injected carriers. In the presence of shallow traps equation (2.3.10) takes the following form [97]:

$$J_{SCLC} = \frac{9}{8}\varepsilon\varepsilon_0\mu\frac{V^2}{d^3}\theta, \text{ with } \theta = \frac{N_c}{N_c + N_t}exp(-\frac{E_t}{kT}) \quad (2.3.12)$$

where θ is a parameter introduced to account for the fraction of the injected charge carriers that are free; whilst N_c and N_t are the densities of charge in the conduction band and trapped charge in the insulator band gap, respectively; and E_t is the trap energy measured from the bottom of the conduction band. On further increase of voltage, at some higher voltage, all traps become essentially filled and then the current increases rapidly back to the trap-free case (see Figure 7). This is the trap-filled limit region and the voltage onset is commonly called trap-filled limit voltage (V_{TFL}). The trap-filled limit voltage is defined as follows:

$$V_{TFL} = \frac{qN_t d^2}{2\varepsilon} \quad (2.3.13)$$

Beyond this limit, any slight change in voltage will increase the current sharply. In fact, the current will increase according to equation (2.3.10). It can be imagined that after all traps are filled up, the subsequently injected carriers will be free to move into the insulator conduction band. Thus, there exists a threshold voltage (V_{TFL}), where the current will rapidly jump from its low trap-limited value to a high trap-free SCL current (see Figure 7). V_{TFL} voltage is defined as the voltage required to fill the traps or, in other words, as the voltage at which Fermi level (E_F) passes through E_t.

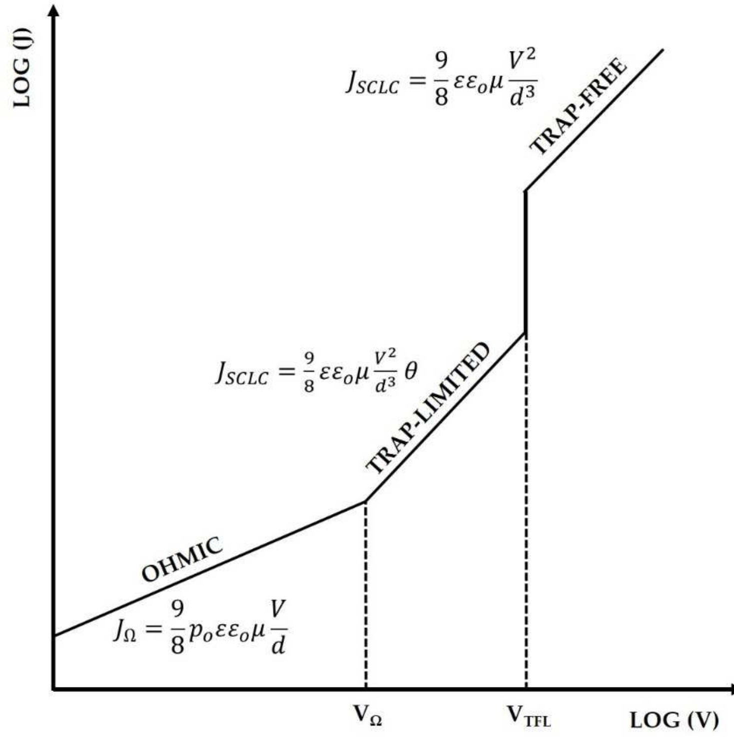

Figure 7. Schematic log (*J*)-log (*V*) plot, showing the current variation as a function of voltage and θ for an insulator with shallow traps confined in a trapping level E_t

Approximate theories to determine such properties as the concentration of traps and their energy distributions have been developed by Rose [98] and others [95]. This information is obtained from the steady state current-voltage characteristic when operating in the SCLC region. SCLC is essentially characterized by (i) current increasing with a power of the voltage equal or greater than two and (ii) current increasing with a power of the reciprocal thickness. Theoretically, the exponent on the thickness is twice that of the voltage

exponent. SCLC technique thus provides a powerful means to interpret the number and energies of present trapping sites.

The basic conduction processes in insulating films with their corresponding dependence with the voltage and the temperature are listed in Table 2.

	Type of conduction	Current density (J) or Conductivity (σ)	Voltage dependence	Temperature dependence
Electrode-limited	Tunneling	$J = cF^2 exp(-\frac{B}{F}\phi_1^{3/2})$	$J \propto V^2 exp(-\frac{b}{V}\phi_1^{3/2})$	Practically independent
	Schottky	$J = AT^2 exp\left[\frac{(\beta_s F^{1/2} - \varphi_0)}{kT}\right]$	$Log(J) \propto V^{1/2}$	$Log(J/T^2) \propto (1/T)$
Bulk-limited	Poole-Frenkel	$J = \sigma_0 F exp\left[\frac{(\beta_{PF} F^{1/2} - \phi_c)}{kT}\right]$	$Log(J/V) \propto V^{1/2}$	$Log(J) \propto (1/T)$
	Hopping	$\sigma = N_F q^2 \alpha \upsilon_{ph} exp(-\frac{E_A}{kT})$	$J \propto V$	$Log(\sigma) \propto (1/T^{1/4})$ at low T
	Space charge-limited	$J = \frac{9}{8}\varepsilon\varepsilon_0\mu\frac{V^2}{d^3}$	$J \propto V^2$	T contributes to the carrier generation

Table 2. Basic mechanisms of electrical conduction in insulators

2.4 Conclusions

In this chapter, the main conduction mechanisms in insulating films have been presented. In the first part, the qualitative expressions for the current density as a function of applied electric field have been described and analyzed for electrode-limited conduction mechanisms. Likewise, the second part has been devoted to the bulk-limited conduction mechanisms. Both temperature and voltage dependences have been also discussed. These conduction mechanisms constitute the basis for explaining and understanding the different behaviors in the current-voltage characteristic of several insulating materials. In particular, the LED materials studied in this thesis.

3 ELECTROLUMINESCENCE AND LED EFFICIENCY: BASIC CONCEPTS

I learned very early the difference between knowing the name of something and knowing something.

— Richard P. Feynman —

3.1 Introduction

In this chapter, the mechanisms of electroluminescence excitation and basic concepts on LED efficiency will be presented. In addition, the procedure for the calculation of the fraction of excited luminescence centers (LCs) in RE ions and Si-based light emitting devices with planar surface is shown. Broadly speaking, we can define the electroluminescence as the excitation (by an applied electric potential) and de-excitation process of a material, whereby the electrical energy is converted to electromagnetic radiation. The electroluminescent mechanisms can be generally classified as (a) energy transfer, (b) impact excitation and (c) impact ionization. Likewise, radiative de-excitation occurs by two processes: (i) direct recombination of conduction electrons and holes in the valence band, and (ii) optical transitions of dopants or activators.

3.2 Energy transfer

The energy transfer process is caused by the radiative recombination of electron-hole pairs through donor-acceptor pairs, whose energy is released to the luminescent centers. For instance, in the material formed by RE-doped Si-nanocrystals, the excitation of RE ion centers could occur via non-radiative resonant energy transfer from Si-nanocrystals to RE ions, as illustrated in Figure 8 (a). This process has shown to be an efficient luminescence mechanism under optical pumping in materials based on Er in Si nanocrystal-doped SiO_2 [99], [100]. On the contrary, under electrical pumping, we have recently demonstrated that this process is no longer dominant [61].

3.3 Impact excitation

Direct impact excitation occurs when inelastic collisions of conduction-band electrons with luminescent ions excite their electrons to higher-energy localized levels at the light-emitting center (the centers are raised to an excited state, without a change in their charge or oxidation state). In the case of RE-doped silicon-based LEDs the EL is mostly dominated by impact excitation process of

hot electrons to the $4f^n$ intra-shell transitions of trivalent RE ions. Basically, hot electrons collide directly with localized RE ions and the ground-state electrons of the ions are excited to higher levels, so that EL is originated, as illustrated in Figure 8 (b). This excitation mechanism is responsible for the EL in the great majority of RE-doped silicon-based light emitting devices.

3.4 Impact ionization

The impact ionization generally occurs when a high-energy carrier (hot electron or hole) can give up enough energy to liberate another electron into the conduction band, which also creates a hole in the valence band. Typically, an electric field of around 7 MeV/cm is sufficient to produce hot electrons in silicon oxide host. Consequently, these hot electrons in the conduction band can ionize the defects by collision, and by creating electron-hole pairs. If defects, acceptor and/or donor states exist in the band gap of the material, the high-energy electrons will have a certain probability of ceding energy to these centers by inelastic collision. These ionized acceptors and donors recapture the electron-hole pairs, and EL is originated because of the recombination of electrons and holes. In addition, if the mean distance for the carrier acceleration up to an ionization event is less than the width of the frictional barrier imposed by nonpolar modes of lattice vibration at high energies, then the effects of carrier multiplication must be considered [101]. Both processes of impact ionization and generation-recombination of electron-hole pairs are illustrated in Figure 8 (c).

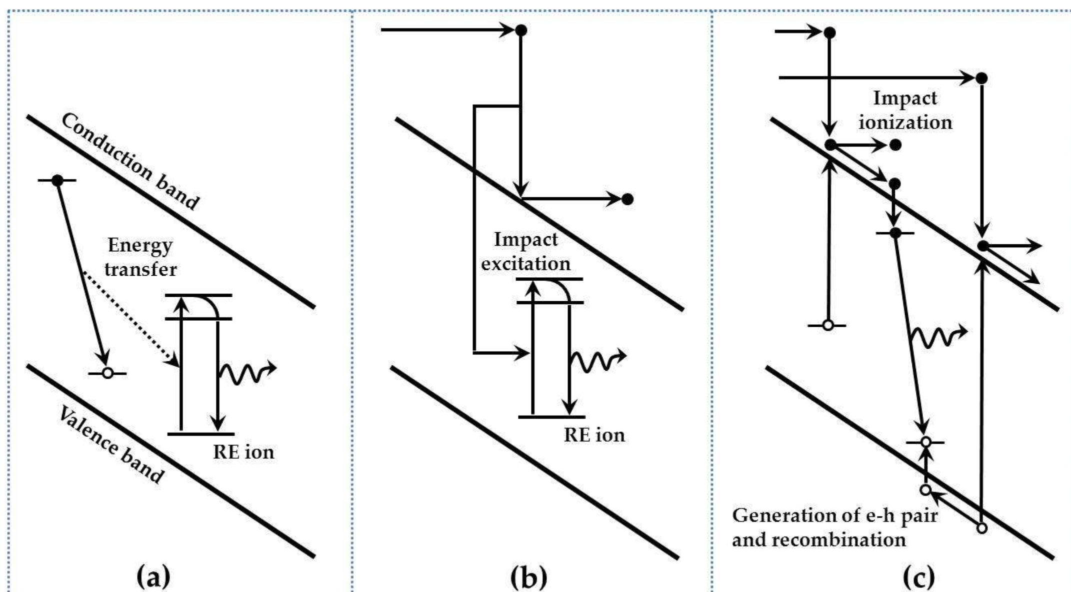

Figure 8. Most usual mechanisms of excitation of luminescent centers in thin-film LED: (a) energy transfer, (b) impact excitation and (c) impact ionization

3.5 Internal, extraction, power and external efficiencies

In an ideal LED, the active region should emit one photon for every injected electron. It means that each charge quantum-particle (electron) gives rise to one light quantum-particle (photon). Therefore, the active layer of an ideal LED has a quantum efficiency of unity. The internal quantum efficiency (η_{IQE}), also termed radiative efficiency, is defined as:

$$\eta_{IQE} = \frac{number\ of\ emitted\ photons\ from\ active\ region\ per\ second}{number\ of\ injected\ electrons\ into\ active\ region\ per\ second} = \frac{P_{int}/(h\nu)}{I/e}$$

(3.5.1)

where P_{int} is the emitted optical power from the active region and I is the injection current.

Once the photons are produced within the device, they have to escape from the active region in order to produce a light-emitting effect. Extraction efficiency ($\eta_{extraction}$), also termed optical efficiency, is the proportion of photons generated in the active region that escape from the device, which is defined as:

$$\eta_{extraction} = \frac{number\ of\ emitted\ photons\ into\ free\ space\ per\ second}{number\ of\ emitted\ photons\ from\ active\ region\ per\ second} = \frac{P_{air}/(h\nu)}{P_{int}/(h\nu)} \quad (3.5.2)$$

where P_{air} is the emitted optical power into the free space.

In a real LED, not all the emitted power from the active region escapes to free space. For instance, the emitted light by the active region may be incident on a metallic contact surface (e.g. electrode) and be absorbed by the metal or by the LED substrate as well. Moreover, the total internal reflection phenomenon, also referred to as the trapped-light phenomenon, reduces the ability of the light to escape from the device. Thus, the extraction efficiency can be a severe limitation for high-performance LEDs.

The power efficiency (η_{PE}), also termed wall-plug efficiency or radiant efficiency, is defined as:

$$\eta_{PE} = \frac{P_{air}}{IV} \quad (3.5.3)$$

where IV is the electrical power provided to the device.

The power efficiency gives the ratio of the radiant flux (i.e the total radiometric optical output power of the device, measured in watt) and the electrical input power, i.e. the efficiency of converting electrical to optical power.

The external quantum efficiency (η_{EQE}) is also defined as:

$$\eta_{EQE} = \frac{\text{number of emitted photons into free space per second}}{\text{number of injected electrons into LED per second}} = \frac{P_{air}/(h\nu)}{I/e} = \eta_{IQE}\eta_{extraction} \quad (3.5.4)$$

or also

$$\eta_{EQE} = \eta_{PE}\frac{e \cdot V}{(h\nu)} \quad (3.5.5)$$

where V is the applied voltage over the device.

The external quantum efficiency is therefore the ratio of the number of photons emitted from the LED to the number of electrons passing through the device. In few words, it indicates how efficiently the device converts electrons into photons and allows them to escape. Additionally, in order to make a fair comparison between different LEDs in terms of their η_{EQE}, the equation (3.5.5) must be divided by the number of luminescent centers in the active region of each LED. Otherwise, we would be neglecting the fact that the higher concentration of luminescent centers, the higher the η_{EQE} value. Nevertheless, it has to be mentioned that a concentration of luminescent centers higher than 10^{21} atoms/cm^3 induces RE ion clustering, which negatively affects the fraction of excitable RE ions and thus decreases the external quantum efficiency [102].

3.6 Calculation of the fraction of excited luminescence centers

The knowledge of the fraction of excited luminescence centers is of paramount importance since it is a necessary step for developing an efficient LED. Therefore, we will devote this section to describe the procedure for estimating the fraction of excited luminescence centers in RE ions and Si-based light emitting devices with planar surface.

Let us call f the fraction of excited luminescence centers, which is defined as:

$$f = \frac{N^*_{LC}}{N_{LC}} \quad (3.6.1)$$

$$\text{or also } N^*_{LC} = fN_{LC} \quad (3.6.2)$$

where N^*_{LC} and N_{LC} are the number of excited luminescence centers and number of total ones, respectively.

For the case of RE ion-implanted devices, we approximate the Gaussian distribution profile by a rectangular one, which is given by:

$$N_{LC} d_{LC} = D \quad (3.6.3)$$

d_{LC} being the thickness of the LC-implanted region taken at full-width at half-maximum (FWHM) and D is the dose of RE ion-implanted, respectively.

Therefore, the flux density of photons produced into the active region is:

$$\phi_{int} = \frac{N^*_{LC}}{\tau_{rad}} d_{LC} \quad (3.6.4)$$

where τ_{rad} is the radiative lifetime of the luminescence species.

Also, from equation (3.6.2) and (3.6.3), the equation (3.6.4) can be rewritten as follows:

$$\phi_{int} = \frac{fN_{LC}}{\tau_{rad}} d_{LC} = \frac{fD}{\tau_{rad}} \quad (3.6.5)$$

Consequently, the internal quantum efficiency (η_{IQE}) is expressed as:

$$\eta_{IQE} = \frac{\phi_{int}}{\phi_e} \quad (3.6.6)$$

$$\phi_e = \frac{J}{e} \quad (3.6.7)$$

where ϕ_e is the flux density of injected electrons.

Hence, from equation (3.6.5) and (3.6.7), the equation (3.6.6) for η_{IQE} can be rewritten in terms of the fraction of excited luminescence centers as follows:

$$\eta_{IQE} = \frac{efD}{J\tau_{rad}} \Leftrightarrow f = \frac{J\tau_{rad}\eta_{IQE}}{eD} \tag{3.6.8}$$

However, equation (3.6.8) takes into account neither the outcoupling efficiency nor the collection efficiency. Therefore, we now proceed to calculate separately both magnitudes.

Let us call η_{outc_eff} the outcoupling efficiency, which is the fraction of light, with respect to the total emitted light from the active region, able to escape from the device to free space. We therefore consider for the outcoupling calculation the total internal reflection phenomenon and the Fresnel reflection.

Let us assume that the angle of incidence in the device at the device-air interface is given by $\theta_{1critic}$. Then, the angle of incidence of the refracted ray, ψ, can be inferred from the Snell's law as follows:

$$n_d sin(\theta_{1critic}) = n_{air} sin(\psi) \tag{3.6.9}$$

where n_d and n_{air} are the refractive indices of the active region of device and air, respectively. It has to be mentioned that the Snell's law has to be applied as many times as the refractive index of each layer changes. This is not however the current case, where both ITO and SiN_x refractive indices are very akin. The critical angle for the total internal reflection is obtained using ψ=90°, as illustrated in Figure 9. Then, using the Snell's law, one obtains:

$$\theta_{1critic} = arcsin\left(\frac{n_{air}}{n_d}\right) \tag{3.6.10}$$

Therefore, the critical angle defines the light escape cone. Light emitted into the cone can escape from the device; whereas light emitted outside the cone is subject to total internal reflection (see Figure 9).

On the other hand, the Fresnel reflection at the active region-air interface has to be calculated. At normal incidence, the Fresnel power transmittance is given by:

$$T = 1 - R = 1 - \left(\frac{n_d - n_{air}}{n_d + n_{air}}\right)^2 = \frac{4n_d n_{air}}{\left(n_d + n_{air}\right)^2} \tag{3.6.11}$$

Thus, the outcoupling efficiency is given by:

$$\eta_{outc_eff} = \frac{2\int_0^{\theta_{1critic}} T(\theta)2\pi r^2 sin(\theta)d\theta}{4\pi r^2} \tag{3.6.12}$$

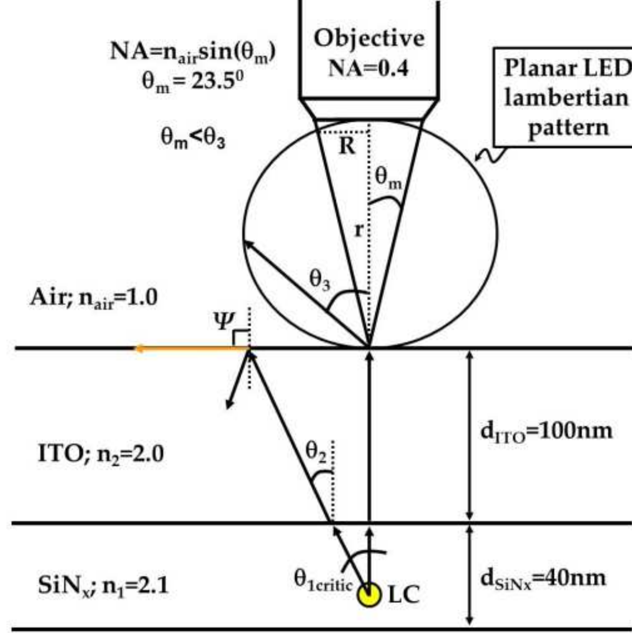

Figure 9. Schema of the light escape cone of a planar surface-LED based on RE-implanted SiN_x

In addition, at normal incidence, equation (3.6.12) can be rewritten as follows:

$$\eta_{outc_eff} = \frac{4n_d n_{air}}{\left(n_d + n_{air}\right)^2}\left[1 - cos(\theta_{1critic})\right] \tag{3.6.13}$$

Now, let us calculate the collection efficiency (η_{col_eff}), which is related with the experimental setup. In particular, not all emitted light that escapes to free space is collected by the detector, but rather than, a fraction that depends on the solid angle subtended by the detector. Thus, the collection efficiency is defined by:

$$\eta_{col_eff} = \frac{P_{measured}}{P_{air}} \tag{3.6.14}$$

where P_{air} is the total emitted power, which can leave the device to free space and $P_{measured}$ is the optical power measured by the detector.

Therefore, the problem is reduced to calculate $P_{measured}$, which is given by:

$$P_{measured} = 2\pi\int_0^{\theta_m} P_0 cos(\theta)sin(\theta)d\theta = 2\pi P_0 \frac{1}{2}sin^2(\theta_m) \quad (3.6.15)$$

where θ_m is the angle related to the numerical aperture of the collection system. In few words, emitted photons to free space with an angle smaller or equal than θ_m can solely arrive to the detector (see Figure 9).

Now, applying the normalization conditions, we can obtain from equation (3.6.15) that:

$$P_{measured} = P_{air} sin^2(\theta_m) \quad (3.6.16)$$

Hence, from equations (3.6.14) and (3.6.16) we can deduce the collection efficiency as follows:

$$\eta_{col_eff} = \frac{P_{measured}}{P_{air}} = sin^2(\theta_m) \quad (3.6.17)$$

Therefore, to get the final fraction of excited luminescence centers (*f*), equation (3.6.8) has to be corrected for both outcoupling and collection efficiencies.

Let us proceed to demonstrate this latter fact. Indeed, by knowing the following expressions:

$$\phi_{air} = \eta_{outc_eff}\phi_{int} \quad (3.6.18)$$

$$\phi_{int} = \eta_{IQE}\phi_e \quad (3.6.19)$$

$$\phi_{measured} = \eta_{col_eff}\phi_{air} \quad (3.6.20)$$

we can rewrite the measured flux density of photons ($\phi_{measured}$) by combining equations (3.6.8), (3.6.18) and (3.6.19) as follows:

$$\phi_{measured} = \eta_{outc_eff}\eta_{col_eff}\frac{fD}{\tau_{rad}} \quad (3.6.21)$$

However, ($\phi_{measured}$) can also be rewritten as:

$$\phi_{measured} = \eta_{col_eff}\eta_{PE}\frac{e \cdot V}{h\nu}\frac{J}{e} \quad (3.6.22)$$

Hence, from matching equation (3.6.21) and (3.6.22), we finally get the fraction of excited luminescence centers (f):

$$f = \frac{1}{\eta_{outc_eff}} \frac{\tau_{rad} V \eta_{PE} J}{h\nu D} \quad (3.6.23)$$

3.7 Conclusions

The different processes that give rise to the electroluminescence and basic concepts on LED efficiency have been revised. Particularly, we have shown that the occurrence of a specific EL mechanism depends on the position of the ground or excited-state energy levels of the luminescent ion with respect to the matrix band edges. We also believe that the three analyzed EL mechanisms are sufficiently comprehensive to include all experimentally realizable systems. Finally, a detailed procedure to calculate the fraction of excited LCs in planar-surface LEDs has been proposed and described. This latter procedure can be also extended to commercial LEDs.

4 RESULTS & DISCUSSION

> An Experiment, like every other event which takes place, is a natural phenomenon; but in a Scientific Experiment the circumstances are so arranged that the relations between a particular set of phenomena may be studied to the best advantage.
>
> — James Clerk Maxwell —

This chapter is dedicated to summarize the most important results of the published papers about the development and characterization of different rare-earth- and Si nanostructure-based light emitting devices. The results have been grouped in two parts, attending to the spectral emission range of the studied LEDs. The first part is devoted to the near-infrared LEDs, whereas the second one focuses on the visible LEDs. The near-infrared LEDs made by magnetron co-sputtering technique have been fabricated at the *Centre de Recherche sur les Ions, les Matériaux et la Photonique* (CIMAP), Caen, France within the framework of the European Project LANCER (FP6-IST 033574). Whereas, the near-infrared LEDs made by ion implantation have been fabricated at the *Laboratoire d'électronique des technologies de L'information* (CEA-Leti), Grenoble, France within the framework of the European Project HELIOS (FP7-ICT 224312). Additionally, the multidieletric gate stack LEDs based on NO and ONO have been fabricated at *Instituto de Microelectrónica de Barcelona* (IMB-CNM, CSIC), Barcelona, Spain under the Spanish Project (ICTS-NGG-31). Finally, the terbium-implanted silicon-rich silicon nitride/oxide LEDs have been fabricated at *Helmholtz-Zentrum Dresden-Rossendorf* in Dresden, Germany under the research stay of the author thanks to the financial support from Grant No. EEBB-I-2012-04552 of the Spanish Ministry of Science and Innovation.

4.1 Near-infrared light emitting devices

The first issue addressed is the one related to light emitting devices in the near-infrared region, whose protagonist is erbium into different silicon-based dielectric matrices with and without embedded Si nanostructures. The electrical conduction mechanisms and electroluminescence excitation processes of erbium

ions as well as the role of Si nanostructures are presented on Papers I and II. Additionally, the electroluminescence efficiency of erbium ions in different host environments and its correlation with the device operation lifetime are tackled on Paper III. This paper also shed light on the excitation process of erbium ions and Si nanostructures in different silicon oxide and silicon nitride environments.

4.1.1 Paper I

Four metal-oxide-semiconductor (MOS) light emitting devices have been fabricated over *p*-type B-doped Si substrates by means of magnetron co-sputtering of three confocal cathodes (viz. SiO_2, Er_2O_3 and Si) under pure Ar plasma. Three different Si excesses, 7%, 18% and 22% on each sample have been introduced. Likewise, four erbium concentrations of around 1×10^{20} at.cm^{-3}, 4.7×10^{19} at.cm^{-3}, 5.2×10^{20} at.cm^{-3} and 8.4×10^{19} at.cm^{-3} have been also practiced accordingly. All layers were annealed at 900 ^{o}C during 1 h. The used top electrode was 60 nm sputtered indium tin oxide (ITO). The mean thickness of the fabricated layers was around 30 nm, which was measured by spectroscopic ellipsometry. Additionally, the erbium concentration was corroborated by time-of-flight secondary ion mass spectrometry (TOF-SIMS), whereas the silicon excess by means of X-ray photoelectron spectroscopy (XPS).

Both electrical and electroluminescence properties of the fabricated devices, as a function of silicon and erbium ions, has been investigated. The conduction mechanism in all devices is found to be field-assisted thermal ionization Poole-Frenkel from Si-nanoclusters to Si-nanoclusters, rather than Fowler-Nordheim tunneling. Moreover, a relevant contribution of the Si-nanoclusters to the electrical conduction in silicon oxide layers is observed. Particularly, the presence of Si-nanoclusters leads to an increase in the current intensity of four to five orders of magnitude with respect to the stoichiometric silicon oxide layer. Electroluminescence emission at 1.5 μm is clearly observed on the layers containing Si-nanoclusters co-doped with erbium ions, in contrast to the erbium-doped stoichiometric silicon oxide layer. Likewise, at lower voltages, no evidence of hot electron injection is detected. Therefore, these two latter facts allowed us to conclude that the 1.5 μm erbium electroluminescence in these layers is mostly produced by energy transfer from Si nanoparticles to erbium ions, rather than by impact ionization of either the Si-nanoclusters or erbium ions. A power efficiency above 10^{-3}% is found for the best device, which was the highest value reported at the time.

4.1.2 Paper II

This study constitutes a complementary work to the one reported on Paper I. The used electro-optical characterization procedure is very akin, but from the structural and compositional viewpoints, the studied layers here differ from the one analyzed on Paper I.

Different thin films of erbium-doped silicon-rich silicon oxide have been deposited over B-doped *p*-type Si substrates by magnetron co-sputtering of three confocal targets of Er_2O_3, SiO_2 and Si under pure argon plasma. Two different materials, (i) low Si excess (9.5%) and Er concentration (2.2×10^{20} at.cm^{-3}) and (ii) high Si excess (18%) and Er concentration (1.0×10^{21} at.cm^{-3}), have been prepared. Additionally, each material has been deposited for two different thicknesses, thus giving rise to four distinct active layers. Annealing at 900 ^{0}C (500 ^{0}C) under N_2 atmosphere during 30 min. of layers with low (high) Si excess and low (high) Er concentration was performed, accordingly. A gold rear contact and a semitransparent 100-nm thick ITO as top contact have been employed, respectively.

From electrical characterization by using current-voltage and capacitance-voltage has been found that defects in the silicon oxide play an important role in the electrical conduction and charge trapping process. In addition, the combination of both electrical techniques showed that the Si-nanoclusters are responsible for the high leakage currents. Different conduction mechanisms in separate low- and high-field have been identified. At low-field, hopping through Si-nanoclusters has been also evidenced by capacitance-voltage measurements as well as at high-field Poole-Frenkel conduction takes place. Interestingly, no evidence of Fowler-Nordheim tunneling has been detected. Both erbium energetic transitions in the visible and infrared ranges have been observed in all devices. The 1.5-µm erbium excitation is more likely to occur by energy transfer from Si-nanoclusters to close Er ions rather than direct impact excitation of erbium ions by hot electrons.

Therefore, although the active layers of the studied LEDs are different in terms of structure and composition in both Papers I and II, we conclude that: i) by magnetron co-sputtering, all layers contain a large density of defects that improve significantly the carrier conduction, and ii) both electrical conduction mechanism and Er excitation process have the same physical origin. These results suggest that the quality of the layers critically depends on the growth techniques.

In particular, for the case of the sputtering technique, the density of defects in the layers is expected to be much higher than, for instance, by low-pressure chemical-vapor deposition (LPCVD), where also both the conduction and the Er excitation mechanisms are different [61].

4.1.3 Paper III

By means of LPCVD, two silicon nitride and two silicon oxide (50-nm-thick) layers have been fabricated over B-doped *p*-type Si substrate. During deposition, silicon excesses of 20% and 12% have been introduced into one of the silicon nitride layers and one of the silicon oxide layers, respectively. Additionally, all layers have been implanted with erbium ions. However, silicon nitride samples have an erbium concentration of around 3.0×10^{20} at·cm^{-3}, whereas silicon oxide samples present a value of 2.0×10^{20} at·cm^{-3}. Post-annealing treatments at 1100 ^{0}C and 900 ^{0}C during 1 h on the silicon oxide and silicon nitride layers have been carried out, respectively. An *n*-type-doped 100-nm-thick semitransparent polysilicon gate electrode has been used. Likewise, an aluminum layer as rear contact has been employed. Both Si excess and Er concentration were confirmed by XPS and TOF-SIMS techniques, respectively.

From the electrical characterization at room temperature, a higher conductivity for layers with Si excess in comparison to stoichiometric ones has been observed, irrespective of the dielectric matrix. Thus, Si-nanoclusters can readily modulate the transport properties on both matrices. Additionally, silicon nitride layers, in contrast to silicon oxide ones, allow higher conductivity. Two well-defined electrical conduction mechanisms have been found depending on the matrix-type. Particularly, electrode-limited conduction (Fowler-Nordheim tunneling) and bulk-limited conduction (Poole-Frenkel) mechanisms for Er-doped silicon oxide and Er-doped silicon nitride layers have been identified, respectively. Interestingly, electrical conduction on the silicon rich-silicon oxide layers obtained by co-sputtering in both Papers I and II was governed by Poole-Frenkel mechanism, irrespective of the Si excess. However, the here studied silicon-rich silicon oxide layers made by LPCVD follow a Fowler-Nordheim-type conduction mechanism. Again, this fact suggests that the electrical conduction mechanism strongly depends on the used fabrication technique.

In all devices, both visible and near infrared erbium energy transitions have been observed. Visible spectra have been used to understand the nature of excitation mechanisms of erbium ions in the different studied matrices. Basically, Er-doped silicon nitride layers are excited by Poole-Frenkel impact ionization, while erbium electroluminescence in silicon oxide layers takes place by direct

impact excitation by means of hot electrons coming from Fowler Nordheim-type tunneling. No evidence of energy transfer process from Si-nanoclusters to erbium ions neither in Er-doped silicon nitride nor in Er-doped silicon oxide layers has been detected. It has been found that erbium ions are better excited by direct impact excitation process rather than by impact ionization, because erbium electroluminescence at 1.5 μm is higher in silicon oxides than in silicon nitrides, although the erbium concentration is slightly lower in silicon oxide samples. This result has been understood taking into account that silicon nitride matrix presents a higher defect density than silicon oxide, which gives rise to major trapping/detrapping events that strongly reduce the amount of hot electrons. At the end, trapping/detrapping on energetically shallow sites in the band gap controls the bulk-limited conduction in silicon nitride layers, and very few electrons are allowed to move freely in the conduction band. As a consequence, silicon oxide matrices are better than silicon nitride ones for generation of hot electrons. In addition, the existence of a tradeoff between power efficiency and device operation lifetimes has been found. Interestingly, the high power efficiency is paid by a short device operation lifetime for Er-doped silicon oxide devices and vice versa for Er-doped silicon nitride ones. Therefore, a suitable combination of these two materials might be a competitive alternative to overcome the existing device limitations.

4.2 Visible light emitting devices

A second argument under investigation in this thesis has been the development and characterization of light emitting capacitors and field-effect transistors in the visible region. For doing so, terbium ions and Si nanostructures, as luminescent centers, into oxide/nitride (ON, bilayer) or oxide/nitride/oxide (ONO, trilayer) gate stacks have been the cornerstone. The first study on the electrical, radiometric and photometric properties of light emitting field-effect transistors based on Si-rich ON and ONO structures and its potential for using in general lighting is reported in Paper IV. Whereas, Paper V discusses the advantage of using a Si-rich NO bilayer structure to achieve a switchable EL from one wavelength to another one depending on the sign of the applied DC voltage to gate. An in-depth study on the nature of the electro-optical properties as well as the correlation between electrical and electroluminescence mechanisms in Si-rich ONO light emitting capacitors is reported in Paper VI. A comparison between light emitting capacitors and field-effect transistors is also addressed. The electroluminescence properties of terbium-implanted silicon-rich silicon

nitride/oxide light emitting devices are reported for the first time in Paper VII. The advantage of using a silicon oxide layer to increase the kinetic energy of electrons and thus favor the terbium excitation by direct impact of hot electrons is presented. This paper also demonstrates the potentiality of this materials platform for the development of integrated light sources fully compatible with Si technology.

4.2.1 Paper IV

In a complete CMOS line, metal-oxide-semiconductor field-effect transistors (MOSFET) have been successfully fabricated. Luminescent layers based on bi- and tri-layers of silicon-rich silicon nitride and silicon-rich silicon oxide, simultaneously, have substituted the oxide layer. This fact makes possible that the present MOSFET devices become electroluminescent devices. For doing so, two gate stack structures have been particularly used. The first one is a bilayer of very thin tunneling silicon oxide (3 nm) and a silicon-rich silicon nitride active layer (26 nm). The second one is a tri-layer which includes an extra-thin silicon oxide layer (3 nm) on top of the previous structure. The purpose of the thin oxide layers is to provide a well-passivated interface with silicon, and to act as tunnel and control dielectrics for the current (hole and electron injection) in the central thick nitride layer. A silicon excess of 19% close to the lower oxide/nitride interface in both gate stacks has been introduced by ion implantation. Whereas, silicon oxide and silicon nitride layers have been fabricated by means of LPCVD.

On one hand, by electro-optical characterization the mechanism of current transport and EL of both bi- and tri-layer has been investigated. Two well-defined peaks (red and blue-green) in both gate stacks have been observed. The red one has been associated to bipolar injection by direct tunneling into Si nanostructures within the silicon-rich silicon layer; whereas Poole-Frenkel ionization has been found to be responsible for blue-green emission coming from Si-related defects in the silicon nitride layer. As a consequence, the combination of these two emission bands appears warm white to the eye.

On the other hand, by means of a photometric study the potentiality of silicon nitride-based light sources for large-area lighting devices has been reported. Under AC excitation conditions with a duty cycle signal of 35%, for the bilayer it has been found that the obtained spectral content is excellent in terms of light quality for its use in general lighting. A color rendering index of 93, correlated color temperature of 4800 K and luminous efficacy of radiation of 112 lm/W have

been obtained. Therefore, based on this finding, this technology has demonstrated that could be competitive with other energy-efficient solid-state lighting options, once the barrier of the 10% in quantum efficiency of extracted light from silicon-based materials can be reached.

4.2.2 Paper V

The studied devices here have followed the same fabrication procedure than one previously described on Paper IV. Specifically, the parameters and routine used to fabricate the silicon-rich silicon nitride/silicon-rich silicon oxide bilayer structures.

The paper reports on two-wavelength switching metal-nitride-oxide-semiconductor light emitting devices based on a silicon-rich silicon oxide/silicon-rich silicon nitride bilayer structure. The bilayer has been *ad hoc* conceived to combine light emission from each Si-rich matrix. By changing the DC voltage sign applied to the gate electrode, the line-shape is completely varied; thus, a switchable EL from a blue-green spectrum at positive DC voltage to a near-infrared spectrum at negative DC voltage has been demonstrated. Under accumulation regime (negative DC voltage applied to the gate), two broad bands peaking at around 525 nm and 800 nm have been simultaneously detected. On the contrary, under inversion regime (positive DC voltage applied to the gate) only one emission peak centered at around 515 nm has been observed. By time-resolved electroluminescence measurements, two lifetimes (135 ns and 3.66 μs) have been measured in accumulation regime. They have been ascribed to Si nitride-related defects (emission at around 525 nm) and excitonic recombination inside the Si-nanoclusters (emission at 800 nm), respectively. However, under inversion regime, solely the fastest lifetime has been detected. These results state that this structure allows the activation of two kinds of luminescent species, due to the injection and transport properties of the whole bilayer.

4.2.3 Paper VI

Different light emitting capacitors with oxide-nitride-oxide (ONO) multidielectric gate stack have been successfully fabricated. The dielectric layers have been deposited by plasma-enhanced chemical vapor deposition (PECVD) over *p*-type B-doped Si substrates. A Si excess of 19% has been introduced by ion implantation followed by a post-annealing at 1000 ^{0}C for 1 h. The peak of Si ion-implanted profile has been centered near the lower oxide/nitride interface. To gain more insight into the physics of electrical and EL properties, light emitting

capacitors in lieu of metal-oxide-semiconductor field-effect transistors have been fabricated and studied here. This is because light emitting capacitors are much simpler devices than transistors from both technological and electro-optical viewpoints.

Both charge transport and EL properties of Si-rich ONO-based light emitting capacitors have been correlated from their temperature dependence. At low voltages, the electrical conduction via variable range hopping mechanism has been observed. On the contrary, at moderate and high voltages, a hybrid conduction simultaneously based on variable range hopping with space charge-limited currents (SCLC) enhanced by Poole-Frenkel (PF) effect have been unambiguously identified. Additionally, at low voltages it has been found that electrical conduction takes place at the Fermi level located at 0.42 eV within the band gap, and the density of states is about 1.18×10^{18} $cm^{-3} \cdot eV^{-1}$. Likewise, at moderate and high voltages, from the SCLC enhanced by PF effect conduction model, a density of traps of 10^{22} cm^{-3} has been estimated.

Two EL peaks have been exhibited, one centered at 1.5 eV and a broader one spanning from 2.0 to 3.0 eV with the maximum at 2.2 eV. The combination of these two EL bands gives rise to a quasi-white light emission extending over the near-infrared region. No remarkable changes on the line-shape of EL spectra with temperature have been observed. However, it has been detected that EL intensity for both peaks drops as the temperature increases, suggesting an increase of non-radiative recombination processes. In addition, two EL decay lifetimes (290 ns and 8.33 μs) have been extracted from time-resolved EL measurements at room temperature. As expected, these lifetime values are in accordance with those reported in Papers IV and V, respectively. Therefore, the luminescence origin of each peak has been related to the previous results accordingly. A univocal correlation between the injected carriers and the excited ones has been inferred since a linear relationship in a log-log plot between the integrated EL and the driving current, in addition to the absence of EL spectral changes, has been observed.

The most distinctive difference observed between Si-rich ONO-based light emitting capacitors presented here and light emitting transistor structures previously studied on Papers IV and V lies on the electrical properties due to the presence of the drain and source currents in the light emitting transistors. As a result, the integrated EL intensity is higher in the transistors than in the capacitors

although the two EL bands have been equally exhibited on both devices in accumulation regime. Nevertheless, the advantage of using MNOS capacitors instead of MNOS transistors rests on its simple structure and simple fabrication process, as well as its simplicity of analysis from the electrical and EL properties viewpoint.

4.2.4 Paper VII

Terbium-implanted silicon-rich silicon nitride/oxide light emitting devices have been designed and fabricated under fully compatible CMOS line. 30 nm-thick silicon oxide and 40 nm-thick silicon-rich silicon nitride layers have been deposited on highly doped *n*-type Si (100) substrates with resistivity of 1-5 mΩ·cm using the PECVD technique. To improve the device conductivity and operation lifetime a 12% of silicon excess has been introduced. Likewise, the introduction of the SiO_2 layer was *ad hoc* conceived for boosting the Tb^{3+} electroluminescence by hot electrons. Indeed, this SiO_2 layer introduces a potential energy step of ~1.3 eV at the interface between the SiO_2 and the Si_3N_4 due to the difference in electron affinities (viz. for SiO_2, it is equal to 0.8 eV, and for Si_3N_4, it is equal to 2.1 eV) which offers the possibility of hot electrons injection into the Tb^{3+}:SiN_x active layer. Additionally, a terbium ion concentration of nearly 1.5% in the depth range of 20-25 nm has been implanted into the silicon-rich silicon nitride layer. The used gate electrode here has been a 100-nm transparent ITO layer (*n*-type) deposited by radio frequency sputtering.

The electrical conduction mechanism has been modulated by introducing the SiO_2 layer, which has facilitated the hot electron generation by tunnel injection at high field in lieu of Poole-Frenkel conduction. A strong 543-nm electroluminescence has been demonstrated thanks to the excitation of the Tb^{3+} luminescent centers by direct impact by means of hot electrons. High optical power density of 0.5 mW/cm^2 and external quantum efficiency of 0.1% have been reported. These values constitute the ones highest ever reported for terbium-implanted silicon-rich silicon nitride light emitting devices. In addition, a terbium-excitation cross section of 8.2×10^{-14} cm^2 in silicon-rich silicon nitride has been calculated. This value is one order of magnitude larger than one reported for Tb^{3+}:SiO_2 light emitting devices [68], which means that terbium ions into silicon nitride host have higher excitation probability than in silicon oxide host. Moreover, a fraction of excited terbium ions of around 7% has been estimated.

The suitability of this materials platform for the realization of integrated Si-based light emitters fully compatible with CMOS technology has been demonstrated.

5 CONCLUSIONS AND FUTURE WORK

As the fruit ripens, so does man mature; after many rains, suns and blows.

— José de la Luz y Caballero —

In this thesis, the electrical and EL properties of rare earth- and Si nanostructure-based light emitting devices have been investigated. In particular, two regions of the electromagnetic spectrum have been covered with the studied LEDs: near-infrared and visible ranges. The realization of the different electroluminescent devices has been successfully achieved by using various CMOS-compatible fabrication techniques such as co-magnetron sputtering, PECVD, LPCVD and ion implantation. In addition, the structure and composition of the studied LED materials have been determined by means of TOF-SIMS, SIMS, XPS, EFTEM, FIB and ellipsometry. Electrical characteristics have been studied by current-voltage at room and high temperature and capacitance-voltage measurements. Additionally, EL properties have been investigated under both quasi-static and dynamic regimes. The fraction of inverted RE ions, device operation lifetimes and LED efficiencies have been also investigated.

For the case of near-infrared light emitting devices at 1.54 μm, we conclude that:

- The most suitable fabrication technique for obtaining the best Si-based host for erbium ions has been identified to be low-pressure chemical-vapor deposition.
- Magnetron co-sputtering technique gives rise to matrices with a huge amount of defects, which induce high leakage currents at the expense of non-radiative channels.
- A strong dependence between the used fabrication technique and electrical conduction mechanisms is found.
- Er-doped SiO_x layers with silicon excess higher than 20% and Er-doped Si_3N_4 layers (highly defective matrices) follow a Poole-Frenkel conduction mechanism, irrespective of the fabrication technique. Whereas, Fowler-

Nordheim tunneling has been proved to be dominant on Er-doped SiO_2 and Er-doped SiO_x with low silicon excess (around 12%).

- Er-doped SiO_2 layers have demonstrated to be the most efficient LED material for the 1.54 μm EL emission with respect to its Er-doped Si_3N_4 counterpart. The high power efficiency that offers Er-doped SiO_2 layers is paid by the short device operation lifetime and vice versa for the case of Er-doped Si_3N_4 layers.
- Direct impact excitation by hot electrons has resulted to be the most efficient EL excitation mechanism in the studied Er-doped LED materials. A power efficiency value at 1.54 μm as high as 0.01% has been obtained.

On the other hand, regarding to the visible light emitting devices, we extract the following conclusions:

- The combination of PECVD and ion implantation techniques gives rise to the best thin-film electroluminescent material in the visible range.
- The main electrical conduction in the NO and ONO gate stacks is mostly a bulk-limited mechanism, irrespective of the fabrication technique. However, for SiO_2 thickness higher than 10 nm in the multidielectic gate stack the conduction changes from a bulk-limited mechanism to electrode-limited one at high voltages.
- Terbium-based silicon-rich silicon nitride/oxide LEDs show higher optical power density, EL efficiency and electrical stability than the non-implanted Tb silicon-rich silicon nitride/oxide LEDs. A 12 % of silicon excess and 1.5% of atomic terbium concentration within the silicon-rich nitride layer render the optimum electro-optical properties.
- The main excitation mechanism of terbium-implanted silicon-rich silicon nitride/oxide LEDs is direct impact by hot electrons. Whereas, PF ionization is the main excitation mechanism of silicon-rich silicon nitride LEDs forming a gate stack as NO and ONO.
- Similar electro-optical properties are obtained by using MNOS capacitors instead of MNOS field-effect transistors. However, MNOS capacitors are more advantageous than MNOS transistors since they present easier structure and fabrication process, as well as simplicity of analysis from the electrical and EL properties viewpoint.
- The optimum gate stack for boosting the EL efficiency is obtained by using a combination of a 30-nm-thick of SiO_2 and a 40-nm-thick of SiN_x layers.

The investigations carried out during this thesis work have allowed to understand and explain the following issues:

- ✓ The influence on the device characteristics of the different fabrication techniques and procedures of Si technology applied to the development of RE- and Si nanostructure-based light emitting devices.
- ✓ The influence of the Si nanostructures and RE ions on the electrical and EL properties of the fabricated LEDs.
- ✓ The correlation between electrical and EL mechanisms of Si-nc and RE-implanted SiO_2 and Si_3N_4 LEDs.
- ✓ The effect on the electrical and EL properties of combining silicon oxide and silicon nitride layers in the form of NO or ONO.
- ✓ The advantage of using capacitor-like devices over field-effect transistors.
- ✓ How through a suitable gate stack design, using SiO_2 and Si_3N_4 layers in form of bilayer (NO), the EL intensity is boosted.

However, there still exist open issues that should be properly clarified in the future by more detailed investigations on the rare earth- and Si nanostructure-based light emitting devices:

- o How could the device operation lifetime be increased up to thousands of hours?
- o How could the non-radiative processes be mitigated?
- o How could both the power and the external quantum efficiencies be enhanced?
- o Is it possible to achieve a lasing action?
- o Will be there any physical limit, from the material viewpoint, which inhibits a significant increase of efficiencies and also the fraction of excited luminescence centers?

6 **RESUMEN EN CASTELLANO**

Hoy día, una fuente de luz basada en Si es el componente primordial requerido para conseguir una completa integración de la fotónica del silicio. No obstante, las limitaciones físicas del silicio masivo como emisor de luz y el conocimiento limitado sobre el entorno más adecuado para excitar de manera eficiente iones de tierras raras, impide la evolución de las actividades de investigación en esta área. Entre los diversos materiales dieléctricos, el óxido de silicio rico en silicio y el nitruro de silicio rico en silicio han sido los más investigados hasta la fecha. Estos materiales tienen muchas ventajas sobre otros sistemas de materiales dieléctricos. Las mismas incluyen una alta compatibilidad con la tecnología existente de Si, un entorno favorable para la segregación de las nanoestructuras de silicio después de un recocido a una temperatura relativamente baja, un alto contraste en términos del índice de refracción que es adecuado para el fuerte confinamiento de fotones (por ejemplo, permite la fabricación de cavidades ópticas de alta calidad) y son excelentes matrices para la excitación óptica y eléctrica de iones de tierras raras y las nanoestructuras de Si. Por lo tanto, esta tesis presenta un trabajo experimental en el desarrollo de iones de tierras raras y nanoestructuras de Si como plataforma de materiales para dispositivos de emisión de luz en el rango visible e infrarrojo cercano. Se han fabricado diferentes dispositivos electroluminiscentes basados en capas simples, dobles o triples de óxido de silicio y/o nitruro de silicio dopados o no con tierras raras. Para ello se han empleado varias técnicas de fabricación compatibles con la tecnología CMOS; a saber, depósito de vapor químico asistido por plasma (PECVD), pulverización catódica mediante magnetrón, depósito de vapor químico a baja presión (LPCVD) e implantación de iones. Así mismo, las propiedades estructurales y de composición de las capas fabricadas han sido determinadas mediante el uso de técnicas de caracterización tales como TOF-SIMS, SIMS, XPS, EFTEM, FIB y elipsometría. Además, a temperatura ambiente y altas temperaturas (25 ^{0}C – 300 ^{0}C) se han estudiado las propiedades electro-ópticas en los regímenes cuasi-estático y dinámico. Por lo general, las técnicas electro-ópticas empleadas fueron corriente-voltaje, capacitancia-voltaje, estudio de carga hasta la ruptura, electroluminiscencia (EL)-corriente, EL-voltaje y EL resuelta en tiempo.

Por un lado, en lo que se refiere a los dispositivos emisores de luz infrarrojos a 1.54 μm, la presencia de nanoestructuras de Si conduce a un aumento en la corriente de cuatro o cinco órdenes de magnitud en las capas de óxido de silicio

ricas en silicio dopadas con Er y fabricadas por pulverización catódica mediante magnetrón. Además, el mecanismo de conducción eléctrica predominante es Poole-Frenkel. Por otra parte, en estas capas activas el mecanismo electroluminiscente principal está asociado a la transferencia de energía entre los iones Er y las nanoestructuras de Si. Por el contrario, en las capas de SiO_2 y SiO_x dopadas con Er y fabricadas por LPCVD, el mecanismo de conducción es tipo túnel Fowler-Nordheim. En tanto, para las capas de Si_3N_4 y SiN_x dopadas con erbio y fabricadas también por LPCVD el mecanismo de conducción es Poole-Frenkel. Además, se ha identificado que los dispositivos basados en SiO_2 dopados con Er tienen más alta eficiencia de EL a 1.54 μm que los basados en Si_3N_4 dopados con Er. No obstante, la alta eficiencia a 1.54 μm que ofrecen los dispositivos con capas activas de SiO_2 dopados con Er, es comprometida a costa del corto tiempo de vida de funcionamiento de los mismos, y viceversa para el caso de los dispositivos basados en capas de Si_3N_4 dopados con Er. El impacto directo mediante electrones calientes (a saber, definido como electrones que no están en equilibrio térmico con la red; típicamente a campos eléctricos elevados, los portadores pueden ganar suficiente energía cinética en la banda de conducción mayor que el nivel de Fermi) ha sido el mecanismo electroluminiscente de excitación más eficiente. Para el mejor dispositivo se ha obtenido un valor de eficiencia de 0.01% a 1.54 μm.

Por otro lado, con respecto a los dispositivos emisores de luz visible, tenemos que mediante la combinación de las técnicas LPCVD e implantación iónica se obtienen capas dobles y triples del tipo (NO) y (ONO) basadas en óxido de silicio y nitruro de silicio. A través de la implantación de Si se obtiene un perfil gaussiano centrado en la interfaz inferior entre las capas de nitruro de silicio y óxido de silicio (NO). El exceso de Si resultante en las capas es del 19%. La conducción eléctrica es fundamentalmente limitada por las capas dieléctricas y no por los electrodos. En particular, el mecanismo de conducción es una combinación de Poole-Frenkel y corriente limitada por carga espacial dependiendo del valor del voltaje aplicado. En particular, a moderados voltajes, tiene lugar el Poole-Frenkel, mientras que a altos voltajes predomina la corriente limitada por carga espacial. No obstante, mediciones eléctricas a altas temperaturas revelaron un mecanismo de conducción eléctrica más complejo en dichas capas multidieléctricas, el cual fue detectado de forma inequívoca en todo el rango de voltajes. Típicamente es un mecanismo híbrido de conducción formado por salto de rango variable (*variable range hopping*, en inglés) y corriente

limitada por carga espacial asistida por Poole-Frenkel. Además, se observan dos bandas de emisión bien definidas (roja y azul-verde) en ambas estructuras de capas, a saber, (NO) y (ONO). La emisión roja está relacionada con una recombinación electrón-hueco en las nanoestructuras de Si embebidas en SiO_2 y cuyo tiempo de decaimiento electroluminiscente es alrededor de 8 μs. En tanto, la banda azul-verde se atribuye a ionización Poole-Frenkel de las trampas asociadas a la implantación de Si en Si_3N_4. El tiempo de decaimiento de EL medido fue del orden de cientos de nanosegundos (alrededor de 290 ns). Adicionalmente, se ha obtenido, mediante un estudio fotométrico detallado y bajo ciertas condiciones de excitación alterna, un índice de reproducción cromática (CRI) de 93, una temperatura correlacionada de color (CCT) de 4800 K y una eficiencia luminosa de la radiación (LER) de 112 lm/W. Dicho resultado muestra el potencial de este tipo de fuentes de luz basadas en nitruro de silicio para dispositivos de iluminación de gran superficie. Además, bajo régimen de corriente continua se demostró en la estructura bicapa (NO), que cambiando el voltaje aplicado de positivo a negativo se consigue conmutar el espectro electroluminiscente de azul-verde a rojo-infrarrojo. También, se estableció la ventaja de utilizar arquitecturas tipo condensador en lugar de transistor de efecto de campo para propósitos de emisión electroluminiscente.

Por último, se fabricó un conjunto complementario de dispositivos formados por estructuras bicapa (NO) e implantados con iones de terbio. Una concentración atómica de terbio del 1.5% fue introducida por implantación iónica. El perfil de implantación fue centrado en el centro de la capa de nitruro de silicio. Dicha capa, además, fue enriquecida con un 12 % de exceso de silicio que fue introducido mediante LPCVD. Una capa de 30 nm de óxido de silicio es introducida intencionalmente, siendo esta más gruesa que las anteriores estudiadas (espesores entre 3-10 nm). Este hecho hace posible cambiar el mecanismo de conducción eléctrica de estar limitado por el volumen (típicamente asociado a las capas de nitruro de silicio) a ser limitado por el electrodo. En particular, a diferencia de los dispositivos anteriores no implantados con terbio, el mecanismo de conducción eléctrica a altos voltajes es el túnel asistido por trampas (*trap-assisted tunneling*, en inglés). Este diseño de bicapa (NO) tiene dos ventajas principales que hacen posible la excitación eficiente de los centros luminiscentes por impacto directo de electrones calientes. Estas son: i) la capa de SiO_2 introduce un escalón de energía potencial de 1.3 eV en la interfaz entre el SiO_2 y el Si_3N_4, el cual es debido a la diferencia en afinidades

electrónicas entre estos dos materiales y ii) se consigue un compromiso entre la eficiencia de EL y la estabilidad eléctrica. Además, este diseño garantiza que el proceso de excitación de los iones de terbio se lleve a cabo a través de la excitación por impacto directo, en lugar de por transferencia de energía de las nanoestructuras de Si a los iones de terbio. Por primera vez, se ha conseguido a 540 nm una densidad de potencia óptica y una eficiencia cuántica externa de 0.5 mW/cm^2 y 0.1%, respectivamente. Además, experimentalmente se ha obtenido una sección transversal de excitación eléctrica del terbio de 8.2×10^{-14} cm^2 en nitruro de silicio rico en silicio, así como una fracción de iones de terbio excitados de alrededor del 7%. Por tanto, este diseño ha demostrado ser adecuado para la excitación eficiente de los iones de terbio por impacto directo mediante electrones calientes. Por otra parte, este diseño podría extenderse para excitar otros elementos de tierras raras tales como iones de erbio, que requieren energías de excitación más bajas (a saber, 0.8 eV) que los iones de terbio. En resumen, se ha establecido la idoneidad de esta plataforma de materiales para la realización de emisores de luz integrados basados en Si y totalmente compatibles con la tecnología CMOS.

7 VITA

7.1 List of all publications

Journal Publications

1. “Electroluminescence efficiencies of erbium in silicon-based hosts” S. Cueff, J. M. Ramírez, J. A. Kurvits, Y. Berencén, R. Zia, B. Garrido, R. Rizk, and C. Labbé; *Applied Physics Letters* **103** (11), 191109 (2013).

2. “Charge transport and electroluminescence of silicon nanocrystals/SiO_2 superlattices” J. López-Vidrier, Y. Berencén, S. Hernández, O. Blázquez, S. Gutsch, J. Laube, D. Hiller, P. Löper, M. Schnabel, S. Janz, M. Zacharias, and B. Garrido; *Journal of Applied Physics* **114** (16), 163701 (2013).

3. “Intense green-yellow electroluminescence from Tb^{+}-implanted silicon-rich silicon nitride/oxide light emitting devices” Y. Berencén, R. Wutzler, L. Rebohle, D. Hiller, J. M. Ramírez, J. A. Rodríguez, W. Skorupa, and B. Garrido; *Applied Physics Letters* **103** (11), 111102 (2013).

4. “Carrier transport and electroluminescence efficiency of erbium-doped silicon nanocrystal superlattices” J. M. Ramírez, Y. Berencén, L. López-Conesa, J. M. Rebled, F. Peiró, and B. Garrido; *Applied Physics Letters* **103** (11) 081102 (2013).

5. “Structural and compositional properties of Er-doped silicon nanoclusters/oxides for multilayered photonic devices studied by STEM-EELS” A. Eljarrat, L. López-Conesa, J. M. Rebled, Y. Berencén, J. M. Ramírez, B. Garrido, C. Magén, S. Estradé, and F. Peiró; *Nanoscale* **5** (20), 9963 (2013).

6. “Er-doped light emitting slot waveguides monolithically integrated in a silicon photonic chip” J. M. Ramírez, F. Ferrarese Lupi, Y. Berencén, A. Anopchenko, J. P. Colonna, O. Jambois, J. M. Fedeli, L. Pavesi, N. Prtljaga, P. Rivallin, A. Tengattini, D. Navarro-Urrios, and B. Garrido; *Nanotechnology* **24** (11) 115202 (2013).

7. “Toward a 1.54 μm electrically driven erbium-doped silicon slot waveguide and optical amplifier” A. Tengattini, D. Gandolfi, N. Prtljaga, A. Anopchenko, J. M. Ramírez, F. Ferrarese Lupi, Y. Berencén, D. Navarro-Urrios, P. Rivallin, K. Surana, B. Garrido, J. M. Fedeli, and L. Pavesi; *Journal of Lightwave Technology* **31** (3) 391 (2013).

8. "Electrical pump & probe and injected carrier losses quantification in Er-doped Si slot waveguides” J. M. Ramírez, Y. Berencén, F. Ferrarese Lupi, D. Navarro-Urrios, A. Anopchenko, A. Tengattini, N. Prtljaga, L. Pavesi, P. Rivallin, J. M. Fedeli, and B. Garrido; *Optics Express* **20** (27) 28808 (2012).

9. “Bulk silica-based luminescent materials by sol-gel processing of non-conventional precursors” J. A. Rodríguez, C. Fernández-Sánchez, C. Domínguez, S. Hernández, and Y. Berencén; *Applied Physics Letters* **101** (10) 171908 (2012).

10. “Structural factors impacting carrier transport and electroluminescence from Si nanocluster-sensitized Er ions” S. Cueff, C. Labbé, O. Jambois, Y. Berencén, A. J. Kenyon, B. Garrido, and R. Rizk; *Optics Express* **20** (20) 22490 (2012).

11. “Correlation between charge transport and electroluminescence properties of Si-rich oxide/nitride/oxide-based light emitting capacitors” Y. Berencén, J. M. Ramírez, O. Jambois, C. Domínguez, J. A. Rodríguez, and B. Garrido; *Journal of Applied Physics* **112** (6) 033114 (2012).

12. "Erbium emission in MOS light emitting devices: from energy transfer to direct impact excitation” J. M. Ramíırez, F. Ferrarese Lupi, O. Jambois, Y. Berencén, D. Navarro-Urrios, A. Anopchenko, A. Marconi, N. Prtljaga, A. Tengattini, L. Pavesi, J.-P. Colonna, J.-M. Fedeli, and B. Garrido; *Nanotechnology* **23** (12) 125203 (2012).

13. “Bipolar pulsed excitation of erbium-doped nanosilicon light emitting diodes” A. Anopchenko, A. Tengattini, A. Marconi, N. Prtljaga, J. M. Ramírez, O. Jambois, Y. Berencén, D. Navarro-Urrios, B. Garrido, F. Milesi,

J.-P. Colonna, J.-M. Fedeli, and L. Pavesi; *Journal of Applied Physics* **111** (6) 063102 (2012).

14. "Effect of the annealing treatments on the electroluminescence efficiency of SiO_2 layers doped with Si and Er" O. Jambois, J. M. Ramírez, Y. Berencén, D. Navarro-Urrios, A. Anopchenko, A. Marconi, N. Prtljaga, A. Tengattini, P. Pellegrino, N. Daldosso, L. Pavesi, J.-P. Colonna, J.-M. Fedeli, and B. Garrido; *Journal of Physics D: Applied Physics* **45** (4) 045103 (2012).

15. "Polarization strategies to improve the emission of Si-based light sources emitting at 1.55μm" J. M. Ramírez, O. Jambois, Y. Berencén, D. Navarro-Urrios, A. Anopchenko, A. Marconi, N. Prtljaga, N. Daldosso, L. Pavesi, J.-P. Colonna, J. M. Fedeli, and B. Garrido; *Materials Science and Engineering B* **177** (10) 734 (2012).

16. "Blue-green to near-IR switching electroluminescence from Si-rich silicon oxide/nitride bilayer structures" Y. Berencén, O. Jambois, J. M. Ramírez, J. M. Rebled, S. Estradé, F. Peiró, C. Domínguez, J. A. Rodríguez, and B. Garrido; *Optics Letters* **36** (14), 2617 (2011).

17. "Metal-nitride-oxide-semiconductor light-emitting devices for general lighting" Y. Berencén, J. Carreras, O. Jambois, J. M. Ramírez, J. A. Rodríguez, C. Domínguez, C. E. Hunt, and B. Garrido; *Optics Express* **19** (10), A234 (2011).

18. "Copropagating pump and probe experiments on Si-nc in SiO_2 rib waveguides doped with Er: The optical role of non-emitting ions" D. Navarro-Urrios, F. Ferrarese Lupi, N. Prtljaga, A. Pitanti, O. Jambois, J. M. Ramírez, Y. Berencén, N. Daldosso, B. Garrido, and L. Pavesi; *Applied Physics Letters* **99** (23) 231114 (2011).

19. "Current transport and electroluminescence mechanisms in thin SiO2 films containing Si nanocluster-sensitized erbium ions" O. Jambois, Y. Berencén, K. Hijazi, M. Wojdak, A. J. Kenyon, F. Gourbilleau, R. Rizk, and B. Garrido; *Journal of Applied Physics* **106** (6), 063526 (2009).

Conference proceedings

20. "Charge trapping and physical parameters of Er-doped light-emitting field-effect transistors" J. M. Ramírez, Y. Berencén, and B. Garrido; *Physica Status Solidi (a)* **211** (2) 467 (2014).

21. "Electroluminescence from Si-based light emitting devices" B. Mundet, Y. Berencén, J. M. Ramírez, J. Montserrat, C. Domínguez, and B. Garrido; *Óptica pura y aplicada* **46** (4) 315 (2013).

22. "Electrically pumped Er-doped light emitting slot waveguides for on-chip optical routing at 1.54 μm" J. M. Ramírez, Y. Berencén, D. Navarro-Urrios, F. Ferrarese Lupi, A. Anopchenko, N. Prtljaga, P. Rivallin, A. Tengattini, J.-P. Colonna, J.-M. Fedeli, L. Pavesi, and B. Garrido; *Proc. SPIE, Integrated Photonics: Materials, Devices, and Applications II* **8767** 87670I (2013).

23. "Role of electron and hole transport processes in conductivity and light emission of silicon nanocrystals field-effect transistors" L. Cattoni, A. Tengattini, A. Anopchenko, J. M. Ramírez, F. Ferrarese Lupi, Y. Berencén, B. Garrido, J.-M. Fedeli, and L. Pavesi; *Proc. SPIE 8629, Silicon Photonics VIII*, **8629** 862914 (2013).

24. "Optimizing Er-doped Layer Stacks for Integrated Light Emitting Devices" J. M. Ramírez, Y. Berencén, L. López-Conesa, J. M. Rebled, A. Eljarrat, S. Estradé, F. Peiró, J.-M. Fedeli, and B. Garrido; *Electro-Chemical Society Transactions* **53** (4) 81 (2013).

25. "Er-doped Si-based electroluminescent capacitors: Role of different host matrices on the electrical and luminescence properties" Y. Berencén, J. M. Ramírez, and B. Garrido; *in Proceedings of the 2013 Spanish Conference on Electron Devices*, 245 (2013).

26. "Opto-Electrical Characterization of Erbium Doped Slot Waveguides" A. Tengattini, D. Gandolfi, A. Marconi, A. Anopchenko, N. Prtljaga, J. M. Ramírez, F. Ferrarese Lupi, Y. Berencén, D. Navarro-Urrios, B. Garrido, J.-

M. Fedeli, P. Rivallin, K. Surana, and L. Pavesi; *Proc. SPIE 8431, Silicon Photonics and Photonic Integrated Circuits III* 843118 (2012).

27. "1.54 μm Er-doped light emitting devices: Role of silicon content" A. Tengattini, A. Marconi, A. Anopchenko, N. Prtljaga, L. Pavesi, J.M. Ramírez, O. Jambois, Y. Berencén, D. Navarro- Urrios, B. Garrido, F. Milesi, J.-P. Colonna, and J.-M. Fedeli; *The 8th IEEE International Conference on Group IV Photonics* 77 (2011).

28. "Effect of the annealing treatments on the transport and electroluminescence properties of SiO_2 layers doped with Er and Si nanoclusters" O. Jambois, J. M. Ramírez, Y. Berencén, D. Navarro-Urrios, S. Hernández, A. Anopchenko, A. Marconi, N. Prtljaga, N. Daldosso, L. Pavesi, J.-P. Colonna, J.-M. Fedeli, and B. Garrido; *Material Research Society (MRS) proceeding* 1289 (2010).

29. "Study of the electroluminescence at 1.5 μm of SiO_x:Er layers made by reactive magnetron sputtering" O. Jambois, Y. Berencén, S. Y. Seo, A. J. Kenyon, M. Wojdak, K. Hijazi, L. Khomenkova, F. Gourbilleau, R. Rizk, and B. Garrido; *in Proceedings of the 2009 Spanish Conference on Electron Devices,* 69 (2009).

Book chapters

1. Authors (signature): José A. Rodríguez; Yonder Berencén
   Chapter Title: Sensores Ópticos
   Book Title: MÉTODOS DE PROCESAMIENTO AVANZADO E INTELIGENCIA ARTIFICIAL EN SISTEMAS SENSORES Y BIOSENSORES
   Publisher: Editorial Reverté, S.A.
   Number or authors: 2
   Pages, Initial: 87 final: 108 Year: 2009 Place of publication: (SPAIN) ISBN: ISBN 978-84-291-8
   Publication code: 255517

7.2 Participation in congresses

Invited speaker

1. **Title:** Si-nanostructures for efficient, tunable and modulable light emission devices
   Authors: B. Garrido, O. Jambois, J. Carreras, M. Perálvarez, and Y. Berencén.
   Conference: MRS 2008 Fall Meeting (Material Research Society) Boston, Massachusetts, USA - Symposium MM: Applications of Group IV Semiconductor Nanostructures
   Date: December 1-5, 2008.

2. **Title:** Si-nanocrystal MOSLEDs: from materials to transistors
   Authors: B. Garrido, M. Perálvarez, Y. Berencén, J. Carreras, and O. Jambois.
   Conference: 217th ECS Meeting (Electrochemical Society) Vancouver, Canada - Symposium E4: Nanoscale Luminescent Materials
   Date: April 25-30, 2010.

3. **Title:** Toward the realization of an efficient Si-based light source emitting at 1.55 μm.
   Authors: O. Jambois, J. M. Ramírez, Y. Berencén, D. Navarro-Urrios, A. Anopchenko, A. Marconi, N. Prtljaga, N. Daldosso, L. Pavesi, J.-M. Fedeli, and B. Garrido.
   Conference: CEN 2010 (2ª Conferencia Española de Nanofotónica) Segovia, Spain
   Date: June 15-18, 2010.

4. **Title:** Light emitting MOS capacitors and transistors with silicon nanocrystals
   Authors: B. Garrido, J. M. Ramírez, Y. Berencén, O. Jambois, and J. Carreras.
   Conference: MRS 2010 Fall Meeting (Materials Research Society) Boston, Massachusetts, USA - Symposium AA: Group IV Semiconductor Nanostructures and Applications
   Date: November 29 - December 3, 2010.

5. **Title:** Light emitting devices based on silicon-rich silicon nitride/oxide for general lighting
   Authors: Y. Berencén, J. Carreras, O. Jambois, J. M. Ramírez, J. A.

Rodríguez, C. Domínguez, C. E. Hunt, and B. Garrido.
Conference: E-MRS 2011 Fall Meeting (European-Materials Research Society) Warsaw University of Technology, Poland - Symposium B: Amorphous nanostructure materials
Date: September 19-23, 2011.

6. **Title:** Si nanostructures and devices for advanced Er-doped LEDs **Authors:** J. M. Ramírez, Y. Berencén, F. Ferrarese Lupi, D. Navarro-Urrios, A. Anopchenko, N. Prtljaga, A. Tengattini, L. Pavesi, J.-P. Colonna, J.-M. Fedeli, and B. Garrido.
Conference: E-MRS 2012 Fall Meeting (European-Materials Research Society) Warsaw University of Technology, Poland - Symposium E: Nanoscaled Si, Ge based materials: Fabrication, characterization, devices
Date: September 17-21, 2012.

7. **Title:** Optimizing Er-doped layer stacks for integrated light emitting devices
Authors: J. M. Ramírez, Y. Berencén, L. López-Conesa, J. M. Rebled, A. Eljarrat, S. Estradé, F. Peiró, J.-M. Fedeli, and B. Garrido.
Conference: 223rd ECS Meeting (Electrochemical Society) Toronto, Ontario, Canada - Symposium E3: Nanocrystal embedded dielectrics for electronic and photonic devices
Date: May 12-16, 2013.

Oral communication

1. **Title:** Current transport and electroluminescence mechanisms in thin SiO_2 films containing Si nanoclusters-sensitized Er ions
Authors: O. Jambois, Y. Berencén, K. Hijazi, M. Wojdak, A. J. Kenyon, F. Gourbilleau, R. Rizk, and B. Garrido.
Conference: IBEDM 2009 (Impurity Based Electroluminescent Devices and Materials Workshop) Tossa del Mar, Girona, Spain
Date: September 30- October 3, 2009.

2. **Title:** Electroluminescence and electrical properties of SiO_2 MOSFET co-implanted with Si and C ions
Authors: Y. Berencén, J. M. Ramírez, O. Jambois, D. Navarro-Urrios, J. Carreras, and B. Garrido.
Conference: IBEDM 2009 (Impurity Based Electroluminescent Devices and Materials Workshop) Tossa del Mar, Girona, Spain

Date: September 30 - October 3, 2009.

3. **Title:** Realization of efficient LED's emitting at 1.55 μm
   Authors: J. M. Ramírez, O. Jambois, D. Navarro-Urrios, S. Hernández, Y. Berencén, F. Ferrarese, A. Martínez, P. Pellegrino, and B. Garrido.
   Conference: IN2UB2010 (3ra Jornada del Institut de Nanociència y Nanotecnologia de la UB) Barcelona, Spain
   Date: April 10-11, 2010.

4. **Title:** Electrical excitation of erbium and energy transfer in efficient silicon nanocomposite LEDs
   Authors: A. Tengattini, A. Anopchenko, A. Marconi, N. Prtljaga, N. Daldosso, J. M. Ramírez, O. Jambois, Y. Berencén, D. Navarro-Urrios, B. Garrido, F. Milesi, J.-P. Colonna, J.-M. Fedeli, and L. Pavesi.
   Conference: 13th Italian National Conference of Photonic Technologies, Fotonica 2011 Geneva, Italy
   Date: May 9-11, 2011.

5. **Title:** Correlation between electrical and electroluminescence properties from temperature studies in silicon nitride MNOSLEDs
   Authors: Y. Berencén, O. Jambois, J. M. Ramírez, J. Carreras, J. A. Rodríguez, C. Domínguez, and B. Garrido.
   Conference: E-MRS 2011 Spring Meeting (European-Materials Research Society) Center Congress Nice, France - Symposium G: Semiconductor Nanostructures: towards optoelectronic and microelectronic device applications.
   Date: May 9-13, 2011.

6. **Title:** Perspectives of light emitting devices based on silicon-rich silicon nitride/oxide for lighting application
   Authors: Y. Berencén, J. Carreras, J. M. Ramírez, O. Jambois, J. A. Rodríguez, C. Domínguez, C. E. Hunt, and B. Garrido.
   Conference: IN2UB2011 (IV Jornada del Institut de Nanociència y Nanotecnologia de la UB) Barcelona, Spain
   Date: April 20-21, 2011.

7. **Title:** Electroluminescence study of $Er:SiO_x$ layers in AC regime

Authors: J. M. Ramírez, O. Jambois, Y. Berencén, D. Navarro-Urrios, A. Anopchenko, A. Marconi, N. Prtljaga, A. Tengattini, L. Pavesi, J.-P. Fedeli, J.-P. Colonna, J.-M. Fedeli, and B. Garrido.
Conference: E-MRS 2011 Fall Meeting (European-Materials Research Society) Warsaw University of Technology, Poland - Symposium J: Rare earth doped semiconductors and nanostructures for photonics
Date: September 19-23, 2011.

8. **Title:** Er^{3+}/silicon nanocrystals co-doped devices: from a light emitting diode to an injected slot waveguide
Authors: A. Tengattini, A. Anopchenko, N. Prtljaga, D. Gandolfi, J. M. Ramírez, F. Ferrarese Lupi, Y. Berencén, D. Navarro-Urrios, O. Jambois, B. Garrido, J.-M. Fedeli, and L. Pavesi.
Conference: EOSAM (European Optical Society - Annual Meeting) Aberdeen, Scotland
Date: September 25-28, 2012.

9. **Title:** Silicon nanocrystal-based light emitting devices
Authors: J. M. Ramírez, A. Tengattini, Y. Berencén, D. Navarro-Urrios, O. Jambois, A. Anopchenko, N. Prtljaga, L. Pavesi, and B. Garrido.
Conference: WODIM 2012 (17th Workshop on Dielectrics in Microelectronics) Dresden, Germany
Date: June 25-27, 2012.

10. **Title:** Electrically excited erbium in slot waveguides
Authors: A. Tengattini, D. Gandolfi, A. Anopchenko, N. Prtljaga, L. Pavesi, J. M. Ramírez, Y. Berencén, F. Ferrarese Lupi, D. Navarro-Urrios, B. Garrido, J.-M. Fedeli, P. Rivallin, and S. Kavitak.
Conference: Fotonica 2012 14º Convegno Nazionale delle Tecnologie Fotoniche, Florence, Italy
Date: May 15-17, 2012.

11. **Title:** Chemical and structural characterization of Si-based electroluminescent and photovoltaic devices through HAADF-EELS
Authors: A. Eljarrat, L. López-Conesa, J. M. Ramírez, Y. Berencén, S. Hernández, J. López-Vidrier, S. Estradé, C. Magén, B. Garrido, and F. Peiró.
Conference: Jounées d'EELS 2012, Aix les Bains, France
Date: May 14-15, 2012.

12. **Title:** Er-doped Si-based electroluminescent capacitors: Role of different host matrices on the electrical and luminescence properties

Authors: Y. Berencén, J. M. Ramírez, and B. Garrido.
Conference: CDE2013 (9th Spanish Conference on Electron Devices) Congress Palace, Valladolid, Spain
Date: February 12-14, 2013.

13. **Title:** Electrically pumped Er-doped light emitting slot waveguides for on-chip optical routing at 1.54 um
Authors: J. M. Ramírez, Y. Berencén, A. Anopchenko, N. Prtljaga, P. Rivallin, A. Tengattini, J.-P. Colonna, J.-M. Fedeli, L. Pavesi, and B. Garrido.
Conference: SPIE microtechnologies 2013 (International Society for Optics and Photonics) Grenoble, France - Session 6 Materials and Devices for Light Emission
Date: April 24-26, 2013.

14. **Title:** Polarization strategies for boosting electroluminescence, efficiency and operation lifetimes from Er-doped Si-based light emitting
Authors: Y. Berencén, L. Rebohle, R. Wutzler, D. Hiller, J. M. Ramírez, W. Skorupa, and B. Garrido.
Conference: E-MRS 2013 Spring Meeting (European-Materials Research Society) Center Congress - Strasbourg, France - Symposium J: Semiconductor Nanostructures towards Electronic and Optoelectronic Device Applications - IV
Date: May 28-30, 2013.

15. **Title:** Correlation between efficiency and stability in Er- and Si-implanted MOS light emitting devices
Authors: L. Rebohle, R. Wutzler, M. Helm, W. Skorupa, Y. Berencén, B. Garrido, and D. Hiller.
Conference: E-MRS 2013 Spring Meeting (European-Materials Research Society) Center Congress – Strasbourg, France - Symposium K: Physics and technology of advanced extra functionality CMOS-based devices
Date: May 28-30, 2013.

16. **Title:** Si-based electroluminescent and photovoltaic devices: EFTEM-HAADF-EELS characterization
Authors: L. López-Conesa, A. Eljarrat, J. M. Ramírez, Y. Berencén, J. López-Vidrier, S. Hernández, S. Estradé, C. Magén, B. Garrido, and F. Peiró.
Conference: 18th Microscopy of Semiconducting Materials (MSMXVIII) Oxford, United Kingdom
Date: April 7-11, 2013.

17. **Title:** Si-based Photonic and photovoltaic devices: a low-loss EELS analysis
    Authors: L. López-Conesa, A. Eljarrat, J. M. Ramírez, Y. Berencén, J. López-Vidrier, S. Hernández, S. Estradé, C. Magén, B. Garrido, and F. Peiró.
    Conference: Microscopy at the Frontiers of Science 2013 Tarragona, Spain
    Date: September 18-20, 2013.

18. **Title:** Electrical and electroluminescence properties of silicon nanocystals/SiO_2 superlattices
    Authors: J. López-Vidrier, Y. Berencén, B. Mundet, S. Hernández, S. Gutsch, D. Hiller, P. Löper, M. Schnabel, S. Janz, M. Zacharias, and Blas Garrido.
    Conference: SPIE Photonics Europe, Square Brussels Meeting Centre Brussels, Belgium - Session 12: Light Emission and Amplification II
    Date: April 14-17, 2014.

19. **Title:** On the photoluminescence of as-deposited Tb-doped silicon oxides and oxynitrides fabricated by ECR-PECVD
    Authors: J. M. Ramírez, J. Wojcik, Y. Berencén, P. Mascher, and B. Garrido.
    Conference: SPIE Photonics Europe, Square Brussels Meeting Centre Brussels, Belgium - Session 2: Light Emission and Amplification I
    Date: April 14-17, 2014.

20. **Title:** The electroluminescence of Er-implanted MOS structures with different silicon oxide and silicon nitride environments
    Authors: L. Rebohle, R. Wutzler, M. Braun, M. Helm, W. Skorupa, Y. Berencén, B. Garrido, and D. Hiller
    Conference: E-MRS 2014 Spring Meeting (European-Materials Research Society) Center Congress – Strasbourg, France - Symposium X: Materials research for group IV semiconductors: growth, characterization and technological developments
    Date: May 26-30, 2014.

Poster presentation

1. **Title:** Study of the electroluminescence at 1.5 μm of different SiOx:Er layers made by reactive magnetron sputtering
   Authors: O. Jambois, Y. Berencén, S. Y. Seo, A. J. Kenyon, M. Wojdak, K. Hijazi, L. Khomenkova, F. Gourbilleau, R. Rizk, and B. Garrido.
   Conference: CDE2009 (7th Spanish Conference on Electron Devices) Poster

Session - Materials, technology and process simulation. Modeling and devices simulation University of Santiago de Compostela, Santiago de Compostela, Galicia, Spain
Date: February 11-13, 2009.

2. **Title:** Toward the realization of an efficient Si-based light source emitting at 1.55 μm
   Authors: J.M. Ramírez, O. Jambois, Y. Berencén, D. Navarro-Urrios, S. Hernández, A. Anopchenko, A. Marconi, N. Prtljaga, N. Daldosso, L. Pavesi, J.-P. Colonna, J.-M. Fedeli, and B. Garrido.
   Conference: MRS 2010 Fall Meeting (Materials Research Society) Boston, Massachusetts, USA - Symposium H: Controlling Material Properties and Charge-Carrier Interactions with Quantum-Dot Coupling
   Date: November 29 - December 3, 2010.

3. **Title:** Metal-oxide semiconductor light emitting transistors for visible and infrared applications
   Authors: J. M. Ramírez, O. Jambois, Y. Berencén, L. López-Conesa, J. M. Rebled, S. Estradé, F. Peiró, D. Navarro-Urrios, A. Anopchenko, A. Marconi, N. Prtljaga, A. Tengattini, L. Pavesi, J.-P. Colonna, J.-M. Fedeli, and B. Garrido.
   Conference: IN2UB2011 (IV Jornada del Institut de Nanociència y Nanotecnologia de la UB) Barcelona, Spain
   Date: April 20-21, 2011.

4. **Title:** Erbium doped silicon-rich silicon oxide layers as competitive materials for Si-based light sources emitting at 1.55 μm
   Authors: J. M. Ramírez, O. Jambois, Y. Berencén, D. Navarro-Urrios, A. Anopchenko, A. Tengattini, A. Marconi, N. Prtljaga, L. Pavesi, J.-P. Colonna, J.-M. Fedeli, and B. Garrido.
   Conference: IN2UB2011 (IV Jornada del Institut de Nanociència y Nanotecnologia de la UB) Barcelona, Spain
   Date: April 20-21, 2011.

5. **Title:** Polarization strategies to improve the emission of a Si-based light source emitting at 1.55 μm
   Authors: J. M. Ramírez, O. Jambois, Y. Berencén, D. Navarro-Urrios, A. Anopchenko, A. Marconi, N. Prtljaga, N. Daldosso, L. Pavesi, J.-P. Colonna, J.-M. Fedeli, and B. Garrido.
   Conference: E-MRS 2011 Spring Meeting (European-Materials Research Society) Center Congress Nice, France - Symposium G: Semiconductor

Nanostructures: towards optoelectronic and microelectronic device applications.
Date: May 9-13, 2011.

6. **Title:** Site specific (EF)TEM characterization of Er^{3+} implanted silicon nanoelectro-optical devices
Authors: L. López-Conesa, J. M. Rebled, S. Estradé, Y. Berencén, F. Ferrarese Lupi, J. M. Ramírez, B. Garrido, J. M. Fedeli, and F. Peiró.
Conference: E-MRS 2012 Spring Meeting (European-Materials Research Society) Center Congress - Strasbourg, France - Symposium N: Control of light at the nanoscale: materials, techniques and applications
Date: May 14-18, 2012.

7. **Title:** Experimental evidences of energy transfer between Si nanoclusters and Er^{3+} ions under electrical pumping
Authors: J. M. Ramírez, F. Ferrarese Lupi, O. Jambois, Y. Berencén, D. Navarro-Urrios, A. Anopchenko, A. Marconi, N. Prtljaga, A. Tengattini, L. Pavesi, J.-P. Colonna, J.-M. Fedeli, and B. Garrido.
Conference: E-MRS 2012 Spring Meeting (European-Materials Research Society) Center Congress - Strasbourg, France - Symposium N: Control of light at the nanoscale: materials, techniques and applications
Date: May 14-18, 2012.

8. **Title:** Silicon-based light sources: En route to the first injected Silicon laser emitting at 1.54 μm
Authors: J. M. Ramírez, F. Ferrarese Lupi, Y. Berencén, D. Navarro-Urrios, O. Jambois, L. López-Conesa, S. Estradé, F. Peiró, B. Garrido, A. Tengattini, N. Prtljaga, A. Anopchenko, L. Pavesi, and J.-M. Fedeli.
Conference: ECIO (16th European Conference on Integrated Optics and Technical Exhibition) Sitges, Barcelona, Spain
Date: April 18-20, 2012.

9. **Title:** Site specific (EF)TEM for Si-based electrophotonic devices
Authors: L. López-Conesa, J. M. Rebled, J. M. Ramírez, Y. Berencén, S. Estradé, B. Garrido, and F. Peiró.
Conference: CDE2013 (9th Spanish Conference on Electron Devices) Congress Palace, Valladolid, Spain
Date: February 12-14, 2013.

10. **Title:** Optimization of integrated Er-doped light emitting devices for

enhanced optoelectronic properties at 1.54 μm
Authors: J. M. Ramírez, Y. Berencén, A. Anopchenko, A. Tengattini, N. Prtljaga, L. Pavesi, J.-M. Fedeli, and B. Garrido.
Conference: E-MRS 2013 Spring Meeting (European-Materials Research Society) Center Congress - Strasbourg, France - Symposium J: Semiconductor Nanostructures towards Electronic and Optoelectronic Device Applications - IV
Date: May 28-30, 2013.

11. **Title:** Electroluminescence from Si-based light emitting devices
Authors: B. Mundet, Y. Berencén, J. M. Ramírez, J. Montserrat, C. Domínguez, and B. Garrido.
Conference: OPTOEL 2013 (VIII Reunión Española de Optoelectrónica 2013) Revista Óptica Pura y Aplicada - Alcalá de Henares, Madrid, Spain
Date: July 10-12, 2013.

12. **Title:** Hot electron-based electroluminescence from silicon-rich silicon nitride/oxide multilayer light emitting devices
Authors: B. Mundet, Y. Berencén, J. M. Ramírez, J. Monserrat, C. Domínguez, and B. Garrido.
Conference: SPIE Photonics Europe, Square Brussels Meeting Centre Brussels, Belgium - Session PS3
Date: April 14-17, 2014.

7.3 Participation in research projects from public calls

1. Title of the project/contract: Micro-nanotecnologies i nanoscòpies per dispositius electrònics i fotònics (MIND)
Kind of contract/Program: Projectes de recerca per potenciar els grups de recerca consolidats
Financing Firm/administration: Agència de Gestió d'Ajuts Universitaris i de Recerca. Generalitat de Catalunya. AGAUR
Number of the project/contract: 2009SGR35 Amount: 49.920,00 € Duration, since: 2009 until: 2013
Main researcher: Albert Cornet Calveras
Number of researchers participating: 22
Keywords: Microscopía electrónica/Polímeros/Microsistemas/Fotónica/Nanotecnología
Code of the project/contract: 052740

2. Title of the project/contract: Acción integrada entre España e Italia. BOE 135 (04/06/2009).
   Kind of contract/Program: Integrated Actions
   Financing Firm/administration: Ministerio de Ciencia e Innovación
   Number of the project/contract: HI2008-0054 Amount: 11.720,00 € Duration, since: 2008 until: 2010
   Main researcher: Blas Garrido Fernández
   Number of researchers participating: 1
   Code of the project/contract: 059056

3. Title of the project contract: PHotonics ELectronics functional Integration on CMOS (HELIOS)
   Kind of contract/Program: COOPERATION. ICT. Seventh Framework Programme (FP7), Information and Communication Technologies.
   Financing Firm/administration: European Union
   Number of the project/contract: 224312 Amount: 222.094,00 € Duration, since: 2008 until: 2012
   Main researcher: Blas Garrido Fernández
   Number of researchers participating: 21
   Keywords: Silicon Photonics
   Code of the project/contract: 049540

4. Title of the project/contract: Interconexión óptica modulable a GHz y Láser a microdisco basados en tecnología CMOS
   Kind of contract/Program: Tecnologías Electrónicas (MIC) y de Comunicaciones (TEC)
   Financing Firm/administration: Ministerio de Ciencia e Innovación
   Number of the project/contract: TEC2009-08359 Amount: 204.200,00 € Duration, since: 2010 until: 2012
   Main researcher: Blas Garrido Fernández
   Number of researchers participating: 8
   Keywords: Nanocristales/Nanomateriales/Láser de silicio/Fotónica CMOS/Fotónica de silicio
   Code of the project/contract: 053920

5. Title of the project/contract: Capacidades metal-oxide-semiconductor (MOS) con nanocristales de silicio embebidos en multi-capas activas basadas en óxido y nitruro de silicio.
   Kind of contract/Program: Infraestructura Programa Nacional de Microelectrónica
   Financing Firm/administration: Centro Nacional de Microelectrónica (CNM-IMB), Barcelona
   Number of the project/contract: NGG-260 Amount: --- Duration, since: 2011 until: 2012
   Main researcher: Yonder Berencén
   Number of researchers participating: 4
   Keywords: Electroluminiscencia/Dispositivos LED/Iluminación/ Fotónica del silicio/Nanocristales de silicio
   Code of the project/contract: 074218

6. Title of the project/contract: Iluminación de estado sólido innovadora e inteligente e interconexiones ópticas a 1.5 micras con fotónica de silicio basada en tecnología CMOS
   Kind of contract/Program: Tecnologías Electrónicas (MIC) y de Comunicaciones (TEC)
   Financing Firm/administration: Ministerio de Economía y Competitividad
   Number of the project/contract: TEC2012-38540-C02-01 Amount: 200.800,00 € Duration, since: 2013 until: 2015
   Main researcher: Blas Garrido Fernández
   Number of researchers participating: 7
   Keywords: Iluminación/Estado sólido/Tierras raras/Nanocristales de silicio
   Code of the project/contract: 077762

7.4 Research stays abroad

Center: Institute of Ion Beam Physics and Materials Research, Helmholtz-Zentrum Dresden Rossendorf, POB 510119, 01314 Dresden, Germany **Place:** Dresden **Country:** Germany **Year:** 2012 **Duration:** 3 Months **Issue:** Electrical and electroluminescence characterization of novel rare-earth implanted MOS structures for optoelectronic and lighting applications **Key:** Pre-Doctoral stay

HZDR

To whom it may concern

Institute of Ion Beam Physics and Materials Research
Semiconductor Materials Division
Dr.-Ing. Wolfgang Skorupa
Division Head
Phone +49 351 260-3612
Fax +49 351 260-3411
w.skorupa@hzdr.de
Our Reference
02.05.2012

Laboratory stay of Yonder Berencén at HZDR, Germany

Dear Ladies and Gentlemen,

In the framework of the Spanish National Programme for Training Human Resources/Subprogram: Predoctoral Research Grants, Mr. Yonder Berencén has worked at the Semiconductor Materials Division of the Helmholtz Center Dresden-Rossendorf (HZDR), Germany, between February 5th and May 4th, 2012.

In the course of this collaboration a comprehensive set of light emitting devices was jointly planned by Y. Berencén and our division. After fabrication, the devices were intensively characterized by Y. Berencén. These investigations comprised electroluminescence (EL) measurements, current-voltage characteristics with a concurrent recording of the EL intensity, capacitance-voltage characteristics and constant current injection characteristics. He held a fine and informative presentation regarding the photonic research activities of his group at the University of Barcelona.

Y. Berencén performed these investigations and the corresponding analysis independently, accurately and in a professional way. He collaborated very well with our group and executed the tasks assigned to him in an excellent and diligent manner!

Due to his successful work and the promising results this stay will surely contribute to an extension of our collaboration with the University of Barcelona.

Dr. Lars Rebohle

Dr. Wolfgang Skorupa

Helmholtz-Zentrum Dresden-Rossendorf e.V.

Visitors' Address:
Bautzner Landstr. 400
D-01328 Dresden
http://www.hzdr.de

Board of Directors:
Prof. Dr. Dr. h. c. Roland Sauerbrey
Prof. Dr. Dr. h. c. Peter Joehnk

Company Registration Number:
VR 1693, Amtsgericht Dresden

Bank Details:
Commerzbank AG
Account No. 0402 657 300
(Bank Code 850 800 00)
BIC DRESDEFF850
IBAN DE42 8508 0000 0402 6573 00

VAT-ID-No.: DE140213784

7.5 European Materials Research Society (EMRS) Student Award 2013

Presenting Author: Yonder Berencén

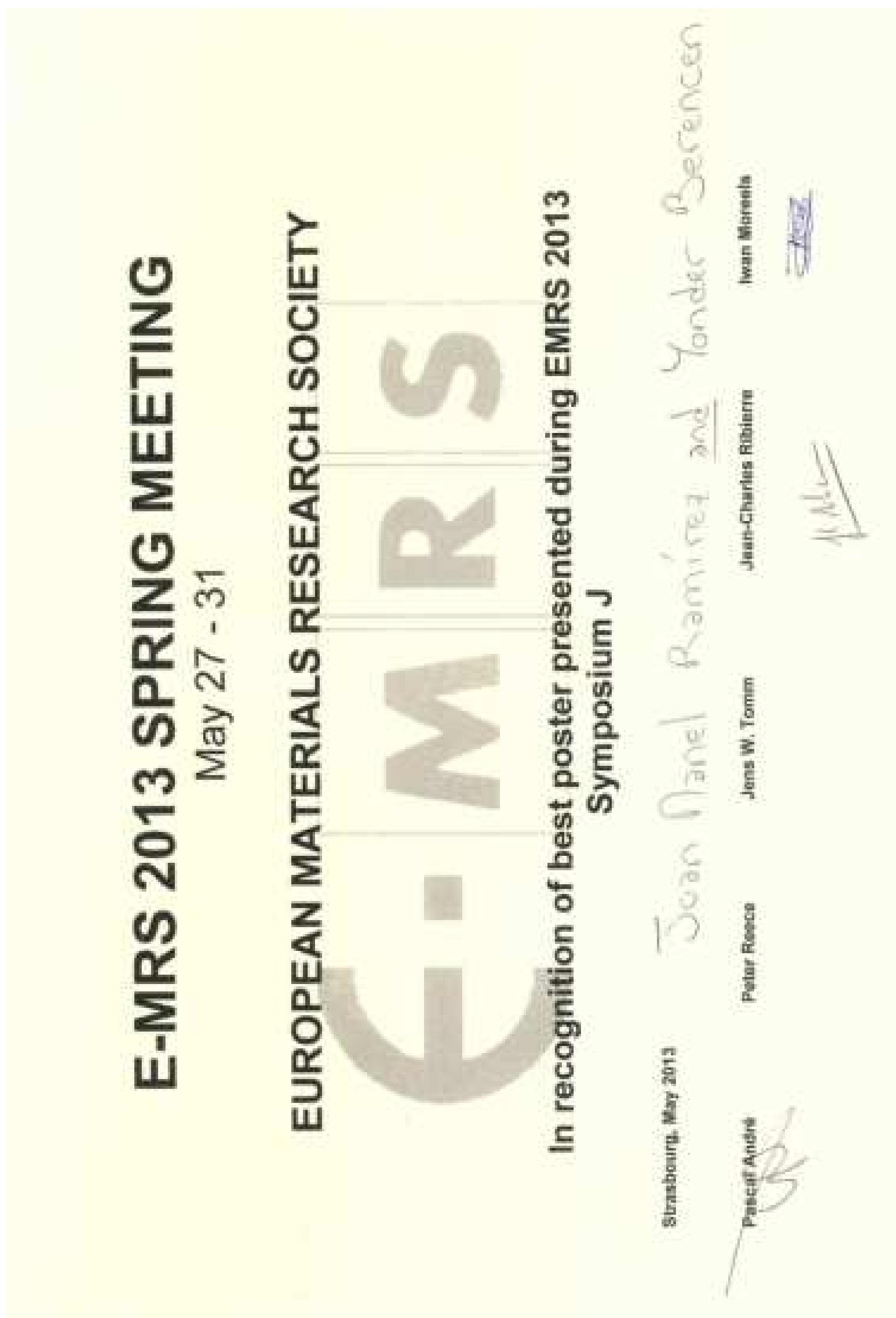

List of tables

Table 1. Power efficiency of different RE- and Si-based materials for light emitting devices ... 21
Table 2. Basic mechanisms of electrical conduction in insulators ... 34
Table 3. Statement of contribution in the presented articles ... 86

List of figures

Figure 1. Concept of chip-to-chip optical interconnection based on Si photonics technology [2]. ... 15
Figure 2. Trends in optical interconnection technology. Active optical cable (AOC), post office protocol version 4 (POP4), multi-source agreement (MSA) and quad small form-factor pluggable (QSFP) [2]. ... 16
Figure 3. Sketch of typical LEDs architecture based on MIS capacitor. ... 17
Figure 4. Schema of different conduction mechanisms and electrical processes in MIM structures. (a) direct tunneling, (b) Fowler-Nordheim tunneling, (c) trap-assisted tunneling, (d) Schottky emission, (e) Poole-Frenkel, (f) hooping of carriers from trap to trap, (g) carrier scattering in the conduction band, and (h) carrier trapping at impurities and/or imperfections ... 24
Figure 5. Potential barrier lowering due to Schottky effect ... 27
Figure 6. Potential barrier lowering at a trapping site due to Poole-Frenkel effect and hopping conduction mechanism ... 30
Figure 7. Schematic *J-V* plot, showing the current variation as a function of voltage and θ for an insulator with shallow traps confined in a trapping level E_t ... 33
Figure 8. Most usual mechanisms of excitation of luminescent centers in thin-film LED: (a) energy transfer, (b) impact excitation and (c) impact ionization .. 36
Figure 9. Schema of light escape cone of planar surface-LED based on RE-implanted SiN_x ... 41

List of references

[1] G. E. Moore, Electronics 38, 114 (1965).

[2] K. Yamada, Y. Urino, T. Nakamura, and Y. Arakawa, NTT Technical Review 11, 1 (2013).

[3] A. Liu, R. Jones, L. Liao, D. Samara-Rubio, D. Rubin, O. Cohen, R. Nicolaescu, and M. Paniccia, Nature 427, 615 (2004).

[4] V. R. Almeida, C. A. Barrios, R. R. Panepucci, and M. Lipson, Nature 431, 1081 (2004).

[5] Y. A. Vlasov, M. O'Boyle, H. F. Hamann, and S. J. McNab, Nature 438, 65 (2005).

[6] F. Xia, L. Sekaric, and Y. A. Vlasov, Nature Photonics 1, 65 (2007).

[7] G. T. Reed, G. Mashanovich, F. Y. Gardes, and D. J. Thomson, Nature Photonics 4, 518 (2010).

[8] L. Sirleto, M. A. Ferrara, T. Nikitin, S. Novikov, and L. Khriachtchev, Nature communications 3, 1220 (2012).

[9] J. Sun, E. Timurdogan, A. Yaacobi, E. S. Hosseini, and M. R. Watts, Nature 493, 195 (2013).

[10] J. P. Mailoa, A. J. Akey, C. B. Simmons, D. Hutchinson, J. Mathews, J. T. Sullivan, D. Recht, M. T. Winkler, J. S. Williams, J. M. Warrender, P. D. Persans, M. J. Aziz, and T. Buonassisi, Nature communications 5, 3011 (2014).

[11] S. S. Iyer and Y.-H. Xie, Science, 260, 40 (1993).

[12] L. T. Canham, Appl. Phys. Lett., 57, 1046 (1990).

[13] F. Iacona, G. Franzò, and C. Spinella, J. Appl. Phys. 87, 1295 (2000).

[14] G. G. Qin, A.P. Li, B.R. Zhang, B.-C. Li, J. Appl. Phys. 78, 2006 (1995).

[15] G. G. Qin, A.P. Li, Y.X. Zhang, Phys. Rev. B 54, R11122 (1996).

[16] P. F. Trwoga, A. J. Kenyon, and C. W. Pitt, J. Appl. Phys. 83, 3789 (1998).

[17] N. Lalic, and J. Linnros, J. Luminesc. 80, 263 (1999).

[18] G. Franzò, A. Irrera, E. C. Moreira, M. Miritello, F. Iacona, D. Sanfilippo, G. Di Stefano, P.G. Fallica, and F. Priolo, Appl. Phys. A 74, 1 (2002).

[19] R. J. Walters, G. I. Bourianoff, and H. A. Atwater, Nat. Mater., 4, 143 (2005).

[20] M. Kulakci, U. Serincan, and R. Turan, Semicond. Sci. Technol. 21, 1527 (2006).

[21] A. Irrera, F. Iacona, I. Crupi, C.D. Presti, G. Franzò, C. Bongiorno, D. Sanfilippo, G. Di Stefano, A. Piana, P.G. Fallica, A. Canino, and F. Priolo, Nanotechnology 17, 1428 (2006).

[22] M. Perálvarez, C. García, M. López, B. Garrido, J. Barreto, C. Domínguez, and J. A. Rodríguez, Appl. Phys. Lett. 89, 051112 (2006).
[23] L. Rebohle, J. von Borany, H. Fröb, and W. Skorupa, Appl. Phys. B 71, 131 (2000).
[24] P. Knàpek, B. Rezek, D. Muller, J. J. Grob, R. Lèvy, K. Luterovà, J. Kocka, and I. Pelant, Phys. Stat. Sol. A 167, R5 (1998).
[25] D. Muller, P. Knàpek, J. Fauré, B. Prevot, J. J. Grob, B. Hönerlage, and I. Pelant, Nucl. Instr. Meth. B 148, 997 (1999).
[26] A. G. Nassiopoulou, V. Ioannou-Sougleridis, P. Photopoulos, A. Travlos, V. Tsakiri, and D. Papadimitriou, Phys. Stat. Sol. A 165, 79 (1998).
[27] G. -R. Lin, and C. -J. Lin, J. Appl. Phys. 95, 8484 (2004).
[28] Y. Liu, T. P. Chen, L. Ding, M. Yang, J. I. Wong, C. Y. Ng, S. F. Yu, Z. X. Li, C. Yuen, F. R. Zhu, M. C. Tan, and S. Fung, J. Appl. Phys. 101, 104306 (2007).
[29] L. –S. Liao, X. –M. Bao, N. –S. Li, X. –Q. Zheng, and N. –B. Min, Solid State Commun. 97, 1039 (1996).
[30] A. Irrera, G. Franzò, F. Iacona, A. Canino, G. Di Stefano, D. Sanfilippo, A. Piana, P. G. Fallica, and F. Priolo, Physica E 38, 181 (2007).
[31] G. G. Qin, S. Y. Ma, Z. C. Ma, W. H. Zong, and Y. Li-ping, Solid State Commun. 106, 329 (1998).
[32] C. L. Heng, B. R. Zhang, Y. P. Qiao, Z. C.Ma, W. H. Zong, and G. G. Qin, Physica B 270, 104 (1999).
[33] L. Heikkilä, T. Kuusela, and H. -P. Hedman, Superlattices Microstruct. 26, 157 (1999).
[34] G. Pucker, P. Bellutti, M. Cazzanelli, Z. Gaburro, and L. Pavesi, Opt. Mater. 17, 27 (2001).
[35] S. Y. Ma, Thin Solid Films 402, 222 (2002).
[36] B. Averboukh, R. Huber, K. W. Cheah, Y. R. Shen, G. G. Qin, Z. C. Ma, and W.H. Zong, J. Appl. Phys. 92, 3564 (2002).
[37] A. Karsenty, A. Sa'ar, N. Ben-Yosef, and J. Shappir, Appl. Phys. Lett. 82, 4830 (2003).
[38] J. H. Kaang, Y. D. Kim, K. M. Cha, H. J. Cheong, Y. Kim, J. -Y. Yi, H. J. Bark, and T. H. Chung, J. Korean Phys. Soc. 45, 1065 (2004).
[39] D. Y. Chen, D. Y. Wei, J. Xu, P. G. Han, X. Wang, Z. Y. Ma, K. J. Chen, W.H. Shi, and Q.M. Wang, Semicond. Sci. Technol. 23, 015013 (2008).
[40] T. Wang, D. Y. Wei, H. C. Sun, Y. Liu, D. Y. Chen, G. R. Chen, J. Xu, W. Li, Z. Y. Ma, L. Xu, and K. J. Chen, Physica E 41, 923 (2009).

[41] A. Marconi, A. Anopchenko, M. Wang, G. Pucker, P. Bellutti, and L. Pavesi, Appl. Phys. Lett. 94, 221110 (2009).
[42] J. López-Vidrier, Y. Berencén, S. Hernández, O. Blázquez, S. Gutsch, J. Laube, D. Hiller, P. Löper, M. Schnabel, S. Janz, M. Zacharias, and B. Garrido, J. Appl. Phys. 114 , 163701 (2013).
[43] K. S. Cho, N. –M. Park, T. –Y. Kim, K. –H. Kim, G. Y. Sung, and J. H. Shin, Appl. Phys. Lett. 86, 071909 (2005). See Erratum: K. S. Cho, N. –M. Park, T. –Y. Kim, K. –H. Kim, G. Y. Sung, and J. H. Shin, Appl. Phys. Lett., 88, 209904 (2006).
[44] R. Huang, K. Chen, B. Qian, S. Chen, W. Li, J. Xu, Z. Ma, and X. Huang, Appl. Phys. Lett. 89, 221120 (2006).
[45] R. Huang, K. Chen, H. Dong, D. Wang, H. Ding, W. Li, J. Xu, Z. Ma, and L. Xu, Appl. Phys. Lett. 91, 111104 (2007).
[46] Z. H. Cen, T. P. Chen, Z. Liu, Y. Liu, L. Ding, M. Yang, J. I. Wong, S. F. Yu, and W. P. Goh, Opt. Express 18, 20439 (2010).
[47] J. Warga, R. Li, S. N. Basu, and L. Dal Negro, Appl. Phys. Lett. 93, 151116 (2008).
[48] L. Rebohle, and W. Skorupa, Rare-Earth Implanted MOS Devices for Silicon Photonics, (Springer Series Materials Science, Germany, 2010).
[49] W. M. Yen, S. Shionoya, and H. Yamamoto, Fundamentals of phosphors, (Taylor & Francis Group, Boca Raton, 2007).
[50] S. Wang, A. Eckau, E. Neufeld, R. Carius, and Ch. Buchal, Appl. Phys. Lett. 71, 2824 (1997).
[51] L. Tsybeskov, S. P. Duttagupta, K. D. Hirschman, P. M. Fauchet, K. L. Moore, and D. G. Hall, Appl. Phys. Lett. 70, 1790 (1997).
[52] G. Z. Ran, Y. Chen, W. C. Qin, J. S. Fu, Z. C. Ma, W. H. Zong, H. Lu, J. Qin, and G. G. Qin, J. Appl. Phys. 90, 5835 (2001).
[53] F. Iacona, D. Pacifici, A. Irrera, M. Miritello, G. Franzò, F. Priolo, D. Sanfilippo, G. Di Stefano, and P. G. Fallica, Appl. Phys. Lett. 81, 3242 (2002).
[54] D. Pacifici, A. Irrera, G. Franzò, M. Miritello, F. Iacona, and F. Priolo, Physica E 16, 331 (2003).
[55] A. J. Kenyon, Semicond. Sci. Technol. 20, R65 (2005).
[56] J. M. Sun, W. Skorupa, T. Dekorsy, M. Helm, and A. M. Nazarov, Opt. Mater. 27, 1050 (2005).
[57] F. Iacona, A. Irrera, G. Franzò, D. Pacifici, I. Crudi, M. Miritello, C. D. Presti, and F. Priolo, IEEE J. Sel. Top. Quant. 12, 1596 (2006).

[58] A. Kanjilal, L. Rebohle, W. Skorupa, and M. Helm, Appl. Phys. Lett. 94, 101916 (2009).
[59] A. Irrera, M. Galli, M. Miritello, R. Lo Savio, F. Iacona, G. Franzò, A. Canino, A. M. Piro, M. Belotti, D. Gerace, A. Politi, M. Liscidini, M. Patrini, D. Sanfilippo, P.G. Fallica, L.C. Andreani, F. Priolo, Physica E 41, 891 (2009).
[60] O. Jambois, F. Gourbilleau, A. J. Kenyon, J. Montserrat, R. Rizk, and B. Garrido, Opt. Express 18, 2230 (2010).
[61] J. M. Ramírez, F. Ferrarese Lupi, O. Jambois, Y. Berencén, D. Navarro-Urrios, A. Anopchenko, A. Marconi, N. Prtljaga, A. Tengattini, L. Pavesi, J. P. Colonna, J. M. Fedeli, and B. Garrido, Nanotechnology, 23, 125203 (2012).
[62] J. M. Ramírez, Y. Berencén, L. López-Conesa, J. M. Rebled, F. Peiró, and B. Garrido, Appl. Phys. Lett., 103, 081102 (2013).
[63] S. Yerci, R. Li, and L. Dal Negro, Appl. Phys. Lett. 97, 081109 (2010).
[64] S. Cueff, J. M. Ramírez, J. A. Kurvits, Y. Berencén, R. Zia, B. Garrido, R. Rizk, and C. Labbé, Appl. Phys. Lett., 103, 191109 (2013).
[65] M. Yoshihara, A. Sekiya, T. Morita, K. Ishii, S. Shimoto, S. Sakai, and Y. Ohki, J. Phys. D 30, 1908 (1997).
[66] S. Wang, H. Amekura, A. Eckau, R. Carius, Ch. Buchal, Nucl. Instrum. Method. B 148, 481 (1999).
[67] C. Buchal, Nucl. Instrum. Method. B 166–167, 743 (2000).
[68] J. M. Sun, W. Skorupa, T. Dekorsy, M. Helm, L. Rebohle, and T. Gebel, J. Appl. Phys. 97, 123513 (2005).
[69] J. M. Sun, W. Skorupa, T. Dekorsy, M. Helm, L. Rebohle, and T. Gebel, Appl. Phys. Lett. 85, 3387 (2004).
[70] W. Skorupa, J. M. Sun, S. Prucnal, L. Rebohle, T. Gebel, A. N. Nazarov, I. N. Osiyuk, and M. Helm, Solid State Phenom. 108–109, 755 (2005).
[71] J. M. Sun, S. Prucnal, W. Skorupa, M. Helm, L. Rebohle, and T. Gebel, Appl. Phys. Lett. 89, 091908 (2006).
[72] M. E. Castagna, S. Coffa, M. Monaco, L. Caristia, A. Messina, R. Mangano, and C. Bongiorno, Physica E 16, 547 (2003).
[73] A. Irrera, F. Iacona, G. Franzò, S. Boninelli, D. Pacifici, M. Miritello, C. Spinella, D. Sanfilippo, G. Di Stefano, P.G. Fallica, F. Priolo, Opt. Mater. 27, 1031 (2005).
[74] S. Prucnal, L. Rebohle, and W. Skorupa, Appl. Phys. B 98, 451 (2010).

[75] A. Irrera, M. Miritello, D. Pacifici, G. Franzò, F. Priolo, F. Iacona, D. Sanfilippo, G. Di Stefano, and P.G. Fallica, Nucl. Instrum. Methods. Phys. Res. B 216, 222 (2004).

[76] S. Prucnal, L. Rebohle, A. Nazarov, I. Osiyuk, I. Tyagulskii, and W. Skorupa, Appl. Phys. B 91, 123 (2008).

[77] S. Prucnal, J.M. Sun, W. Skorupa, and M. Helm, Appl. Phys. Lett. 90, 181121 (2007).

[78] Y. Berencén, R. Wutzler, L. Rebohle, D. Hiller, J. M. Ramírez, J. A. Rodríguez, W. Skorupa, and B. Garrido, Appl. Phys. Lett., 103, 111102 (2013).

[79] B. Gelloz and N. Koshida, J. Appl. Phys., 88, 4319 (2000).

[80] A. G. Cullis, L. T. Canham, and P. D. J. Calcott, J. Appl. Phys. 82, 909 (1997).

[81] C. –H. Cheng, Y.-C. Lien, C. –L. Wu, and G. –R. Lin, Opt. Express, 21, 391 (2013).

[82] S. M. Sze, Physics of semiconductor devices, 2nd ed. (Wiley, New York, 1981).

[83] D. R. Lamb, Electrical conduction mechanisms in thin insulating films, (Methuen & Co. Ltd., London, 1967).

[84] R. H. Fowler and L. Nordheim, Proc. Roy. Soc. London, 73, A119 (1928).

[85] J. G. Simmons, Electronic conduction through thin insulating films, Handbook of thin film technology, (L. I. Maissel and R. Glang (Ed.), Mc-Graw Hill, 1970).

[86] W. Schottky, Physik Z., 15, 872 (1914).

[87] S. R. Pollack, J. Appl. Phys., 34, 877 (1963).

[88] W. E. Flannery and S.R. Pollack, J. Appl. Phys., 37, 4417 (1967).

[89] J. Frenkel, Phys. Rev., 54, 647 (1938).

[90] C. A. Mead, Phys. Rev., 128, 2088 (1962).

[91] J. G. Simmons, Phys. Rev., 155, 657 (1967).

[92] R. B. Hall, Thin Solid Films, 8, 263 (1971).

[93] J. Tyczkowski, M. Ziclinski and M Kryszewski, Thin Solid Films, 55, 253 (1978).

[94] A. C. Rastogi and K. L. Chopra, Thin Solid Films, 26, 61 (1975).

[95] N.F. Mott, Phil. Mag., 19, 835 (1969).

[96] M. A. Lampert, Phys. Rev, 103, 1648 (1956).

[97] Kwan Chi Kao, Dielectric phenomena in solids, (Academic Press, California, 2004).

[98] A. Rose, Phy. Rev., 97, 1538 (1955).

[99] C. E. Chryssou, A. J. Kenyon, T. S. Iwayama, C. W. Pitt and D. E. Hole, Appl. Phys. Lett. 75, 2011 (1999).

[100] P. G. Kik, M. L. Brongersma, and A. Polman, Appl. Phys. Lett. 76, 2325 (2000).

[101] F. Seitz, J. Chem. Phys. 6, 454 (1938).

[102] N. Prtljaga, D. Navarro-Urrios, A. Tengattini, A. Anopchenko, J. M. Ramírez, J. M. Rebled, S. Estradé, J. –P. Colonna, J. –M. Fedeli, B. Garrido, and L. Pavesi, Opt. Mater. Express 2, 1278 (2012).

Appendix

A1. Statement of contribution in the presented articles

Article number	Did the author participate in the discussion of ideas that lead to this article?	Did the author participate in the design of samples or their processing?	Did the author take active part in the experimen-tal work?	Did the author take active part on the writing of the article?	Other useful comments for the evaluation of participation
I	YES	NO	YES	YES	Joint work
II	YES	NO	YES	YES	Joint work
III	YES	YES	YES	YES	Major contributions by Y. Berencén
IV	YES	YES	YES	YES	Major contributions by Y. Berencén
V	YES	YES	YES	YES	Major contributions by Y. Berencén
VI	YES	YES	YES	YES	Major contributions by Y. Berencén
VII	YES	YES	YES	YES	Major contributions by Y. Berencén

Table 3. Statement of contribution in the presented articles

A2. Copy of the published articles included as part of the thesis

PAPER I

JOURNAL OF APPLIED PHYSICS **106**, 063526 (2009)

Current transport and electroluminescence mechanisms in thin SiO_2 films containing Si nanocluster-sensitized erbium ions

O. Jambois,[1,a)] Y. Berencen,[1] K. Hijazi,[2] M. Wojdak,[3] A. J. Kenyon,[3] F. Gourbilleau,[2] R. Rizk,[2] and B. Garrido[1]

[1]*Dept. Electrònica, MIND-IN2UB, Universitat de Barcelona, Martí i Fanquès 1, 08028 Barcelona, CAT, Spain*
[2]*CIMAP, UMR CNRS 6252, 6 Boulevard Marchal Juin, 14050 CAEN, France*
[3]*Department of Electronic and Electrical Engineering, University College London, Torrington Place, London WC1E 7JE, United Kingdom*

(Received 30 June 2009; accepted 7 August 2009; published online 24 September 2009)

We have studied the current transport and electroluminescence properties of metal oxide semiconductor (MOS) devices in which the oxide layer, which is codoped with silicon nanoclusters and erbium ions, is made by magnetron sputtering. Electrical measurements have allowed us to identify a Poole–Frenkel conduction mechanism. We observe an important contribution of the Si nanoclusters to the conduction in silicon oxide films, and no evidence of Fowler–Nordheim tunneling. The results suggest that the electroluminescence of the erbium ions in these layers is generated by energy transfer from the Si nanoparticles. Finally, we report an electroluminescence power efficiency above $10^{-3}\%$. © *2009 American Institute of Physics*. [doi:10.1063/1.3213386]

I. INTRODUCTION

There are various methods to obtain electroluminescence (EL) from silicon-based devices, but there is also a need for optimization of devices and better understanding of underlying photogeneration and current transport processes. For the EL signal from silicon-rich silica thin films, the emission is usually attributed to silicon nanocrystals[1,2] or nanoclusters[3,4] (Si-ncls) dispersed in the SiO_2 matrix. In order to maximize potential applications, other approaches, including doping stoichiometric silica with rare earth ions, have been studied.[5,6] In most of the cases, the mechanism of conductivity was identified to be Fowler–Nordheim tunneling, and the emission was attributed to impact excitation of the ions by hot electrons. Different strategies are proposed at the device level in order to improve EL efficiency in metal oxide semiconductor (MOS) structure, such as the insertion of a nitride layer to control the energy of injected electrons,[7] or the design of plasmon-enhanced MOS devices.[8]

Because Si-ncls are capable of efficient energy transfer to erbium and other rare earth ions, silicon-rich erbium-doped silica as a material for EL devices became a subject of research.[9–11] However, the role of the Si-ncls in the EL of Er and conduction mechanisms is not clear. It is agreed that the presence of Si-ncls introduces more efficient conduction mechanisms, including variable range hopping,[12] direct tunneling (DT), trap-assisted tunneling, Poole–Frenkel (PF) conduction,[13] or space charged limited current (SCLC).[11] Si nanoparticles favor the injection of charge carriers, improve device lifetime,[14] reduce the population of hot electrons,[15] and consequently reduce impact excitation of Er.[10,16] It has also been argued that other mechanisms of EL can be introduced, including energy transfer from electrically excited Si-ncls to erbium ions.[13] In general, different processes can be dominant depending on material composition, film thickness, or voltage regimes. An understanding of injection and transport of carriers in erbium-doped silicon-rich silica (SiO_x:Er) is a prerequisite to the design of efficient devices.

We have tested a series of MOS structures that enabled us to study the carrier transport and EL from Er^{3+} ions as a function of both silicon and erbium contents. The goal of the present paper is to determine the influence of the Si-ncls on Er EL, on the conductivity of the layers, and on the power efficiency of the device. Finally, our measurements have enabled us to develop a model for the charge transport and EL mechanisms.

II. EXPERIMENTS

The layers were grown on *p*-type B-doped Si substrates by magnetron cosputtering of three confocal cathodes, SiO_2, Er_2O_3, and Si, under a pure Ar plasma. The rf power applied to each cathode permits the control of the film composition, i.e., the incorporation of Si and Er in the thin layer. More details on the deposition process can be found elsewhere.[17] In total, three different SiO_x:Er layers were fabricated, with thicknesses around 30 nm. Thickness was determined by spectroscopic ellipsometry measurements. The layers were annealed at 900 °C for 1 h in nitrogen.

X-ray photoelectron spectroscopy (XPS) spectra were measured with a Perkin-Elmer PHI-5500 instrument using Al $K\alpha$ radiation. XPS depth profiles were obtained by measuring the spectra after sputtering the samples to different thicknesses with an Ar^+ ion beam at 4 keV. The time-of-flight secondary ion mass spectrometry (TOF-SIMS) analyses were performed using a TOF-SIMS IV (ION-TOF, Munster, Germany), equipped with a Bi primary ion source, a

[a)]Author to whom correspondence should be addressed. Electronic mail: ojambois@el.ub.es.

 © 2009 American Institute of Physics

Downloaded 13 Oct 2009 to 161.116.95.84. Redistribution subject to AIP license or copyright; see http://jap.aip.org/jap/copyright.jsp

TABLE I. Results for Si excess and Er concentration of the four monitor layers.

Material	Si excess (%)	Er concentration (at. cm^{-3})	Thickness (nm)
C422	0	1×10^{20}	30
C426	7	4.7×10^{19}	27
C446	18	5.2×10^{20}	35
C439	22	8.4×10^{19}	30

Cs/O_2 electron impact dual source column, and a low-energy electron flood gun (for charge compensation of insulating samples).

Photoluminescence (PL) measurements were performed with a DPSS laser emitting at 473 nm, a Bentham M300 single grating monochromator, and a NIR-sensitive Hamamatsu photomultiplier (R5509-72).

The electrical contacts on the back side of the wafers were deposited by successive evaporation of chromium and gold. The top contacts were 60 nm sputtered indium tin oxide (ITO). Different areas from 1.56×10^{-2} to 1 mm^2 were used. To test the transparency of ITO, a series of test samples on glass was prepared, and they showed more than 90% transmission at 1.55 μm. Current-voltage characteristics were performed with an Agilent B1500A semiconductor parameter analyzer. EL measurements were performed with a Hamamatsu G8605 photodiode cooled to −30 °C and a long pass filter with cut-on at 1.4 μm to integrate the light coming from the band at 1.55 μm or an Oriel MS257 monochromator to spectrally resolve the light. The electrical excitation was continuous, not pulsed.

III. RESULTS AND DISCUSSION

A. Structural characterization and PL properties of the layers

XPS measurements were performed to characterize the Si excess. To determine the concentration of Er that is below the resolution of XPS, the sensitive TOF-SIMS technique was used and calibrated with Rutherford backscattering spectroscopy on another SiO_x:Er reference sample. The results for Si excess and Er concentration are given in Table I.

The PL of the four layers was characterized before depositing the electrodes. For each Si-rich layer, a luminescence band at 1.54 μm is observed when pumped at 473 nm, which is clearly attributed to the $^4I_{13/2}$-$^4I_{15/2}$ transition in the internal 4f shell of the Er^{3+} ions. A typical PL spectrum can be seen in Fig. 1. As Er is not pumped at a wavelength corresponding to a resonant transition, this suggests that Er ions are indirectly excited by the Si-ncls thanks to energy transfer, as proposed in literature.[18,19] In the inset of Fig. 1, the PL intensity of the three Si-rich samples has been normalized to the layer thickness and the Er concentration. Different intensities are found, but no clear dependence on Si excess or Er concentration can be inferred. These differences in PL intensities are attributed either to different fractions of optically active Er in the layers, or a different fraction of Er ions coupled to Si-ncls. The fact that the layer with the

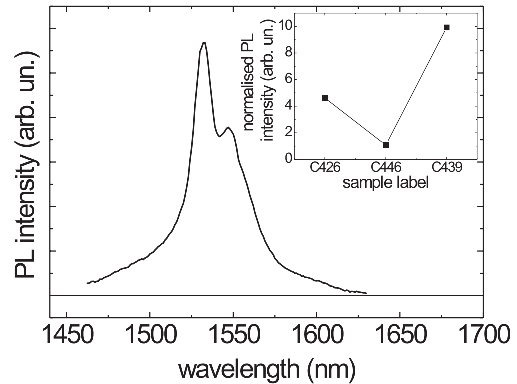

FIG. 1. PL spectrum of sample C446 by indirect pumping of Er. The inset shows the integrated PL intensity normalized to layer thickness and Er concentration for the three Si-rich layers.

higher Er content has the lower PL intensity suggests also that for this layer there is some Er agglomeration.

B. Conduction and EL properties

In Fig. 2, we present a typical J-V characteristic obtained for one device in both polarities. By convention, positive voltage to the p-type substrate corresponds to forward polarization. It can be seen that the current increases by several orders of magnitude over the range of voltages used here, which is typical of strong insulators. At lower voltages, the J-V curves are symmetric for both polarities, which suggests that the current is limited by the bulk of the active layer, and not by the electrode.[20] However, note that this is not true at higher voltages, as a saturation of the current can be observed in reverse polarization. This can be attributed to the lower density of electrons in the p-type substrate in inversion that can be injected in the dielectric so the injection becomes interface limited.

In the inset of Fig. 3, we present an EL spectrum showing an EL band at 1.55 μm, which is clearly attributable to the Er ions in the active layer. Note that the EL spectrum appears broader than the PL spectrum as for EL the slits of the monochromator were opened to the maximum to detect as much light as possible. This leads to a higher signal but lower resolution and a broadening of the spectrum. This kind of spectrum was obtained for samples that contain excess Si (C426, C446, and C439) when in forward bias. As can be

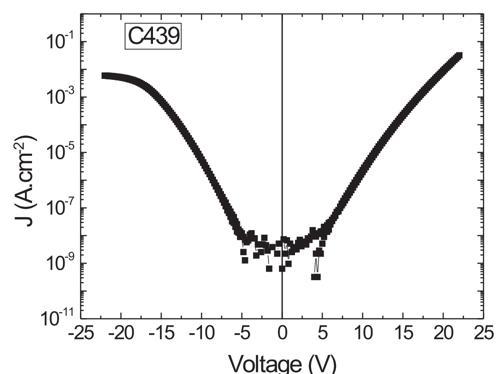

FIG. 2. J-V characteristic of sample C439.

Downloaded 13 Oct 2009 to 161.116.95.84. Redistribution subject to AIP license or copyright; see http://jap.aip.org/jap/copyright.jsp

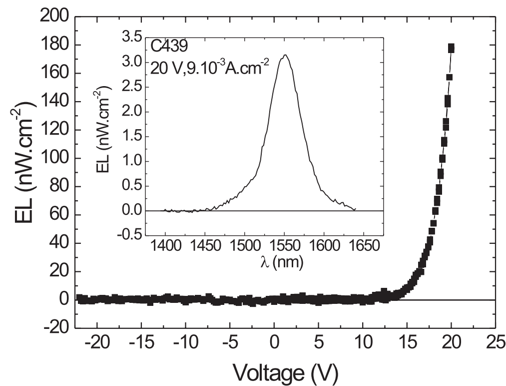

FIG. 3. EL power vs voltage of sample C439. The inset shows an EL spectrum

seen in Fig. 3, the EL intensity increases with the applied voltage. Under negative voltage, no EL was observed. It is also worth mentioning that sample C422, which has no Si excess, does not show any EL at 1.55 μm for any polarization.

In order to understand the conduction mechanisms, we present in Fig. 4(a) the current density–electric field (J-E) characteristics of the four samples. The electric field, given by the voltage divided by the active layer thickness, has been increased as much as possible before seeing breakdown of the device. In Fig. 4(a), we can see a strong variation of the current with applied field, in particular for the Si-rich samples (C426, C439, and C446). Moreover, the current is

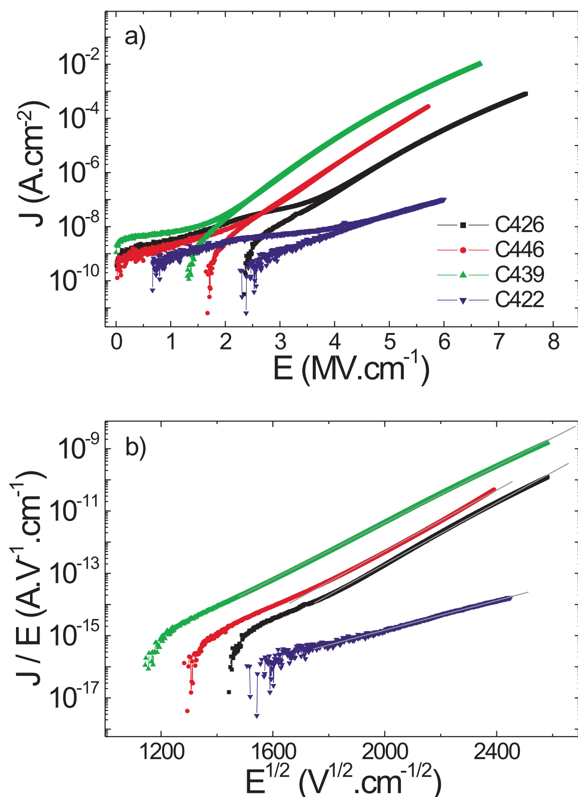

FIG. 4. (Color online) J-E characteristics of the layers (a) in log scale and (b) in PF representation. The legend that appears in (a) applies for both pictures.

strongly enhanced when a Si excess is introduced in the silicon oxide, as the current is increased by four or five orders of magnitude. This shows that the transport of charges occurs through the Si nanoparticles. This is also supported by the increase in conductivity with Si excess. If we compare the current densities to the ones given by other groups on similar materials made by sputtering,[11] the values found in the present study are much lower. This could suggest that the layer we have fabricated contains fewer matrix defects, leading to a lower conductivity.

Different models are known to describe current transport in silicon oxides through defects—for example, phonon-assisted tunneling, DT, field assisted thermal ionization, or SCLC.[20,21] The first two correspond to tunnel escape of charges from trap to trap. At higher electric fields, transport is generally well described by the Fowler–Nordheim mechanism, which corresponds to injection of charges from the electrode into the conduction band of the dielectric by tunneling through a triangular potential barrier. In our case, the data for the Si-rich samples are best described by the PF model, that is to say, the field-enhanced thermal emission of carriers from trapping sites in the insulator. This law is generally described by the following equation:

$$J \propto E \times \exp\left(\frac{1}{kT}\sqrt{\frac{e^3 E}{\pi \varepsilon_0 \varepsilon_r}}\right),$$

where kT is the thermal energy, e is the electron charge, ε_0 is the vacuum permittivity, and ε_r is the relative permittivity of the film.[20] From the fit, the value of ε_r can be deduced. From the effective medium theory, the value of ε_r can vary between 4 and 12, corresponding to the permittivities of SiO_2 and of pure Si, respectively. Figure 4(b) shows the J-E curve in the PF representation, i.e., the logarithm of the ratio J/E versus the square root of E. A straight line in a large range of J/E can be found for the Si-rich samples, giving values of permittivity consistent with the effective medium theory. For samples C426, C446, and C439, values of permittivity of 6.6, 6.9, and 7.9 were found. The increasing value of the permittivity with the Si excess is further evidence of the role of the Si-ncls in charge transport. The dominance of this mechanism in these kinds of layers is in agreement with what has previously been reported,[13,14,21] but contradicts other results,[11] in which a SCLC-type mechanism and much higher current density current even at low electric field were reported. We attribute this difference to the lower matrix defect density in the samples presented here than in Ref. 11, consistent with the lower currents we measure. It was also intended to fit the I-V characteristics with the Fowler–Nordheim law discussed above. In principle this kind of mechanism can lead to the injection of hot electrons in the active layer. This process is well known to be dominant for silicon oxides or silicon oxides with Si-ncls at high electric fields, when the films contain a much lower content of matrix defects. For example, we reported that layers of thermal SiO_2 implanted with Si and annealed at high temperature show good agreement with Fowler–Nordheim injection, and the EL mechanism of excitation of the Si-ncls was attributed to impact ionization.[22] This is also the case reported by Nazarov *et al.*,[10] who observed a Fowler–Nordheim-type injec-

Downloaded 13 Oct 2009 to 161.116.95.84. Redistribution subject to AIP license or copyright; see http://jap.aip.org/jap/copyright.jsp

tion in SiO_x:Er layers that have been fabricated by sequential implantation of Si and Er in a SiO_2 layer made by thermal oxidation of a Si substrate. In this study, the higher density of defects due to the preparation method seems to favor the injection of charges inside the dielectric, preventing hot electron injection, when the electric field is not too high. In the case of sample C422 (no silicon excess), different behavior is observed. Although the fit with the PF model seems reasonable, a permittivity of about 20 is found. This suggests that a mechanism of thermal ionization assisted by electric field could occur, but with some differences. In fact, a better fit with the SCLC mechanism could be found. This law is generally well fitted by a power dependence of I with V. In the ideal case, the exponent is equal to 2, as can be analytically found if we consider a dielectric free of traps or with shallow traps situated at a constant energy below the conduction band. In the case of a distribution of deeper states, higher values of exponent can be found.[23] In our case, an exponent of 7 has been found, which suggests that the defects present in the layers that assist conduction show a large energy distribution; this is understandable as the medium is essentially amorphous.

The power efficiency of EL is defined as the ratio between the power of the emitted light and the input electrical power. This value has been estimated for the three Si-rich layers by carefully calibrating the EL setup. We obtained power efficiencies of $2.3\times10^{-4}\%$, $1.2\times10^{-3}\%$, and $1.1\times10^{-4}\%$, for samples C426, C446, and C439, respectively. There is no clear tendency that appears with Si excess or Er concentration. This is because the system is governed by several parameters, including the Si-ncl density and the fraction of coupled Er. In fact, the EL results are contrary to the PL results of Fig. 1; i.e., the sample with the highest PL intensity has the lowest EL power efficiency. Actually, PL and EL do not necessarily coincide as, on one hand, for optical pumping the luminescent centers have to be well isolated to ensure the best confinement, whereas for electrical pumping the luminescent centers have to be close to one another to allow charge transport.[11,24] Moreover, even if the layers can be optimized by PL in terms of Er coupled to Si-ncls, we have to deal with different paths for the flow of charges, which can be matrix defects, Si-ncls not coupled to Er ions, or Si-ncls that are coupled to the Er ions. Among these three, only the last one allows excitation of Er, and the samples have to be prepared in order to favor this mechanism. The low matrix defect density has allowed us to obtain a power efficiency of $1.2\times10^{-3}\%$ for the best result, corresponding to an external quantum efficiency of 0.03%. In general, authors only report external quantum efficiency, which is the upper limit for power efficiency,[25] but power efficiency values are the one required for application purposes. To our knowledge, the value of power efficiency we report is the highest reported in Si-ncl sensitized Er ion systems. One expects a significant increase in this number for optimized material that is currently the object of intense effort.

C. Excitation mechanisms

Having clearly demonstrated the role of Si-ncls in the enhancement of the conductivity of the stoichiometric layer, we have studied the mechanism of Er excitation. We can imagine three scenarios that may occur in those layers leading to excitation of the Er ions: (i) impact ionization of Er directly, so the Si-ncls act only as paths for conduction; (ii) impact ionization of the Si-ncls and transfer of the excitonic energy to the nearest Er; or (iii) injection of electron and hole in the same Si-ncls, formation of an exciton, and transfer to the closest Er. In the case of impact ionization, the electron needs to reach a high kinetic energy. When it is high enough, the collision of this electron with a Si-ncl allows the creation of an exciton confined inside the Si-ncls, which can transfer its energy to the Er ions. Also, the hot electron can excite Er directly by collision. If the electron does not collide with the scattering centers (Si-ncls, Er, and matrix defects), it will impact the Si substrate. Thus, if hot electrons can be created by field ionization, radiative emission of the Si substrate due to impact ionization should be observable. In Fig. 5, an EL spectrum has been measured from 1 to 1.7 μm, to observe luminescence of Er at 1.55 μm, and that from the Si substrate at around 1.15 μm. The spectrum is measured at a bias of 22 V, and the device has never previously been subjected to voltages larger than 22 V. By increasing the electric field the EL intensity at 1.55 μm increases, as has already been seen in Fig. 3. However, when the applied voltage becomes higher than 35 V, the EL at 1.55 μm drops suddenly, and a new band appears at 1.15 μm. At the same time, the current shows also a noticeable increase (not shown). When reducing the bias to 22 V, the spectrum remains changed across the whole measured range, as can be seen in Fig. 5; the new band at 1.15 μm remains, and the EL of Er is lower.

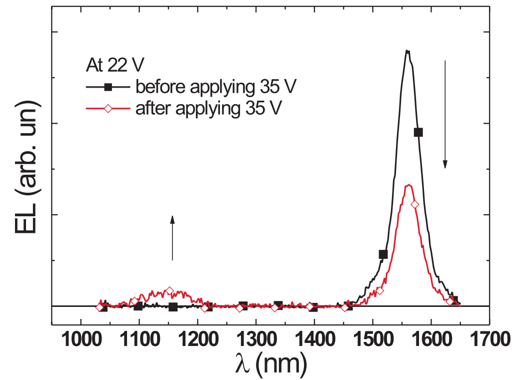

FIG. 5. (Color online) EL spectrum from 1000 to 1700 nm at 22 V before applying 35 V (full squares) and after applying 35 V (empty diamonds).

In Fig. 5, before applying voltages higher than 35 V, no luminescence from the Si substrate is observed, suggesting that hot electrons are not injected in the active layer. This is supported by the fact that no Fowler–Nordheim injection was observed. Instead, the charges are trapped by the matrix traps (Si-ncls or matrix defects) with a high probability because of their high density. If the electrons increase their kinetic energy (become hot) due to the electric field, they would thermalize very quickly. This suggests that the light emitted from Er does not come from impact ionization either of Er or of the Si-ncls. It appears more likely that in these layers we see bipolar injection of electrons from the ITO electrode and of holes from the accumulation region in the Si

Downloaded 13 Oct 2009 to 161.116.95.84. Redistribution subject to AIP license or copyright; see http://jap.aip.org/jap/copyright.jsp

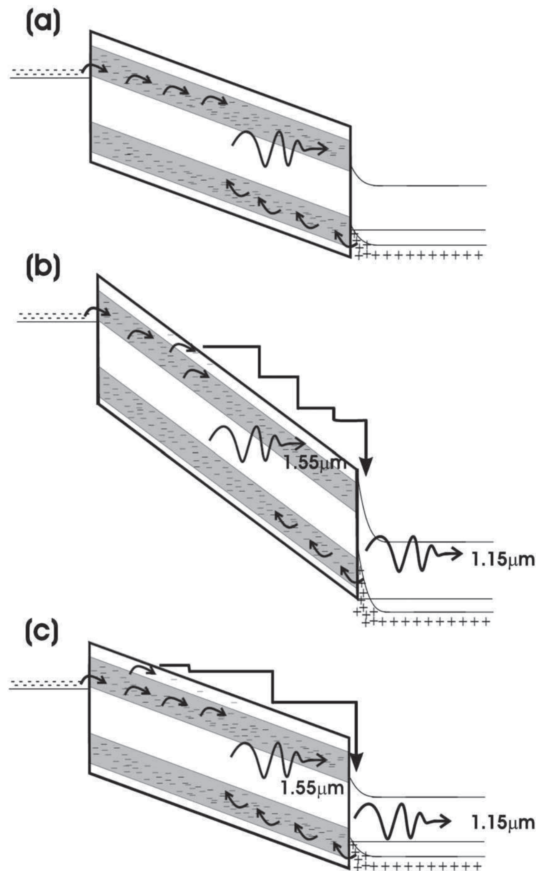

FIG. 6. Energy diagrams of the ITO/SiO_x:Er/*p*-Si structure. (a) At low voltage before applying 34 V, (b) at higher voltage, and (c) back to low voltage.

substrate into the Si-ncls, and that a transfer of the excitonic energy to the Er ions occurs. The fact that no EL is observed in reverse polarization suggests that holes are necessary to obtain Er EL. Moreover, another indication of the indirect excitation of Er is the fact that the SiO_2:Er layer does not show any EL. If we now consider the regime where very high electric fields are applied to the device—close to the layer breakdown—additional traps can be generated by the applied field. These new traps constitute a new channel for the conduction of charges, leading to a higher current, and some of the charges can reach the conduction band of the matrix. As the mobility is much higher there, electrons can remain hot and reach the Si substrate. This explains the appearance of a luminescence band at 1.15 μm. Finally, when coming back to 22 V, the defects generated by the high electric field are still there; hence it is still possible to generate hot electrons and the EL band due to the Si substrate remains. The decrease in the intensity of the EL band could be due either to a lower fraction of charges that flow through the traps inside the gap, or to a nonradiative interaction between excitons and hot electrons (Auger).

From all the above results, we propose a model describing the conduction of charges in our sample for different regimes of electric field, and explaining the different EL bands emitted from the device. We schematize in Fig. 6(a) the mechanism in an energy-space diagram at low voltage. The active layer in the center is sandwiched between the ITO semimetallic electrode and the *p*-type Si substrate. The high density of traps characterizing the films (Si-ncls or matrix defects) allows conduction of charges with a reduced mobility compared to an electron in the conduction band, and hence a PF mechanism occurs. At low voltages in forward bias, electrons are injected from the ITO electrode, and holes from the Si substrate. EL from Er can be observed: we symbolize it by the twisted arrow in the center of the active layer. When a higher voltage is applied, the electric field is close to breakdown [see Fig. 6(b)], and it is likely that defects are created inside the layer. The charges follow these new channels, and are injected into the conduction band of the silicon oxide matrix. There the electrons can become hot, as they suffer less scattering than in the pseudoconduction band created in the gap of the oxide. They are thus able to impact with the substrate, and this explains the luminescence of the substrate that appears at high fields, as observed in Fig. 5, as well as the observed increase in the current intensity. Finally, when coming back to lower field [see Fig. 6(c)], the defects created by the high electric field are still there, and charges can still be injected into the conduction band of the matrix. This leads to a new situation in which a new luminescence band appears at 1.15 μm. As a fraction of electrons are deviated from their original trajectory, less EL at 1.55 μm is obtained.

IV. CONCLUSIONS

In summary, we have studied the conduction and EL mechanisms in SiO_x:Er layers of different compositions, as well as their power efficiency. The presence of Si-ncls leads to an increase in the current of four to five orders of magnitude. The conduction mechanism is found to be dominated by field assisted thermal ionization (PF) from Si-ncls to Si-ncls. At lower voltages, no evidence of hot electron injection has been seen. The experiments allow us to attribute the erbium EL to a transfer of the excitonic energy of the Si-ncls to Er ions, and to discount impact ionization of either the Si-ncls or Er ions. A power efficiency above 10^{-3}% has been found for the best device. A model is proposed to explain the different regimes of luminescence with the applied voltage that occurs in these devices.

ACKNOWLEDGMENTS

This work is supported by the European Community through the LANCER Project (FP6-IST 033574). O.J. acknowledges financial support from the Spanish Ministry of Science (Juan de la Cierva Program).

[1]G. Franzò, A. Irrera, E. C. Moreira, M. Miritello, F. Iacona, D. Sanfilippo, G. Di Stefano, P. G. Fallica, and F. Priolo, Appl. Phys. A: Mater. Sci. Process. **74**, 1 (2002).
[2]R. J. Walters, G. I. Bourianoff, and H. A. Atwater, Nature Mater. **4**, 143 (2005).
[3]A. Irrera, F. Iacona, I. Crupi, C. D. Presti, G. Franzò, C. Bongiorno, D. Sanfilippo, G. Di Stefano, A. Piana, P. G. Fallica, A. Canino, and F. Priolo, Nanotechnology **17**, 1428 (2006).
[4]V. Filip, H. Wong, C. K. Wong, and D. Nicolaescu, J. Vac. Sci. Technol. B **26**, 813 (2008).
[5]S. Prucnal, J. M. Sun, W. Skorupa, and M. Helm, Appl. Phys. Lett. **90**,

Downloaded 13 Oct 2009 to 161.116.95.84. Redistribution subject to AIP license or copyright; see http://jap.aip.org/jap/copyright.jsp

181121 (2007).
[6]H. Jeong, S.-Y. Seo, and J. H. Shin, Appl. Phys. Lett. **88**, 161910 (2006).
[7]M. Perálvarez, J. Carreras, J. Barreto, A. Morales, C. Domínguez, and B. Garrido, Appl. Phys. Lett. **92**, 241104 (2008).
[8]A. Hryciw, Y. C. Jun, and M. L. Brongersma, Opt. Express **17**, 185 (2009).
[9]F. Iacona, D. Pacifici, A. Irrera, M. Miritello, G. Franzò, F. Priolo, D. Sanfilippo, G. Di Stefano, and P. G. Fallica, Appl. Phys. Lett. **81**, 3242 (2002).
[10]A. Nazarov, J. M. Sun, W. Skorupa, R. A. Yankov, I. N. Osiyuk, I. P. Tjagulskii, V. S. Lysenko, and T. Gebel, Appl. Phys. Lett. **86**, 151914 (2005).
[11]K. Sun, W. J. Xu, B. Zhang, L. P. You, G. Z. Ran, and G. G. Qin, Nanotechnology **19**, 105708 (2008).
[12]M. Fujii, Y. Inoue, S. Hayashi, and K. Yamamoto, Appl. Phys. Lett. **68**, 3749 (1996).
[13]F. Priolo, C. D. Presti, G. Franzò, A. Irrera, I. Crupi, F. Iacona, G. Di Stefano, A. Piana, D. Sanfilippo, and P. G. Fallica, Phys. Rev. B **73**, 113302 (2006).
[14]S. Prezioso, A. Anopchenko, Z. Gaburo, L. Pavesi, G. Pucker, L. Vanzetti, and P. Bellutti, J. Appl. Phys. **104**, 063103 (2008).
[15]D. J. DiMaria, T. N. Theis, J. R. Kirtley, F. L. Pesavento, D. W. Dong, and S. D. Brorson, J. Appl. Phys. **57**, 1214 (1985).
[16]M. E. Castagna, S. Coffa, M. Monaco, L. Caristia, A. Messina, R. Mangano, and C. Bongiorno, Physica E (Amsterdam) **16**, 547 (2003).
[17]K. Hijazi, L. Khomenkova, J. Cardin, F. Gourbilleau, and R. Rizk, Physica E (Amsterdam) **41**, 1067 (2009).
[18]A. J. Kenyon, P. F. Trwoga, M. Federighi, and C. W. Pitt, J. Phys.: Condens. Matter **6**, L319 (1994).
[19]M. Fujii, M. Yoshida, Y. Kanzawa, S. Hayashi, and K. Yamamoto, Appl. Phys. Lett. **71**, 1198 (1997).
[20]S. M. Sze, *Physics of Semiconductor Devices*, 2nd ed. (Wiley, New York, 1981).
[21]J. G. Simmons, Phys. Rev. **155**, 657 (1967).
[22]O. Jambois, A. Vilà, P. Pellegrino, J. Carreras, A. Pérez-Rodríguez, B. Garrido, C. Bonafos, and G. BenAssayag, J. Lumin. **121**, 356 (2006).
[23]R. M. Hill, Thin Solid Films **1**, 39 (1967).
[24]P. M. Fauchet, Mater. Today **8**, 26 (2005).
[25]B. Gelloz and N. Koshida, J. Appl. Phys. **88**, 4319 (2000).

Downloaded 13 Oct 2009 to 161.116.95.84. Redistribution subject to AIP license or copyright; see http://jap.aip.org/jap/copyright.jsp

PAPER II

Proceedings of the 2009 Spanish Conference on Electron Devices - Feb 11-13, 2009. Santiago de Compostela, Spain.

Study of the electroluminescence at 1.5 μm of SiO_x:Er layers made by reactive magnetron sputtering.

O. Jambois*, Y. Berencen*, S.-Y. Seo* A.J. Kenyon†, M. Wojdak†, K. Hijazi‡, L. Khomenkova‡, F. Gourbilleau‡, R. Rizk‡ and B. Garrido*

*MIND-IN2UB, Dept. Electrònica, Universitat de Barcelona, Martí i Fanquès 1, 08028, Barcelona, CAT, Spain

†Department of Electronic and Electrical Engineering, University College London, Torrington Place, London WC1E 7JE, United Kingdom

‡CIMAP, UMR CNRS 6252, 6 Boulevard Marchal Juin, 14050 CAEN, France

***Abstract*—We have studied the current transport and electroluminescence mechanisms of four layers of Si oxide co-doped with Si nanoclusters and erbium ions. Electrical measurements have identified different conduction mechanisms in separate high-field and low-field regimes, including Poole-Frenkel hopping. In particular, hopping through the Si-ncl is evidenced by C-V measurements. We have also observed an important contribution of defects from the oxide in the conduction, and no evidence of Fowler-Nordheim tunnelling. The results suggest that the electroluminescence from erbium ions in silicon-rich silicon dioxide is generated by electrons transported through the active layer by hopping from localised states, which we associate with silicon nanoclusters.**

I. Introduction

Si photonics is an emerging field of active research, which aims to achieve the integration of both photonic and electronic functions on the same chip. This would allow to open the route to potential applications that would revolutionize current microelectronics. However, an efficient Si-based electrically driven light source is still lacking to obtain a photonic technology truly compatible with integrated electronic circuits. One of the promising materials studied is the system of Er doped silicon rich silica matrix. Indeed, the luminescence of Er at 1.5 μm is eminently strategic as it corresponds to the C band in telecommunications. Moreover, the presence of Si nanoclusters (Si-ncl) with sizes typically less than 5 nm is doubly beneficial: i) an efficient sensitizing effect for the excitation of the RE ions, well established for the ions Er3+ [1], [2] and ii) an enhancement of the injection and the transport of electrical carriers in the insulating layer. This material has been demonstrated already as prmising for light emitting diode devices [3], as power efficiency as high as 0.1% has already been observed. Moreover, the higher absorption cross section of about four order of magnitude of the Si-ncl could allow to obtain optical amplification with reduced dimension devices, which could be a real breakthrough to the actual optical fiber amplifiers.

We have previously reported the sensitization effect of Si nanoclusters in Er luminescence by optical pumping [4], and internal gain by optical pumping has been shown by us [5] and others [6]. But it seems that a major limitation to optical pumping is that Er needs to be in the close vicinity of Si-ncl (less than 1 nm) to be efficiently sensitized. Thus, net gain is still difficult to achieve by optical pumping. However, by electrical pumping, it should be possible to excite the Er ions indirectly through the Si-ncl, or directly. Moreover, it has been reported that the excitation cross section of Er is 2 order of magnitude higher by electrical pumping than by optical pumping [7], which makes electrical pumping a better alternative. However, a clear comprehension of the Er excitation in Si-ncl based material and on the conduction mechanisms is still lacking.

We report here the conduction and electroluminescence (EL) mechanisms of 4 SiOx:Er layers made by reactive magnetron sputtering containing different Si excess and Er concentrations. Electrical characterisation by current voltage (I-V) and capacitance- voltage (C-V) has been performed to understand the conduction mechanisms. It is found that defects of the oxide play an important role in the conduction of the charges. Moreover, the combination of both techniques allow us to identify the Si-ncl as responsible of the high leakage currents. The EL of the layers is presented and the EL mechanisms analyzed. It is suggested that the injection of electrons and holes inside the Si-ncl and the transfer of the excitonic energy to the close Er ions is more likely to occur than direct impact ionisation of Er ions through hot electrons. Finally, EL in the visible range is presented and its origin discussed.

978-1-4244-2839-7/09/$25.00 (C)2009 IEEE

II. Experimental

The thin films of Er-doped Silicon Rich Silicon Oxide (Er-SRSO) layers were deposited by magnetron co-sputtering of three confocal targets, SiO_2 and Er_2O_3 and Si under a plasma of pure argon. The content of Er and Si excess can be finely and independently tuned through the monitoring of the RF power applied on each cathode. The layers were grown at a substrate temperature of 500˚C on a rotating holder for good homogeneity of both thickness and composition. After deposition, the layers were subsequently annealed under a nitrogen flux for one hour at different temperatures T_a between 500˚C and 900˚C [8]. Two different materials have been prepared, one with low Si excess and low Er concentration (samples S1a and S1b), and the other with high Si excess and high Er concentration (samples S2a and S2b). Each material has been deposited for two different thicknesses, leading to a total of 4 wafers for this study. The annealing temperatures have been chosen to optimize the photoluminescence properties of the films. After annealing, the Si rich Si oxide separate in two phases thermodynamically stable, one of Si and a second one of SiO_2. It is known that the Si phase appears in the form of Si nanoclusters (Si-ncl) [9]. Then a gold back contact has been deposited and for the top contact, Indium Tin Oxide (ITO) has been chosen, as it is known that this material can be transparent and conductive by playing on the Indium content. In this study, the top contact is 6mm^2 and 100 nm thick.

The table I details the characteristics of the different layers.

sample	nominal thickness (nm)	annealing conditions	Si excess (%)	Er concentration (at.cm^{-3})
S1a	30	900˚C, 30 minutes	9.5	2.2×10^{20}
S2a	15	900˚C, 30 minutes	9.5	2.2×10^{20}
S1b	18	500˚C, 30 minutes	18	1×10^{21}
S2b	42	500˚C, 30 minutes	18	1×10^{21}

TABLE I
RESUME OF THE DIFFERENT LAYERS OF THIS STUDY.

Si excess have been determined by X-ray Photoelectron Spectroscopy (XPS), and Er concentration by Time of Flight Second Ion Mass Spectroscopy (ToF-SIMS) with a calibration sample of known Er concentration. Current-Voltage (I-V) and Capacitance-Voltage (C-V) of the devices have been performed at room temperature with a semiconductor device analyzer (Agilent B1500A) and a probe station (Cascade Microtech). Electroluminescence spectra were obtained with a an InGaAs infrared photodiode (Hamamatsu G8605 serie) and lock-in amplification for infrared spectroscopy, and a CCD camera cooled at 160K for visible spectroscopy. Spectra were corrected from the setup response.

III. Results and discussion

The I-V of the four different wafers are shown in figure 1. First of all, we can observe that the layers are very conductive. Typically, when 5 V are applied on a sample that is around 30 nm thick, we have more than 3×10^{-4} A for an area of the electrode of 6mm^2 i.e. 5×10^{-3}A.cm^{-2}. This contrast with thermal SiO_2 layers implanted with Si, where the defect density is expected to be much lower (the defects due to implantation are expected to be removed during annealing), current density may be 4 order of magnitude lower for such electric field [10]. This suggest that the layers are full of defects that improve significantly the conduction. This is understandable as the quality of the oxide depends critically on the growth conditions. In the case of deposition techniques like sputtering, the defect density is expected to be much higher than in a thermal oxide. Secondly, we can see that for the same material, the thinner sample has higher current than the thicker one. This suggests strongly that although the layer are very thin, the current is still limited by the bulk of the active layer, and not by the injection at the interface. Indeed, if that was the case, the value of the current should remain the same whatever the thickness of the layer. Finally, it is observed that the sample with the higher Si content and Er concentration, and annealed at lower temperature has a lower conductivity. This is quite surprising, as at 500˚C, the phase separation of SiO_x in a nanophase of Si and a phase of SiO_2 has already begun. And as there is much more Si in this sample, this last observation suggests that there are fewer defects when the Si excess is made higher.

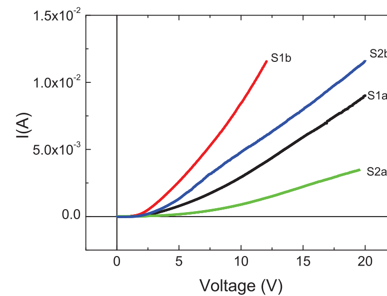

Fig. 1. I-V characteristics of the different wafers in forward bias.

Figure 2 shows the C-V characteristics for all samples. The maximum absolute applied gate voltage was 10 V (negative with respect to substrate), the AC level signal was 100 mV and the frequency was fixed at 100 kHz for all measurements. We can observe that an hysteresis cycle appears for all the curves of the figure 2 while this effect is absent for a reference sample free of Si-ncl and Er ions (not shown). The hysteresis evidences a shift of the flat band voltage V_{FB} showing a charging effect of the layers, through the Si-ncl or the defects of the matrix both inducing traps for the charges. Moreover, the hysteresis measured under the same maximum absolute

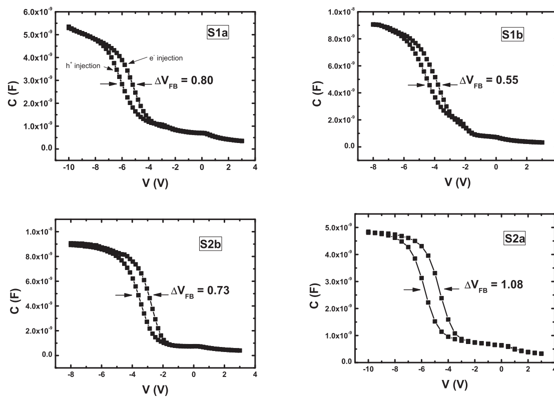

Fig. 2. C-V characteristics of the different wafers.

applied gate voltage (10 V) is more pronounced for sample C2a than for sample C1a which contains less Si excess and lower Er concentration. The same observation can be made for samples C2b and C1b, for which the C-V characteristics were measured under a maximum absolute gate voltage-value of 8 V. These results shows that the Si-ncl plays a role on the conduction of the charges. This is important, because the Si-ncl are expected to be sensitizers to the Er excitation.

It is possible to find out the permittivity from the C-V measurements. It is well-known that in the accumulation regime, the expression of the total capacitance is practically the oxide capacitance:

$$C_{Ox} \quad = \quad \frac{\varepsilon_r \times \varepsilon_0 \times S}{d_{Ox}} \tag{1}$$

where C_{Ox} is the oxide capacitance in the accumulation regime,ε_0 the vacuum dielectric constant, equal to 8.85×10^{-12} F.m^{-1}, ε_r the relative permittivity, d_{Ox} the thickness of the active layer and S, the area of the electrode.

Hence, starting from equation (1) we can obtain the value of the relative permittivity for each sample as shown in the table II.

sample	d_{Ox} (nm)	C_{Ox} (F)	ε_r
S1a	30	529×10^{-11}	2.98
S1b	15	905×10^{-11}	2.55
S2a	18	906×10^{-11}	3.07
S2b	42	480×10^{-11}	3.80

TABLE II
VALUES OF PERMITTIVITY OF EACH LAYERS DEDUCED FROM C-V MEASUREMENTS.

From this table, if we compare two wafers having around the same thickness, for examples S1a with S2a, or S1b with S2b, we can see that the permittivity is higher for the sample that has the larger Si content. From the theory of effective medium, it is expected that the effective permittivity of our layers are between the value of both phases of SiO_2 and Si, that is to say between 3.9 and 12. Thus, as the permittivity is higher for the wafers S2, this support our previous conclusion that the higher content of Si that we have introduced is effectively used by the carriers for flowing from one electrode to the other. So this suggest also that there are more Si-ncl in the S2 layers. The fact that the conductivity is higher for the wafers S1 as we have seen in figure 1 suggests that the material S1 contains much more defects, and less Si-ncl.
If we look now to the quantitative results, we can see that the permittivity is lower than 3.9 in all the cases. This is quite surprising, and this could be due to the fact that the films present some porosity, and that the real thickness is larger than the nominal one.

We are interested now in modeling the conduction in the layers. Different models are known to describe conduction through defects like phonon-assisted tunneling, direct tunneling or field assisted thermal ionisation. The first two one correspond to tunnel escape of charges from trap to trap. The last mechanism, known as Poole-Frenkel mechanism, gives a dependance of the current with voltage with the following law:

$$I \propto V exp\left(\frac{1}{kT}\sqrt{\frac{e^3V}{\pi c^2\varepsilon_0\varepsilon_r d_{Ox}}}\right) \tag{2}$$

where I and V are the current and the applied voltage, kT is the thermal energy, d_{Ox} is the thickness of the layer and c is a correction factor depending on the kind of traps, their energy distribution or the number of dimensions considered in the model [11]. This law consists in the thermal ionization of the traps, that have their energy barrier reduced by the electric field. From the fit, the product $c^2\varepsilon_r$ can be deduced. From the models $1 < c < 2$, and as commented before $3.9 < \varepsilon_r < 12$. So a good quantitative fit should give $3.9 < c^2\varepsilon_r < 48$. Here we are only interested in this figure, but not in deducing quantitative values of ε_r, because c is unknown and is strongly dependent on the environment, and some uncertainty on the thickness may also be possible.
In the figure 3, we have plotted the I-V characteristic of samples S1a and S2a in Poole-Frenkel representation. This representation allows to see a straight line in the medium field region, suggesting that this model is valid to describe the current conduction in our samples at lower fields. At higher electric fields, we have a linear dependence of the current with the voltage, as has been seen in figure 1. So, this results suggest that at lower field, the injected charges hops from traps to traps by thermal ionization and drift due to the electric field. At higher voltage, more defects are accessible to the injected charges, and the density of defects is so high, that an almost ohmic law can be observed.

The EL has been obtained from all the layers in forward bias. Figure 4 shows the typical EL band at 1.55 μm coming from sample S1b. This band is clearly attributed to the $^4I_{13/2}$-$^4I_{15/2}$ transition in the internal 4f-shell of the Er^{3+} ions. It is observed that the EL intensity is increasing with the

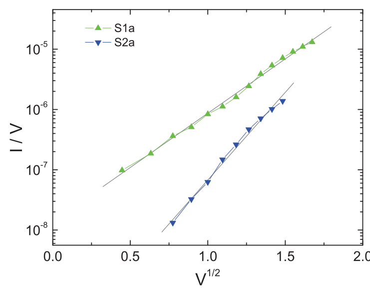

Fig. 3. I-V characteristics represented in Poole-Frenkel representation for the thicker samples.

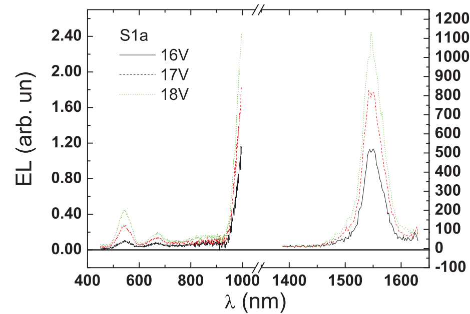

Fig. 4. Electroluminescence spectra of sample S1a for different voltages in the visible and infrared spectral ranges.

voltage, as more charges are injected in the layer to excite the luminescent centers. We have also measured the EL spectrum in the visible range, and have observed different bands in the visible at around 540 nm, 670 nm and 870 nm. It is more difficult to assign precisely the origin of these bands, as in this spectral range, a lot of contribution could arise. For example, it has already been observed by photoluminescence spectroscopy measurements that Si-rich Si oxide have NBOHC (Non Bridging Oxygen Hole Center) defects that emit at 650 nm, and oxygen vacancy that may emit between 560 nm and 620 nm. Also, Er ions have higher energy transition, which energy depends on the matrix, but value as 550 nm and 670 nm have been reported, which could clearly be at the origin of the visible EL observed here. Finally, in our samples, the annealing temperature is lower than 900°C, so it is probable that most of the nanoparticles of Si are amorphous. It has been reported that amorphous Si nanoclusters can emit in the near infrared region, and this could explain the band at 870 nm [7]. About the mechanism of excitation of the Er ions, as we have seen that the layers are full of defects that allow large leakage current even at low voltage, it seems easy to the charges (electrons and holes) to be injected and travel through the oxide layer. This suggest that there is a low probability that the electrons may reach the SiO_2 conduction band and become hot electrons (that is to say with energy higher than the SiO_2 conduction band). It seems more likely that the charges flow inside the gap through the traps. Therefore, as it is unlikely that impact ionisation occurs in our devices, a mechanism of excitonic energy transfer as already reported for optical pumping [1], [4] from Si nanoparticles to Er ions seems more likely to occur. This result is supported by the fact the current is not limited by interface injection, so the direct injection of hot electrons from the electrode is not likely to occur. Other measurements are on-going to support further this interpretation.

IV. Conclusion

In conclusion, four layers with different Si excess, Er concentration and thicknesses have been studied, in order to anlyse the charge transport and the EL excitation mechanisms in SiO_x:Er layers. Electrical characterization by I-V and C-V has been performed. It allows to show that matrix defect induce leakage current, but a significant role of the Si-ncl on the conduction has also been evidenced. The EL at 1.5 μm of each layer has been obtained. This EL band is clearly attributed to the Er ions, and the results suggest that the Er ions are excited through the Si-ncl sensitization and not by direct impact ionization.

Acknowledgment

This work was supported by European Commission under the Sixth Framework (LANCER, FP6-033574). O.J. acknowledges financial support from the Spanish Ministry of Science (Juan de la Cierva Program), and Anna Gil for technical assistance.

References

[1] A. J. Kenyon, P. F. Trwoga, M. Federighi, and C. W. Pitt, J. Phys.: Condens. Matter 6, L319 (1994).
[2] M. Fujii, M. Yoshida, Y. Kanzawa, S. Hayashi, and K. Yamamoto, Appl. Phys. Lett. 71, 1198 (1997).
[3] F. Priolo, C. D. Presti, G. Franzò, A. Irrera, I. Crupi, F. Iacona, G. Di Stefano, A. Piana, D. Sanfilippo, and P. G. Fallica , Phys. Rev. B 73, 113302 (2006).
[4] B. Garrido, C. García, S.-Y. Seo, P. Pellegrino, D. Navarro-Urrios, N. Daldosso, L. Pavesi, F. Gourbilleau, and R. Rizk, Phys. Rev. B 76, 245308 (2007).
[5] N. Daldosso, D. Navarro-Urrios, M. Melchiorri, L. Pavesi, F. Gourbilleau, M. Carrada, R. Rizk, C. García, P. Pellegrino, and B. Garrido, Appl. Phys. Lett. 86, 261103 (2005).
[6] Hak-Seung Han, Se-Young Seo, and Jung H. Shin, Appl. Phys. Lett. 79, 4568 (2001) .
[7] A. Irrera, D. Pacifici, M. Miritello, G. Franzò, F. Priolo, F. Iacona, D. Sanfilippo, G. Di Stefano, and P. G. Fallica Appl. Phys. Lett. 81 1866 (2002)
[8] K. Hijazi, L.Khomenkova, J. Cardin, F. Gourbilleau and R. Rizk., accepted for publication in Journal of Luminescence
[9] O. Jambois, H. Rinnert, X. Devaux and M. Vergnat Journ. of Appl. Phys. 98, 046105 (2005)
[10] O. Jambois, B. Garrido, P. Pellegrino, Josep Carreras, A. Pérez-Rodríguez, J. Montserrat, C. Bonafos, G. BenAssayag, and S. Schamm Appl. Phys. Lett. 89, 253124 (2006)
[11] J. G. Simmons, Phys. Rev. 155, 657 (1967)

PAPER III

Er-doped Si-based electroluminescent capacitors: Role of different host matrices on the electrical and luminescence properties

Y. Berencén,* J. M. Ramírez, and B. Garrido

MIND-IN2UB, Dept. Electrònica, Universitat de Barcelona, Martí i Fanquès 1, 08028, Barcelona, Spain.
*Corresponding author: yberencen@el.ub.edu

***Abstract*—We report on the electrical and electroluminescence properties of four different layers based on Er-doped silicon oxide (or nitride) with (or without) silicon nanocrystals. Electrical measurements have allowed us to identify that samples composed by silicon nitride matrices present a Poole-Frenkel-type conduction, whereas those ones formed by silicon oxide matrices show a Fowler-Nordheim tunneling mechanism. In addition, infrared power efficiency at 1.54 µm has shown to be two orders of magnitude larger for Er-doped silicon oxide layers than for Er-doped silicon nitrides. Moreover, an interesting trade off between power efficiency at 1.54 µm and device operation lifetime has been observed by comparing both Er-doped silicon oxides and Er-doped silicon nitride layers.**

Keywords—Erbium; silicon nanocrystals; silicon oxide; silicon nitride; electrolumincescence.

I. Introduction

Silicon oxide- and silicon nitride-based materials have been widely employed for decades in mainstream complementary metal-oxide-semiconductor (CMOS) technology as dielectric materials [1]. Later on, these materials together with silicon were also proposed to develop new integrated functional building blocks based on photon management for high data transmission rates [2]. By this time, a new appealing area of research came up: the silicon photonics. Nowadays, one of the most important research activities on such a topic is the integration of electrical and optical functionalities in the same chip [2]. This fact opens the possibility to develop photonic integrated circuits (PICs) that would solve most of the present microelectronics drawbacks (i.e. interconnections). Nevertheless, a mature photonic technology able to develop an efficient Si-based electrically driven light source has not yet been obtained. Erbium ions and Silicon nanocrystal (Si-ncs) inclusions embedded into either silicon oxide or silicon nitride matrices have been considered as suitable candidates for the realization of light sources emitting at 1.54 µm [2], [3]. This Er emission line is ideal for telecom purposes as it lies within the minimum of absorption for silica fibers [2]. Moreover, the presence of Si-ncs brings additional benefits such as: i) reduction of the effective barrier height for electrical injection and ii) acts as efficient sensitizers for the Er excitation under optical pumping [4].

In this work, we report on the electrical and electroluminescence properties of four different matrices based on silicon oxide (or nitride) co-doped with Er ions and Si-ncs. The different conduction mechanisms and their correlation with luminescent properties are investigated. In addition, an assessment of the electroluminescence (EL) at 1.54 µm in terms of efficiency and device operation lifetimes is carried out.

II. Experimental Detalis

Four different layers of 50nm-thick were fabricated on <100>, 0.001 Ω·cm, p-type substrate by means of low pressure chemical vapor deposition (LPCVD) technique with similar annealing treatments (see Table I). All samples were implanted with Er ions. Whereas, Si-ncs implantation were solely accomplished on B1 and B3, with a silicon excess of 20 % and 12 % for silicon nitride and silicon oxide layers, respectively. Si excess was determined by X-ray Photoelectron Spectroscopy (XPS) and Er concentration by means of Time of Flight Secondary Ion Mass Spectroscopy (ToF-SIMS) using a reference sample of known Er concentration. An n-type doped semitransparent polysilicon gate electrode has been performed (100 nm thick). Additionally, an aluminium layer has been deposited and used as a back contact.

Quasi-static electrical measurements were accomplished in MOS capacitor devices with area of 300 x 300 µm^2 using a semiconductor parameter analyzer (Agilent B1500A) coupled to a probe station (Cascade Microtech Summit 11000) electrically isolated by a Faraday cage (microchamber). The devices are forward biased, i.e. a negative voltage is applied to the gate. This corresponds to an accumulation regime in the p-type Si substrate. The microchamber was optically coupled to a long working distance Mitutoyo objective. Thus, light emitted by the devices was then conducted to an Acton 2300i grating spectrometer for analysis and detection through a cryogenically-cooled PI Spec-10-100B/LN charge-coupled device for the visible range or by a PMT detector (H10330-25) for the infrared. EL spectra were corrected using the optical transfer function of the system, calibrated with measurements from a white-emission Xe lamp.

TABLE I. DIFFERENT LAYERS UNDER STUDY.

Sample	Matrix	Annealing conditions	Si excess (%)	Er concentration (at./cm^3)
B1	Si_3N_4	1100°C, 60min.	20	3.0x10^{20}
B2	Si_3N_4	1100°C, 60min.	0	3.0x10^{20}
B3	SiO_2	900°C, 60min.	12	2.0x10^{20}
B4	SiO_2	900°C, 60min.	0	2.0x10^{20}

III. RESULTS AND DISCUSSIONS

Room temperature I-V curves are shown on Fig. 1. Notice that at one fixed voltage, layers with Si excess show better conductivity than stoichiometric layers irrespective of the dielectric matrix. This fact suggests that Si-ncs can modulate the transport properties on both matrices. Moreover, silicon nitrides as matrix for erbium ions and/or Si-ncs, in contrast with silicon oxides, allow higher conductivity (i.e. lower band offsets with respect to Si and higher defect density than silicon oxide).

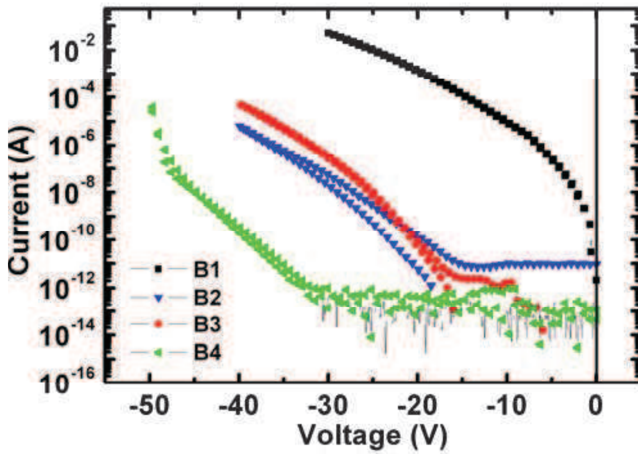

Figure 1. Current-voltage (I-V) characteristics of the devices under study (forward bias).

Furthermore, to better understand the differences observed in the conductivity of the layers, two models commonly used in the literature have been applied to examine the I-V characteristics in amorphous materials. The first one is the Poole-Frenkel (PF) model, which is associated to thermally activated conduction between localized states in the gap assisted by the electric field [5]. It is also known as a bulk-limited conduction mechanism. The second one is the Fowler-Nordheim (FN) that describes the tunnelling of charges through a triangular barrier from the electrode into the active layer [6], or between localized states. However, it has to be mentioned that for the FN case, localized states may refer to shallow defects in the insulator, produced either by a strong electric field or by implantation procedures of additives such as Si or Er ions. In the PF mechanism, the current and the voltage are related by the expression:

$$I \propto V \exp\left[1/k_BT\left(\sqrt{e^3V/\pi\varepsilon_0\varepsilon_r d}\right)\right] \qquad (1)$$

where I is the electrical current, V is the applied voltage on the active layer of thickness d, k_BT is the thermal energy, e is the electron charge, ε_0 is the vacuum permittivity and ε_r is the relative permittivity of the insulator. On other hand, the FN mechanism is governed by the law:

$$I \propto V^2 \exp\left[-\frac{4d\sqrt{2m_{ox}^*\left(e\phi_b\right)^3}}{3\hbar eV}\right] \qquad (2)$$

where m_{ox}^* is the effective mass of electrons in the conduction band, ϕ_b the potential barrier height and $\hbar$ the reduced Planck's constant. Therefore, Fig. 2 shows the curve fitting of such mechanisms using the experimental I-V curves of the studied layers. Indeed, samples containing silicon nitride as host matrices for Er ions present a good agreement with the PF mechanism (Fig. 2 (a)). Likewise, FN mechanism is in better accordance with silicon oxide matrices (Fig. 2 (b)). Hence, this suggests that the conduction for silicon oxides is electrode-limited independently of the probability of having residual defects created during the Er and Si implantation. The implanted Si will only contribute to the barrier height lowering. On the contrary, a bulk-limited conduction is observed for Er-doped silicon nitride samples.

To further analyze the electrical characteristics we have examined either the extracted relative permittivity from PF fitting, or the deduced barrier height from the FN expression. These values are summarized in Table II accordingly. A relative permittivity of 14±1 and 7±1 were deduced for B1 and B2 layers, respectively. The value of 14 is too high to be acceptable; while 7 is physically acceptable with respect to the value of silicon-rich silicon nitride obtained in previous works [7]. Nevertheless, a more complex conduction model is probably needed to better fit the experimental I-V curves (e.g. a model which also takes into account the charge/discharge effects). On the other hand, different barrier height values were extracted from the FN model for Er-doped silicon oxide layers. In particular, those values were (1.6 ± 0.2) eV and (2.7 ± 0.2) eV for B3 and B4, respectively. It has to be mentioned that the obtained values are in agreement with the ones reported in similar layers [8]. In addition, such values also corroborate that mostly electrons are involved in the transport, as larger barrier heights would have been found if holes were responsible for the electric conduction. Even though, it is worth noticing that hole injection in a region close to the Si substrate cannot be discarded [7].

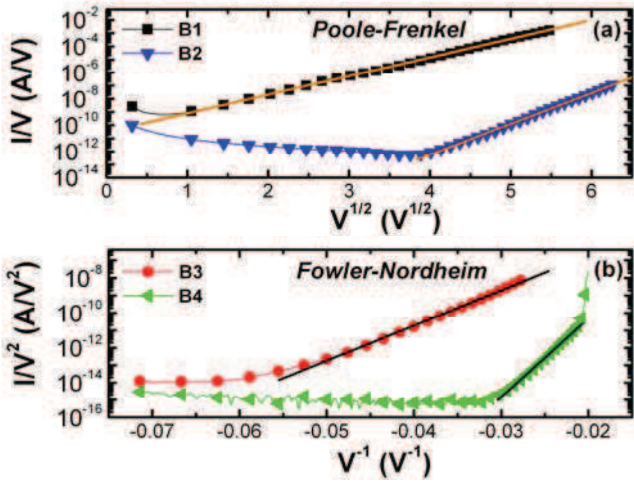

Figure 2. Conduction mechanims of the devices (a) Poole-Frenkel representation for Er-doped silicon nitride matrices (b) Fowler-Nordheim representation for Er-doped silicon oxide matrices.

TABLE II. RELATIVE PERMITTIVITY AND BARRIER HEIGHT OF THE LAYERS EXTRACTED BY FITTING THE I-V CURVES BY THE MODEL PF AND FN, RESPECTIVELY.

Sample	Relative permittivity	Barrier height (eV)
B1	14 ± 1	-
B2	7 ± 1	-
B3	-	1.6 ± 0.2
B4	-	2.7 ± 0.2

Fig. 3 shows the visible and near infrared Er transitions at a fixed current (I=100 µA). In particular, the visible spectrum of B3 shows the typical Si-nc broad emission superimposed to various peaks, whose energy coincides with the higher excited Er transition levels. Interestingly, sample B1 exhibits a broad band spectrum that spans from 500 nm to 990 nm. Two peaks are clearly observed at around of 622 nm and 870 nm, respectively. The emission peak at 622 nm is associated to Si-related defects in the silicon nitride matrix and originated by the implanted Si [9], [10]. Whereas the other band at around 870 nm is ascribed to electron-hole recombination within Si-ncs via quantum confinement [10], whose electron-hole pairs are generated by PF ionization. In addition, Fig. 3 depicts that layers without Si-ncs have higher EL intensity at 1.54 µm at a fixed current than their counterparts with Si-ncs, irrespective of the matrix-type. Therefore, this fact suggests that Si-ncs act as scattering centres for Er ions, competing with them for the impact excitation. Interestingly, this phenomenon can be evidenced on the visible spectra, where B1 (highest Si-ncs excess) does not show any visible Er transition levels. On the contrary, the line-shape of B3, which has lower Si-excess than B1, presents both visible Er levels and Si-ncs contributions. Likewise, we believe that Er excitation in silicon nitrides takes place through impact excitation of hot electrons in the conduction band [3]. Similarly, the impact excitation by means of hot electrons coming from FN-type injection predominates in the Er-doped silicon oxide samples. Also, this latter excitation mechanism of Er ions seems to be more efficient since we observe higher Er emission at 1.54 µm in silicon oxides than in silicon nitride layers, as shown in Fig. 3, although the Er concentration is slightly lower in silicon oxide samples.

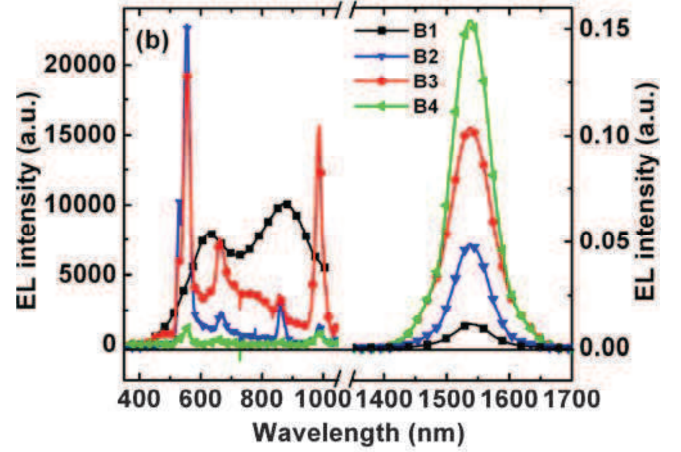

Figure 3. Visible and near infrared EL spectra at constant current (I=100 µA) of the set of devices.

Fig. 4 depicts both how EL at 1.54 µm increases linearly with the injected current and the EL saturation at high injection current regime. This latter fact suggests two possible explanations; (i) all luminescence centers (Er ions) optically active are being excited or (ii) other non-radiative current pathways start to be competitive, diminishing the optoelectronic properties of devices [8].

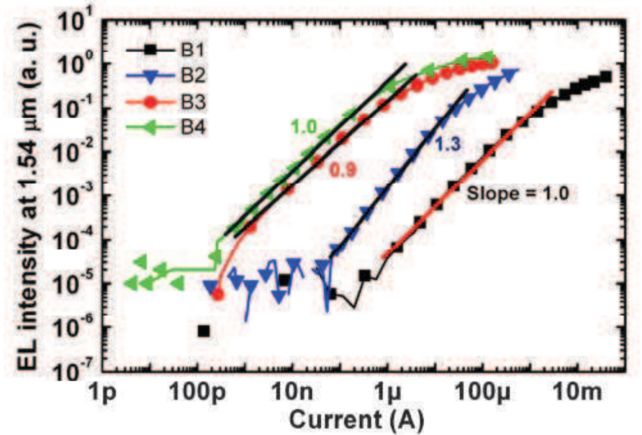

Figure 4. Evolution of the electroluminescence at 1.54 µm as a function of the injected current.

Er-doped silicon oxide devices show better power efficiency (PE) values than Er-doped silicon nitrides. A value around of 0.01 % (highest PE) was found for samples B3 and B4 (see Fig. 5). In addition, silicon nitrides present higher

conductivity than silicon oxides for a given EL level (lower external quantum efficiency). These results suggest that Si-ncs could not be necessary as Er sensitizers under electrical pumping. Moreover, Fig. 5 indicates that high efficiency is paid by a short device operation lifetime (as observed in Er-doped silicon oxide layers) and vice versa (the gain in stability is also paid by a loss of efficiency, as seen in Er-doped silicon nitride layers).

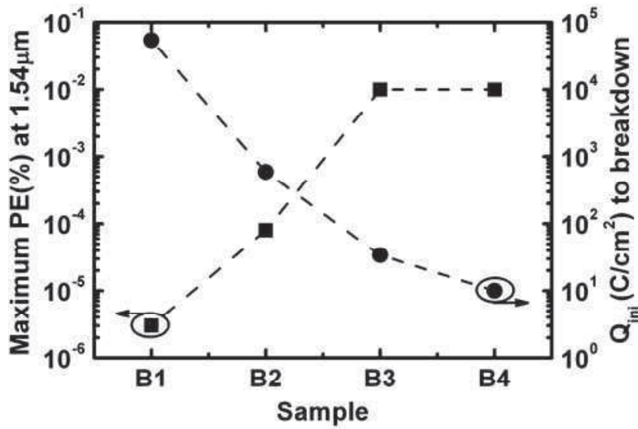

Figure 5. Values of the maximum power efficiency (%) and injected charge (Q_{inj}) to breakdown, both at constant current (-50μA), for each sample.

IV. CONCLUSIONS

In summary, electro-optical properties of four different layers based on Er-doped silicon oxide (or nitride) with (or without) Si-ncs have been studied. From electrical characterization Fowler-Nordheim tunneling mechanism was identified in Er:SiO_2 and Er:SRO layers. Whereas, Poole-Frenkel transport was observed in Er:Si_3N_4 and Er:SRN. The EL of Er ions and Si-ncs either in the visible or in the infrared range were accordingly compared. In addition, Er ions into SiO_2 (or Si-rich oxide) matrices present higher EL and PE at 1.54 μm than Er ions into Si_3N_4 (or Si-rich nitride) layers. Moreover, the existence of a trade off between PE and device operation lifetime was demonstrated. In particular, the high efficiency is paid by a short device operation lifetime (as seen in Er-doped silicon oxide layers) and vice versa (observed in Er-doped silicon nitride layers). Therefore, we believe that the combination of these two materials (e. g. oxynitride matrices or multilayer structures like $SiO_2/Si_3N_4/SiO_2$) might be a competitive alternative to overcome the current device limitations.

ACKNOWLEDGMENT

This work was supported by the European Community through the HELIOS Project (ICT-FP7-224312). Y.B. acknowledges financial support from the Subprograma de Formación de Personal Investigador FPI-MICINN (TEC2009-08359).

REFERENCES

[1] S. M. Sze, and Kwok K. NG, Physics of Semiconductor Devices, 3rd ed. Wiley, New York, 2007.

[2] D. J. Lockwood, and L. Pavesi "Silicon Photonics II, components and integration", Springer, 2011.

[3] O. Jambois, Y. Berencén, K. Hojdak, A. J. Kenyon, F. Gourbilleau, R. Risk, and B. Garrido. "Current transport and electroluminescence mechanisms in thin SiO2 films containing Si nanocluster-sensitized erbium ions", J. Appl. Phys. vol. 106, pp. 063526-063532, (2009).

[4] In Young Kim, Kyung Joong Kim, and Jung H. Shin, "Nanocluster Si sensitized Er luminescence: Excitation mechanisms and critical factors for population inversion", Appl. Phys. Lett. vol. 101, pp. 141907-141911, (2012).

[5] D. M. Pai, "Electric-field-enhanced conductivity in solids", J. Appl. Phys. vol. 46, pp. 5122-5127, (1975).

[6] G. Pananakakis, G. Ghibaudo, R. Kies, and C. Papadas, "Temperature dependence of the Fowler-Nordheim current in metal-oxide-semiconductor structures", J. Appl. Phys. vol. 78, pp. 2635-2642, (1995).

[7] Y. Berencén, Josep Carreras, O. Jambois, J. M. Ramírez, J. A. Rodríguez, C. Domínguez, Charles E. Hunt, and B. Garrido, "Metal-nitride-oxide-semiconductor light-emitting devices for general lighting", Opt. Express vol. 19, pp. A234-A244, (2011).

[8] J. M. Ramírez, F. Ferrarese Lupi, O. Jambois, Y. Berencén, D. Navarro-Urrios, A. Anopchenko, A. Marconi, N. Prtljaga, A. Tejgattini, L. Pavesi, J. P. Colonna, J. M. Fedeli, and B. Garrido "Erbium emission in MOS light emitting devices: from energy transfer to direct impact excitation", Nanotehcnology vol. 23, pp. 125203-125211, (2012).

[9] Z. H, Cen, T. P. Chen, L. Ding, Y. Liu, J. I. Wong, M. Yang, Z. Liu, W. P. Goh, F. R. Zhu, and S. Fung, "Evolution of electroluminescence from multiple Si-implanted silicon nitride films with thermal annealing", J. Appl. Phys. vol. 105, pp. 123101-123104, (2009).

[10] J. Warga, R. Li, S. N. Basu, and L. Dal Negro, "Electroluminescence from silicon-rich nitride/silicon superlattice structures", Appl. Phys. Lett. vol. 93, pp. 151116-151118 (2008).

PAPER IV

Metal-nitride-oxide-semiconductor light-emitting devices for general lighting

Y. Berencén,[1,*] Josep Carreras,[2] O. Jambois,[1]
J. M. Ramírez,[1] J. A. Rodríguez,[3] C. Domínguez,[4] Charles E. Hunt,[2,5] and B. Garrido[1]

[1]*MIND-IN2UB, Dept. Electrònica, Universitat de Barcelona, Martí i Fanquès 1, 08028, Barcelona, Spain*
[2]*IREC, Catalonia Institute for Energy Research, Jardí de les Dones de Negre 1, PL2, 08930, Barcelona, Spain*
[3]*Physics Faculty, University of Havana, San Lázaro y L, Vedado, 10400 Havana, Cuba*
[4]*Instituto de Microelectrónica de Barcelona (IMB-CNM, CSIC), Bellaterra 08193, Barcelona, Spain*
[5]*California Lighting Technology Center,University of California 633 Peña Ave, Davis California, 95618, USA*
**yberencen@el.ub.es*

Abstract: The potential for application of silicon nitride-based light sources to general lighting is reported. The mechanism of current injection and transport in silicon nitride layers and silicon oxide tunnel layers is determined by electro-optical characterization of both bi- and tri-layers. It is shown that red luminescence is due to bipolar injection by direct tunneling, whereas Poole-Frenkel ionization is responsible for blue-green emission. The emission appears warm white to the eye, and the technology has potential for large-area lighting devices. A photometric study, including color rendering, color quality and luminous efficacy of radiation, measured under various AC excitation conditions, is given for a spectrum deemed promising for lighting. A correlated color temperature of 4800K was obtained using a 35% duty cycle of the AC excitation signal. Under these conditions, values for general color rendering index of 93 and luminous efficacy of radiation of 112 lm/W are demonstrated. This proof of concept demonstrates that mature silicon technology, which is extendable to low-cost, large-area lamps, can be used for general lighting purposes. Once the external quantum efficiency is improved to exceed 10%, this technique could be competitive with other energy-efficient solid-state lighting options.

©2011 Optical Society of America

OCIS codes: (230.2090) Electro-optical devices; (150.2950) Illumination.

References and links

1. S. Nakamura, M. Senoh, and T. Mukai, "Highly P-Typed Mg-Doped GaN Films Grown with GaN Buffer Layers," Jpn. J. Appl. Phys. **30**(Part 2, No. 10A), 1708–1711 (1991).
2. F. A. Ponce and D. P. Bour, "Nitride-based semiconductors for blue and green light-emitting devices," Nature **386**(6623), 351–359 (1997).
3. S. Nakamura, M. Senoh, and T. Mukai, "High-power InGaN/GaN double-heterostructure violet light emitting diodes," Appl. Phys. Lett. **62**(19), 2390–2393 (1993).
4. S. Nakamura, M. Senoh, N. Shin-ichi, N. Iwasa, T. Yamada, T. Matsushita, Y. Sugimoto, and H. Kiyoku, "Room-temperature continuous-wave operation of InGaN multi-quantum-well structure laser diodes," Appl. Phys. Lett. **69**(26), 4056–4059 (1996).
5. A. Zukauskas, M. S. Shur, and R. Gaska, *Introduction to Solid State Lighting* (John Wiley and Sons, New York, 2002).
6. E. F. Schubert and J. K. Kim, "Solid-state light sources getting smart," Science **308**(5726), 1274–1278 (2005).
7. Photonics 21 Strategic Research Agenda, http://www.photonics21.org/AboutPhotonics21/SRA.php
8. Multi-Year Program Plan, Solid State Lighting Research and Development, US Department of Energy, http://apps1.eere.energy.gov/buildings/publications/pdfs/ssl/ssl_mypp2009_web.pdf
9. Y.-L. Wang, F. Ren, H. S. Kim, D. P. Norton, and S. J. Pearton, F. Ren, D. P. Norton, and S. J. Pearton, "Materials and Process Development for ZnMgO/ZnO Light-Emitting Diodes," IEEE J. Quantum Electron. **14**(4), 1048–1052 (2008).
10. W. I. Park and G.-C. Yi, "Electroluminescence in n-ZnO Nanorod Arrays Vertically Grown on p-GaN," Adv. Mater. (Deerfield Beach Fla.) **16**(1), 87–90 (2004).

#141485 - $15.00 USD Received 20 Jan 2011; revised 10 Mar 2011; accepted 11 Mar 2011; published 29 Mar 2011

11. L. T. Canham, “Silicon quantum wire array fabrication by electrochemical and chemical dissolution of wafers,” Appl. Phys. Lett. **57**(10), 1046–1048 (1990).
12. L. Pavesi, L. Dal Negro, C. Mazzoleni, G. Franzò, and F. Priolo, “Optical gain in silicon nanocrystals,” Nature **408**(6811), 440–444 (2000).
13. R. J. Walters, G. I. Bourianoff, and H. A. Atwater, “Field-effect electroluminescence in silicon nanocrystals,” Nat. Mater. **4**(2), 143–146 (2005).
14. T. P. Chen, Y. Liu, M. S. Tse, O. K. Tan, P. F. Ho, K. Y. Liu, D. Gui, and A. L. K. Tan, “Dielectric functions of Si nanocrystals embedded in a SiO2 matrix,” Phys. Rev. B **68**(15), 153301 (2003).
15. J. Bu and M. H. White, “Design considerations in scaled SONOS nonvolatile memory devices,” Solid-State Electron. **45**(1), 113–120 (2001).
16. M. Perálvarez, C. García, M. López, B. Garrido, J. Barreto, C. Domínguez, and J. A. Rodríguez, “Field effect luminescence from Si nanocrystals obtained by plasma-enhanced chemical vapor deposition,” Appl. Phys. Lett. **89**(5), 051112–051115 (2006).
17. O. Jambois, Y. Berencen, K. Hijazi, M. Wojdak, A. J. Kenyon, F. Gourbilleau, R. Rizk, and B. Garrido, “Current transport and electroluminescence mechanisms in thin SiO2 films containing Si nanocluster-sensitized erbium ions,” J. Appl. Phys. **106**(6), 063526–063532 (2009).
18. J. F. Ziegler, J. P. Biersack, and U. Littmark, *The Stopping and Range of Ions in Solids* (Pergamon, New York, 1985).
19. M. Perálvarez, J. Barreto, J. Carreras, A. Morales, D. Navarro-Urrios, Y. Lebour, C. Domínguez, and B. Garrido, “Si-nanocrystal-based LEDs fabricated by ion implantation and plasma-enhanced chemical vapour deposition,” Nanotechnology **20**(40), 405201 (2009).
20. S. M. Sze, *Physics of Semiconductor Devices* 2nd ed. (Wiley, New York, 1981).
21. S. Habermehl, R. T. Apodaca, and R. J. Kaplar, “On dielectric breakdown in silicon-rich silicon nitride thin films,” Appl. Phys. Lett. **94**(1), 012905–012908 (2009).
22. W. Chandra and L. K. Ang, “Space charge limited current in a gap combined of free space and solid,” Appl. Phys. Lett. **96**(18), 183501 (2010).
23. J. Warga, R. Li, S. N. Basu, and L. Dal Negro, “Electroluminescence from silicon-rich nitride/silicon superlattice structures,” Appl. Phys. Lett. **93**(15), 151116 (2008).
24. R. Hattori and J. Shirafuji, “Longitudinal electron drift mobility of hydrogenated amorphous silicon/silicon nitride multilayer structures revelealed by time-of-flight measurements,” Appl. Phys. Lett. **54**(12), 1118–1120 (1989).
25. J. Robertson and M. J. Powell, “Gap states in silicon-nitride,” Appl. Phys. Lett. **44**(4), 415–417 (1984).
26. Z. H. Cen, T. P. Chen, Z. Liu, Y. Liu, L. Ding, M. Yang, J. I. Wong, S. F. Yu, and W. P. Goh, “Electrically tunable white-color electroluminescence from Si-implanted silicon nitride thin film,” Opt. Express **18**(19), 20439–20444 (2010).
27. L. Dal Negro, J. H. Yi, L. C. Kimerling, S. Hamel, A. Williamson, and G. Galli, “Light emission from silicon-rich nitride nanostructures,” Appl. Phys. Lett. **88**(18), 183103 (2006).
28. K. A. Nasyrov, S. S. Shaimeev, and V. A. Gritsenko, “Trap-Assisted Tunneling Hole Injection in SiO2: Experiment and Theory,” J. Exp. Theor. Phys. **109**(5), 786–793 (2009).
29. M. Perálvarez and J. Josep Carreras, M. Perálvarez, J. Carreras, J. Barreto, A. Morales, C. Domínguez, and B. Garrido, “Efficiency and reliability enhancement of silicon nanocrystal field-effect luminescence from nitride-oxide gate stacks,” Appl. Phys. Lett. **92**(24), 241104 (2008).
30. CIE, (1995), *Method of Measuring and Specifying Colour Rendering Properties of Light Sources* Publication 13.3, Vienna: Commission Internationale de l'Eclairage, ISBN 978–3900734572.
31. CIE, (1926), *Commission internationale de l'Eclairage proceedings* (Cambridge University Press, Cambridge) p. 1924.
32. W. Davis and Y. Ohno, “Color quality scale,” Opt. Eng. **49**(3), 033602 (2010).
33. J. Carreras, J. M. Quintero, and C. E. Hunt, “Theoretical limits of natural light emulation,” Second CIE Expert Symposium on Appearance, Ghent, Belgium (2010).
34. J. Carreras, J. Quintero, and C. E. Hunt, “Towards the Definition of New Visual Color Quality Representations,” Illuminating Engineering Society (IES) Meeting, Toronto, Canada, (2010).

1. Introduction

The luminous efficacy of Solid State Light (SSL) sources has soared in the last decade from a few lm/W (less than incandescent bulb) to astonishing values in excess of 150 lm/W (superior to high-pressure Na lamps). This has been largely due to the development of III-V nitride compound technology (GaN, GaInN, AlGaN, AlGaInN) in the 90’s, with breakthroughs such as the attainment of p-type doping in GaN [1,2] and the subsequent demonstration of blue and green GaInN double-heterostructure, high-power LEDs and lasers [3,4]. Further improvements in doping, reduction of dislocation density, improved thermal management and the use of multiple quantum wells have made possible the fabrication of high-power LEDs with ever increasing efficacies and emitted power, making them promising for lighting

purposes [5]. Nevertheless, LEDs are quite monochromatic light sources and, their use as white lighting sources requires wavelength conversion either by phosphors or semiconductor wavelength converters [5]. Large Stokes losses (i.e. higher-energy photons are converted into lower-energy photons), integration with phosphor packaging and color drift are limitations of this approach. Other approaches for white-light emission use multicolored LEDs (tri-chromatic and tetra-chromatic) together with color mixing optics. The absence of Stokes loss and good color rendering are promising features, whereas the poor efficiency in current green LEDs, and the color drift of red AlGaInP LEDs, give poor color mixing and low overall efficacy [6]. Normally, the addition of more wavelengths by adding more LED sources facilitates better adjustment of color temperature and color rendering, but this is accomplished at the expense of efficacy, stability and increased cost.

SSL sources for general lighting could save enormous amounts of energy as about 20% of all electricity is consumed for lighting purposes. Environmental savings, in terms of less green-house (CO_2) and poisonous gas emissions (e.g. containing Hg), would also be major benefits [7,8]. Although nitride compound technology has made possible the introduction of SSL, its massive deployment is hampered by the significant cost inherent to III-V technologies and the lack of a suitable substrate for mass fabrication. Additionally, III-V technology does not provide simple routes for integrated white-light emitters without the use of phosphor converters. While organic LEDs (OLEDs) can be made cheaper and have suitable substrates, they are mainly used for diffuse areal lighting in large area devices. Some other disruptive approaches have been proposed such as ZnMgO on ZnO substrates [9] and GaN and ZnO nanowires on cheap substrates [10]. These last approaches circumvent the need of expensive sapphire substrates. However, they still require expensive epitaxial reactors for fabrication.

A new and disruptive approach towards Solid State Lighting is presented here. It is suitable for developing white-light monolithically integrated emitters for lighting purposes. This approach, that we call "Silicon-based Lighting (SiL)," is based on the employment of novel SSL procedures using Silicon and CMOS (or large-area a-Si compatible technology) in its manufacturing. This is accomplished by merging the experience gained from both Silicon Photonics and Solid State Lighting Technology. The scalability, cost-effectiveness and mass-production potential already demonstrated by the silicon semiconductor industry would enable reduced costs and significant penetration of energy-efficient solutions in the marketplaces where nitrided-semiconductor LEDs are challenged for economical massive deployment.

Si-based integrated light sources were first reported in the early 90's, after the discovery of porous silicon and Si-nanocrystals/nanoclusters (Si-nc) visible emission [11–13]. Nanostructuring Silicon produces a dramatic increase in luminescent emission because of quantum confinement of excitons in Si-nc. Confinement brings about relaxation of selection rules for radiative transitions in indirect band-gap silicon. Furthermore, band-gap enlargement dependency on Si-nc size makes possible the tuning of the emission in the red-orange part of the visible spectrum. A suitable matrix that passivates non-radiative centers in Si-nc, and promotes conduction, is desirable for device manufacturability as well as for large internal quantum efficiency of electroluminescence (EL). SiO_x (Silicon Rich Silicon Oxide, SRSO) has been thoroughly studied as a suitable matrix for Si-nc [11–14]. Nevertheless, Si-nc embedded in SiN_x (Silicon Rich Silicon Nitride, SRSN) has emerged as an alternative for its superior transport properties and better color rendering. By combining red-orange emission of Si-nc in SiO_x with green-blue emission of Si-nc in SiN_x we have been able of synthesizing a white light emitting efficient EL material. Although efficacy for the moment remains quite low in our LEDs (less than 1 lm/W), there is room for orders of magnitude of improvement by optimizing the material, improving charge injection and transport, and enhancing extraction efficiency. We believe that this route for developing efficient light sources will eventually become successful, provided the efficacy of devices nears that of existing OLEDs (5-10 lm/W). Silicon or glass wafers are low-cost suitable substrate material for these devices. In

#141485 - $15.00 USD Received 20 Jan 2011; revised 10 Mar 2011; accepted 11 Mar 2011; published 29 Mar 2011
(C) 2011 OSA

addition, Si-based materials open the possibility of integrating LEDs with drivers and control in the same chip, making affordable the concept of System on Chip (SoC) lighting. Economical deposition technology is available in CMOS foundries and large area devices can be fabricated -with application to areal lighting- in a way similar than for solar cells.

In this investigation, we present a metal-nitride-oxide-semiconductor light-emitting device (MNOSLED) as a proof of concept for "Silicon-based Lighting" (SiL). These first non-optimized MNOSLEDs are driven as MOS capacitors and transistors. Experimental details and electrical and electro-optical studies are presented in Sections 2 and 3, respectively. Photometric analysis of the MNOSLED is presented in section 4, including color rendering, color quality and luminous efficacy of radiation. The emphasis is to assess the applicability of this device as a potentially low-cost, high-quality SSL white-light source.

2. Experimental details

Generally speaking, we define a MOSLED as a metal-oxide-semiconductor field-effect capacitor or transistor (MOSFET) with a transparent gate electrode. The 'oxide', depending on design and material properties, is frequently substituted by a gate stack or a composite material, although we use to maintain the MOSLED name. For the particular type of device presented here we also use the term MNOSLED to enhance the fact that we have introduce a bi-layer (or tri-layer) in a similar way as for the MNOS memories [15]. The electrodes used in previous designs include semitransparent metals, thin polysilicon and indium tin oxide (ITO) [16,17]. The electrode preferred in current devices is a thin (100 nm), semitransparent n-type (phosphorous) heavily-doped polysilicon. This choice emphasizes compatibility; and for this reason the devices have been entirely fabricated in a standard CMOS line. The drawback of using a thin 100 nm polysilicon gate is its varying (non-flat) transmission in the visible spectrum due to a Fabry-Perot interference pattern and its low transmission in the blue [16]. Two dielectric or gate stack structures have been designed and fabricated in this investigation, as depicted in Fig. 1(a). The first one is a bi-layer of very thin tunneling silicon oxide (3 nm) and a silicon nitride transport layer (26 nm). The second one is a tri-layer which includes an extra-thin silicon oxide layer (3 nm) on top of the previous structure. The purpose of the thin oxide layers is to provide a well-passivated interface with silicon, and to act as tunnel and control dielectrics for the current (hole and electron injection) in the central thick nitride layer.

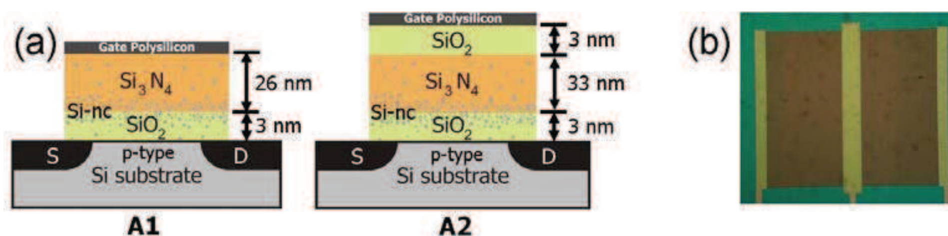

Fig. 1. (a) Cross-sectional view of the two Silicon Nitride MNOSLED structures under study. A1: Tunnel oxide (SiO_2) + Si_3N_4 and A2: Tunnel oxide (SiO_2) + Si_3N_4 + control oxide (SiO_2). (b) Top view of a typical device. The semi-transparent gate electrode is the central rectangle with dimensions 10µm x 500 µm.

The excess Si which (upon thermal annealing) forms the Si-nc has been introduced by ion implantation. A single dose of $4x10^{16}$ atoms/cm^2 of Si has been implanted at 20 keV to form the structure A1 and at 30 keV to form the structure A2, shown in Fig. 1. These implant parameters were chosen after SRIM [18] simulations performed to obtain a Si excess of 19% with its peak distribution close to the lower oxide/nitride interface in both cases (Fig. 2). After ion implantation, the wafers were annealed in an N_2 atmosphere at 1000°C for 1 hr to induce phase separation forming the Si-nc. Transmission electron microscopy (not shown) was performed and revealed Si nanoclusters in the bottom SiO_2 layer, whereas no Si-nc could be observed in the Si nitride, either because they are too small to be observed, or because Si-

#141485 - $15.00 USD Received 20 Jan 2011; revised 10 Mar 2011; accepted 11 Mar 2011; published 29 Mar 2011
(C) 2011 OSA

based defects are more likely to be created in Si nitrides. Additionally, the top control oxide in A2 is completely free of Si-nc and should act as a current-flow limiting layer.

The Source/Drain regions of the n-channel MNOSLEDs were formed by phosphorous implantation. The thin polysilicon gate electrode was deposited by low-pressure chemical vapour deposition (LPCVD) at 780°C and degenerately doped with $POCl_3$. The process sequence employed standard MOS procedures, resulting in the final transistor structure, as seen (top view) in Fig. 1(b). P-type silicon substrates were used for both structures.

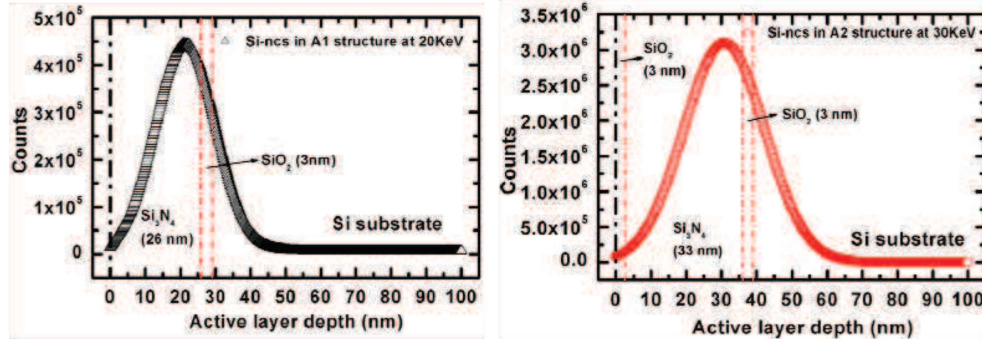

Fig. 2. SRIM simulation profile for each structure.

Quasi-static current-voltage (I-V) measurements were performed using a semiconductor parameter analyzer (Agilent B1500A) with high-power/high-resolution units coupled to a probe station (Cascade Microtech Summit 11000) using Faraday isolation (microchamber). The devices are forward biased, that is, a negative voltage is applied to the gate. This corresponds to an accumulation regime in the p-type Si substrate. As seen later, this enables the activation of the Si-nc in the SRSO layer that are expected to emit in the red [13,16]. The microchamber was optically coupled to a long working distance Mitutoyo objective. The EL spectra in AC excitation were obtained by applying a square waveform to the gate by means of an Agilent 8114A Pulse Generator. Thus, light emitted by the devices was then conducted to an Acton 2300i grating spectrometer for analysis and detection by a cryogenically-cooled PI Spec-10-100B/LN charge-coupled device. Device emission spectra were corrected using the optical transfer function of the system, calibrated with measurements from a white-emission Xe lamp.

3. Electro-optical characterization

Figure 3(a) depicts the J-V characteristics of structures A1 and A2 in the accumulation regime (negative voltage to the gate, p-type substrate). The devices show clear rectifying behavior. In the inversion regime (not shown), the limited flow of minority carriers from the substrate (electrons) saturates the current at μA levels. For accumulation, electrons are injected from the polysilicon gate and get through the silicon nitride and eventually through the whole structure to the substrate. Although holes from the accumulation layer in the substrate find a much larger band offset, the presence of Si-nc in the oxide layer constrains a certain injection level to traps close to the interface. Hole injection, from silicon substrate to Si-nc, has been demonstrated from negative flat band voltage shifts in similar structures [19]. J-V characteristics confirm that structure A2 has a much higher onset voltage and resistive behavior than structure A1. This is due to the presence of the 3 nm thick control oxide at the top. The maximum current density is –65.6 A/cm^2 and –8.8 A/cm^2 for A1 and A2, at the maximum voltage before breakdown, which is –25V and –28V, respectively. These voltages correspond to an electric field of approximately 10 MV/cm. These current density values are three orders of magnitude higher than those reported for a silicon oxide matrix [13,16]. Thus, silicon nitride as a matrix for Si-nc - in contrast with silicon oxide - allows for higher bulk-

#141485 - $15.00 USD Received 20 Jan 2011; revised 10 Mar 2011; accepted 11 Mar 2011; published 29 Mar 2011
(C) 2011 OSA

limited currents (higher conductivity) and higher injection-limited currents (lower band offsets with Si).

We have plotted in Fig. 3(b) the J-V curves in the Poole-Frenkel representation. The Poole-Frenkel model is a conduction mechanism based on bulk-limited currents and is well suited for silicon nitride and other dielectrics with a significant concentration of traps [20]. Electrons or holes are hopping from thermally-activated traps assisted by the electric field. The Poole-Frenkel expression is:

$$J \propto E \exp\left[\left(1/k_B T\right)\sqrt{e^3 E / \pi\varepsilon_0\varepsilon_r}\right],$$

where J is the electrical current density, E is the applied field on the active layer of thickness d, k_BT is the thermal energy, e is the electron charge, ε_0 is the vacuum permittivity and ε_r is the relative permittivity of the insulator. Good agreement is found with the Poole-Frenkel conduction model from low to medium voltage (roughly to 5-6 MV/cm, Fig. 3 (b)). From the fits we have found a relative permittivity of approximately 7, which is consistent with the value for a SRSN layer [21]. At higher electric fields, the J-V curves depart from the exponential behavior and enter in a regime where the current is increasing with the square of the voltage, as can be seen in Fig. 3 (c). Such behavior in dielectrics is generally attributed to space charge limited current (SCLC) [20,22]. This corresponds to more carriers being trapped in the defects of the dielectric at higher voltages, resulting in space-charge build-up which limits the current [20,22]. The SCLC regime is given by:

$$J = 9\varepsilon_0\varepsilon_r\mu E^2 / 8d,$$

where μ is the drift mobility and the other parameters are as in the previous equation. In Fig. 3(a), such a change in the conduction regime can be appreciated in the change of slope of the J-V curves at 15-20V for A1. A SCLC type of conduction has been reported for SRSN by Warga et al [23]. Following this equation, we find an electron mobility of 1.25 x 10^{-5} $cm^2/(V{\cdot}s)$ which is one order of magnitude lower than the value reported in ref [24] for Si nitrides.

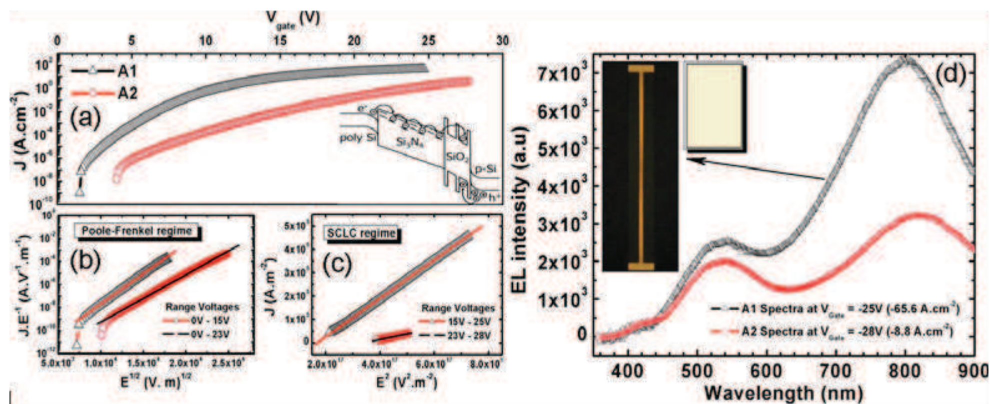

Fig. 3. (a) Current density (J) vs. gate voltage (V) plot for the MNOSLED. The inset shows the band diagram for struture A1 (b) Poole-Frenkel representation at low voltages. (c) Space charge-limited current representation at high voltages. (d) EL spectra at maximum voltage for both devices. The inset shows the EL emission of A1. This photograph was taken with a standard digital commercial camera. The white square on the right side represents the color extracted directly from the spectrum, which may be interpreted as a true-white correction.

Si implant profiles, shown in Fig. 2, have been designed to form Si-nc inside the oxide layer and in the nitride layer close to the interface with the oxide. The EL spectra of the devices under study with two broad peaks around 805 nm and 535nm are shown in Fig. 3(d).

#141485 - $15.00 USD Received 20 Jan 2011; revised 10 Mar 2011; accepted 11 Mar 2011; published 29 Mar 2011
(C) 2011 OSA

The inset of Fig. 3(d) shows a photograph of the MNOSLED device (A1) with the emitted orange-white light. A bi-layer or tri-layer structure like those reported here are expected to have red-infrared luminescence from Si-nc in the oxide and/or nitride and blue-green luminescence of Si based defects in the silicon nitride [19,25,26]. Note that when silicon precipitates have been observed (by electron microscopy) in a silicon nitride matrix, red emission is reported as well [23]. However, in our case, Si-ncs have not been observed into silicon nitride. Consequently, the peak around 535 nm is attributed to the luminescence of the SRSN. In particular, it has been reported that luminescent centers associated to defects, such as Si-dangling bonds located in the middle of the band-gap, as well as bonding states of Si-Si units that are close to the valence band edge, emit at this wavelength [25,26]. In similar layers, luminescence lifetimes in the ns and µs range are ascribed to silicon nitride defects and Si-nc into silicon oxide matrix, respectively, according to dynamic studies reported [19,27]. It should also be noted that the transmittance spectrum of a 100 nm thick polysilicon layer has resonances at 470 nm and 760 nm. Therefore, it is expected that the measured spectra are reinforced at those frequencies. Transparent conducting oxides (TCO) will be used in subsequent optimized devices.

It is desired to emit light using the mechanism of excitation of the luminescent centers (Si-nc in oxide and Si-defects in nitride). It is extremely important to engineer the active material to enhance radiative recombination and/or decrease non-radiative recombination and thus optimize the internal quantum efficiency (IQE). Excitation efficiency of luminescent centers is closely related to the mechanism of injection. Tunnel bipolar injection of electrons and holes from opposite electrodes into Si-nc is an efficient way to create excitons in Si-nc from cold carriers. This tunnel injection is expected for a defective layer where the Poole-Frenkel mechanism of conduction takes place, and is attributed to the excitation mechanism of Si-nc in SRSO and defects in SRSN. Electrons do travel by Poole-Frenkel from the poly gate to the Si-nc and defects in the oxide and nitride, while holes are injected into a few nanometers of the SRSO by tunneling from the accumulation layer in the p-type Si substrate (see inset of Fig. 3(a)) [19,28]. To add in favor of this, when we bias the structure in inversion, only the green-blue peak is detected. This is clearly due to the lack of injected holes from the gate electrode. With regards to the emission from Si-related defects in SRSN, the injected electrons activate the luminescent centers by Poole-Frenkel ionization. The two different structures analyzed in this work only differ in external quantum efficiency (EQE). The relative intensity of the red and green bands is related to the details of the Si-excess profile in the nitride/oxide bi-layer and can be tailored due to photometric requirements, as we will demonstrate in the next section. The best emitting devices obtained, thus far, belongs to a series of bi-layer devices emitting in the red, with almost negligible Si-excess in the nitride layer and a peak up to 0.1% power efficiency which corresponds to a 1% EQE [29].

4. Photometric characterization

In order to investigate the potential impact of this technology as a candidate to replace mainstream lighting, the photometric characteristics have to be analyzed in-depth. In particular, we are interested in the determination of color rendering and quality as well as in the overall efficacy of such a device. Although the former can be straightforwardly analyzed by using standard CIE color rendering metrics for broadband sources, like general color rendering index (CRI) [30], the latter is not easy to determine, because of the impossibility to presently evaluate all of the potential available for improvement in the external quantum efficiency which exists for this technology.

Considering that a lighting device's total wall-power to illuminant efficiency, η, is the product of multiple efficiency elements, e.g. $\eta = \Pi\ \eta_i$, Luminous Efficacy of Radiation (LER) is one of the critical multiplicative factors affecting η of a source. In this section, we restrict our energy analyses to the study of LER, which means that we are leaving aside other energy loss mechanisms occurring inside the device such as non-radiative recombination, charge

#141485 - $15.00 USD Received 20 Jan 2011; revised 10 Mar 2011; accepted 11 Mar 2011; published 29 Mar 2011
(C) 2011 OSA

injection, light extraction (that were treated in the preceding sections), as well as external factors such as power-supply efficiency.

In order to maximize LER, it would be ideal to keep the spectral content of the light source in a small region around 555 nm, where the sensitivity of the human eye peaks according to the CIE Luminosity Function [31]. However, doing so limits the color span that the source can correctly render. Obviously, the choice to prioritize energy efficiency or color reproduction depends ultimately upon the particular application under consideration. In Fig. 4 are shown the spectra obtained under different excitation conditions that involve changes in excitation voltage (Fig. 4(a)), period of the excitation signal (Fig. 4(b)), and duty cycle of the excitation signal (Fig. 4(c)). Moreover, the right columns in the same plot show color trajectories in the CIE 1931 diagram that are experienced under these excitation changes.

The XYZ CIE 1931 diagram is a color map that contains all the perceivable colors to humans. Blackbody radiators, such as the sun and other hot objects, including flames, are considered natural. This means that the color coordinates of any artificial light source intended for general lighting should lie very close to the blackbody locus plotted in dotted white lines in the CIE diagrams of Fig. 4. The tolerance of deviation from the blackbody locus is usually measured in the U*V*W* space by a distance termed Δ_{uv} (or simply D_{uv}), and usually the general rule of $D_{uv}<0.0054$ is applied for white light sources targeting natural appearance. However, this is not an absolute requirement, since it has been argued that slight out-of-blackbody-locus illumination is acceptable, as long as it is supported by color preference schemes in detriment of naturalness of the light source [32].

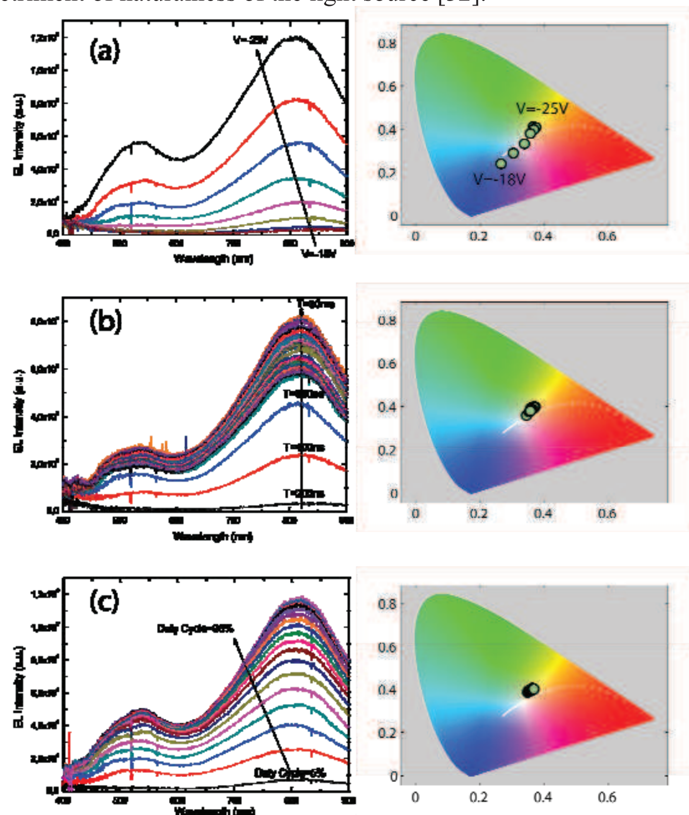

Fig. 4. Color shifts in the CIE 1931 diagram produced under a change in (a) excitation voltage (T = 10µs and DC = 50%), (b) period of the excitation signal (V = –25V and DC = 50%) and (c) duty cycle of the excitation signal (V = –25V and T = 10µs).

#141485 - $15.00 USD   Received 20 Jan 2011; revised 10 Mar 2011; accepted 11 Mar 2011; published 29 Mar 2011
(C) 2011 OSA

The most remarkable fact derived from the XY trajectories followed under different excitation conditions, is that important color shifts can only be obtained by changing the voltage amplitude of the excitation waveform. This procedure gives rise to a Correlated Color Temperature (CCT) span of 3310K, from 4385K to 7695K, covering a great number of important applications in lighting ("normal white" being considered CCT = 5500K). However, it does not cover the interesting warm CCT of around 3000K that is typical of the omnipresent incandescent light bulb. This warmer white could be easily worked out through the material's optimization by slightly shifting the peak centered at 535nm towards the red region.

As shown in the detailed photometric study of the spectra set in Fig. 5, changes of 90% in the duty cycle (DC), allow only modest changes in the perceived CCT, covering the range between 4500K and 5000K. It is worth noting that this occurs without a substantial change in D_{uv}, thus preserving the naturalness of the original spectrum. In other words, time-related changes in the excitation waveform lead to modest shifts in color but preserve D_{uv} or "follow" the blackbody locus, while changes in the excitation voltage give rise to notable color shifts but at the expense of bringing about instabilities in the naturalness of the light produced.

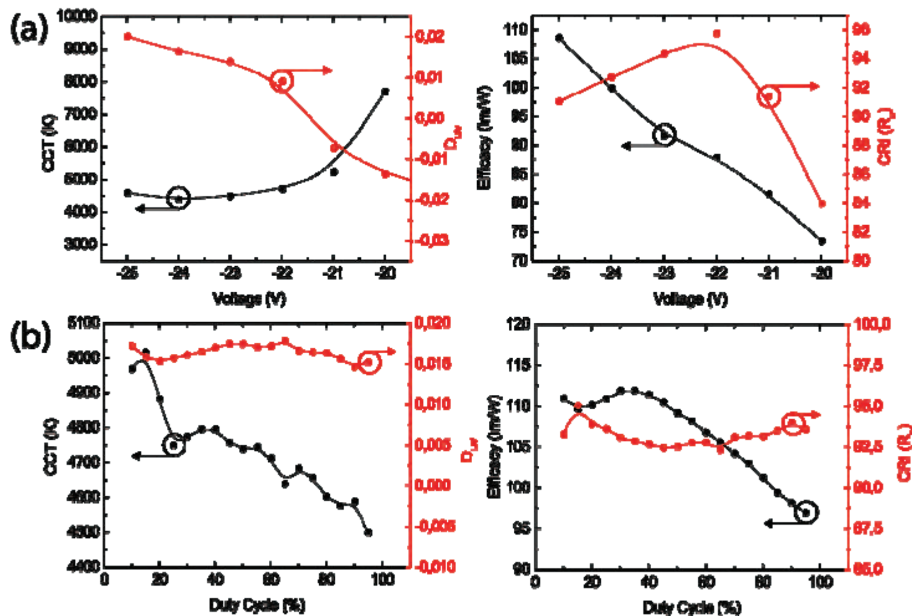

Fig. 5. Dependence of Correlated Color Temperature (CCT), deviation from the blackbody locus (D_{UV}), Luminous Efficacy of Radiation (LER) and Color Rendering Index (CRI) on Voltage (a) and on Duty Cycle (b).

In addition to control of spectral content, the present international energy-conservation effort mandates the consideration of the luminous efficacy of radiation or LER. At the same time, LER optimization alone cannot result in a light source which correctly reproduces colors, because low acceptance by the public would limit its market penetration. Recent studies have established theoretical limits up to where these two inversely correlated variables can be jointly optimized [33]. These studies demonstrate that for [3000K,5500K,8000K] spectra, it is physically possible to obtain efficacies of [363,313,288] lm/W while maintaining general CRIs over 90, ensuring outstanding light quality within the most important regions of the Munsell gamut.

These theoretical values indicate that efficacies shown in the second column plots of Fig. 5 can be substantially enhanced by optimizing the materials to emit only in the visible range,

#141485 - $15.00 USD Received 20 Jan 2011; revised 10 Mar 2011; accepted 11 Mar 2011; published 29 Mar 2011
(C) 2011 OSA

eliminating the loss of efficacy that arises from the near-infrared portion of the spectra shown in Fig. 4 as was mentioned in the section 3.

Similar to what is observed with color shifts (CCTs), the dependence of CRI and efficacy on voltage, is much stronger than on duty cycle. In addition, luminous efficacies as high as 112 lm/W and general CRIs above 93 are achievable for DCs of 35%. By analyzing in detail this optimized spectrum of about CCT = 4800K, we can further evaluate up to what extent it would render colors in a wide color gamut by utilizing the so-called Color Rendering Map (CRM) presented elsewhere [34]. In Fig. 6, a set of scores are represented by color-coding (from blue to red, corresponding to R_m values from 0 to 100) and plotting over a tracing of the Munsell gamut area of an original CIE 1931 color-space chart as illustrated in the inset of Fig. 6(b). The plot created by these scores represents the most significant saturation levels and hues, as defined in the Munsell color system. This system is widely accepted by both the display and lighting communities. For the Reader's reference, the Munsell gamut color space, around the CIE white point from the CIE 1931 chart, is depicted in Fig. 6(a). From it, the identification of the color that a particular score represents (visually depicted in the color bar of the Fig. 6(b)) is directly found by comparison.

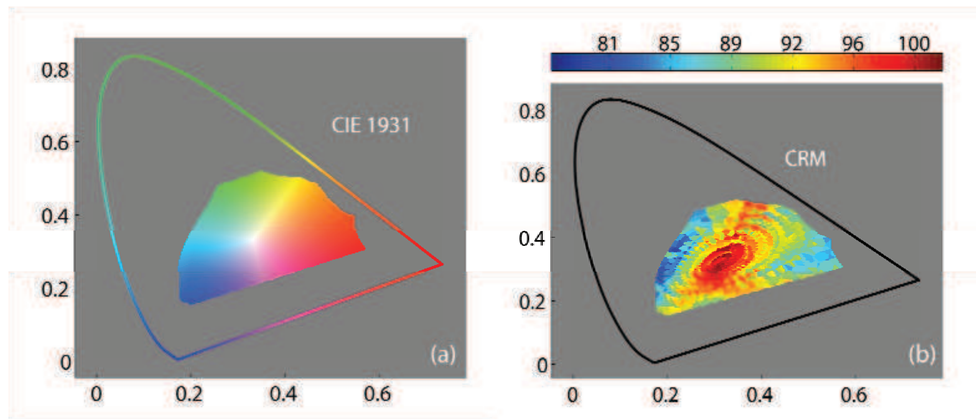

Fig. 6. (a) Musell region in the CIE 1931 diagram. (b) Color Rendering Map (CRM) of the spectrum excited through a waveform of –25V amplitude, 10µs period and 35% duty cycle.

By direct inspection, one sees that the optimized 4800K spectrum that has an general CRI of 93, presents good color rendering all along the Munsell region, always satisfying R_m>80 no matter what color is trying to reproduce. This is indeed the most convincing argument that enables us to conclude that the light produced by MNOSLEDs with Si_3N_4 and Si nanocrystals fulfills all the requirements required in the lighting industry in terms of color rendition and quality.

The external quantum efficiency of all-silicon light sources represents, at this time, the most important challenge. In fact, although the promise of omnipresent and high color quality silicon lighting is quite appealing because of the price reduction, integration, large area, etc., the small wall-plug (W) to light (W) efficiency in this technology is clearly the most limiting factor that prevents its general application at this point. The fact the emission spectrum can be adjusted depending on particular needs through material and/or device engineering indicates that superior LER than in the results presented here can be achieved.

For the sake of illustration, if the target total efficacy for this technology was fixed to 30 lm/W, to compete with commercial OLEDs, assuming a LER of approximately 300 lm/W would indicate that external quantum efficiencies near 10% would be required. This requires a challenging one order of magnitude increase, minimum, in the emission efficiency. It is worth noting that the spectral content can potentially be narrowed to the visible region by means of material's optimization (basically by eliminating part of the near-infrared tail produced by the

#141485 - $15.00 USD Received 20 Jan 2011; revised 10 Mar 2011; accepted 11 Mar 2011; published 29 Mar 2011
(C) 2011 OSA

Si nanocrystals EL), so that it is realistic to anticipate that the LER could be increased up to 300 lm/W, without a detriment in color quality.

5. Conclusion

We have presented in this work some potential of silicon-based white-lighting SSL devices for general lighting. From the two structures studied, the SiO_2 + Si_3N_4 bilayer structure shows better electro-optical properties in terms of injected current and optical power. Emission visible to naked eye was exhibited. Furthermore, for this bilayer it is found that the spectral content obtained is excellent in terms of light quality for use in general lighting. Several spectra for these devices have been analyzed, and the most promising has been identified as a 4800K spectrum, with general CRI of 93 and LER of 112 lm/W. We believe that this technology can start to be competitive as commercial SSL once the barrier of the 10% in quantum efficiency of light extracted from silicon-based materials can be reached.

Acknowledgments

YB acknowledges financial support from the Subprograma de Formación de Personal Investigador FPI-MICINN (TEC2009-08359). JC acknowledges funding from the Ministry of Science and Innovation (MICINN) through project SILENCE[2] (TEC2010-17472) and for sample fabrication in the Integrated Nano and Microelectronics Clean Room at IMB-CNM through the ICTS access program, (project ICTS-NGG-31).

#141485 - $15.00 USD Received 20 Jan 2011; revised 10 Mar 2011; accepted 11 Mar 2011; published 29 Mar 2011
(C) 2011 OSA

PAPER V

Blue–green to near-IR switching electroluminescence from Si-rich silicon oxide/nitride bilayer structures

Y. Berencén,[1,*] O. Jambois,[1] J. M. Ramírez,[1] J. M. Rebled,[1,4] S. Estradé,[1,5] F. Peiró,[1] C. Domínguez,[2] J. A. Rodríguez,[3] and B. Garrido[1]

[1]*MIND-IN2UB, Dept. Electrònica, Universitat de Barcelona, Martí i Fanquès 1, 08028, Barcelona, Spain*

[2]*Instituto de Microelectrónica de Barcelona (IMB-CNM, CSIC), Bellaterra 08193, Barcelona, Spain*

[3]*Physics Faculty, University of Havana, San Lázaro y L, Vedado, 10400, Havana, Cuba*

[4]*Institut de Ciència de Materials de Barcelona-CSIC, Campus UAB, Bellaterra 08193, Barcelona, Spain*

[5]*TEM-MAT, CCiT-UB, Solé i Sabarís 1, 08028, Barcelona, Spain*

**Corresponding author: yberencen@el.ub.es*

Received March 2, 2011; revised May 27, 2011; accepted June 14, 2011; posted June 14, 2011 (Doc. ID 143511); published July 11, 2011

Blue–green to near-IR switching electroluminescence (EL) has been achieved in a metal-oxide-semiconductor light emitting device, where the dielectric has been replaced by a Si-rich silicon oxide/nitride bilayer structure. To form Si nanostructures, the layers were implanted with Si ions at high energy, resulting in a Si excess of 19%, and subsequently annealed at 1000 °C. Transmission electron microscopy and EL studies allowed ascribing the blue–green emission to the Si nitride related defects and the near-IR band with the emission of the Si-nanoclusters embedded into the SiO_2 layer. Charge transport analysis is reported and allows for identifying the origin of this two-wavelength switching effect. © 2011 Optical Society of America

OCIS codes: 250.0250, 230.2090, 230.6080, 260.3800.

Silicon-rich silicon oxide (SRSO) and silicon-rich silicon nitride (SRSN) have drawn great interest in the last decades as active dielectric matrices in optoelectronic devices [1–4]. Particularly, these materials have been used in the fabrication of low-cost light emitting devices compatible with the mainstream Si technology, They also provide a solution to the monolithic integration of electronic and optical technologies on the same Si chip. Different electroluminescence (EL) excitation mechanisms have been reported, such as hot electrons [5] and optically active defects [6] or field-effect EL using pulsed excitation [1]. The EL emission of the Si-nanocrystals (Si-ncs) embedded in SiO_2 is usually in the red-IR and shows a narrow shift capability depending on Si-nc size [1,3]. Regarding Si nitrides, luminescence in the blue–green is also reported, ascribed either to Si nitride related defects or Si-ncs [4,7]. In addition, some strategies have been employed in order to extend the EL emission to different spectral region. For instance, defects created by dopants such as rare-earth ions can lead to light emission from UV to near-IR, depending on their specific energy level structure [8].

In this Letter we report two-wavelength switching metal-nitride-oxide-semiconductor light emitting devices (MNOSLED) based on a SRSO/SRSN bilayer structure.

The devices are similar to metal-oxide-semiconductor field-effect transistors with a 100 nm thick polycrystalline silicon layer used as an optically transparent gate electrode. Since its transmittance spectrum peaks at 470 nm and 760 nm [3], the final EL spectra of the devices are modulated accordingly. In order to combine light emission from different matrices, a SRSO/SRSN bilayer structure was designed *ad hoc* to form the insulator of the transistor. The Si excess in the SiO_2 and Si_3N_4 layers was introduced by ion implantation. A subsequent annealing treatment at 1000 °C during one hour was performed to recover the matrices and precipitate the Si-ncs. The implantation parameters (energy and dose) were chosen by stopping and range of ions in matter simulations to obtain a Si excess of 19%, attending to photoluminescence studies in previous works [7]. Energy filtered transmission electron microscopy (EFTEM) measurements were performed using a JEOL 2010-FEG (200 kV) microscope equipped with a Gatan imaging filter for EFTEM imaging mode. Moreover, due to the importance of the proper localization of the geometry of the devices, the cross section was defined by a focused ion beam. (Dual Strata- FEI Company).

Electrical measurements using a semiconductor parameter analyzer (Agilent B1500A) and a probe station (Cascade Microtech Summit 11 000) were accomplished at room temperature. Both source and drain were grounded during forward (or backward) bias, in order to improve the injection into the bilayer. By convention, it is considered that a negative direct current (dc) voltage applied to the polysilicon electrode corresponds to forward polarization (accumulation regime). Room temperature EL spectra were measured through an Acton 2300i grating spectrometer and a cryogenically cooled PI Spec-10-100B/LN charge-coupled device. The final spectra were corrected for the spectral response of the optical system.

Figure 1(a) shows an EFTEM cross section picture of the bilayer structure of the device under study. The zone at the border of the polycrystalline silicon (pc-Si) is formed by a silicon nitride layer about 28 nm thick. No Si-ncs were observed inside this region, in accordance with Ref. [9]. Moreover, the zone between silicon nitride and crystalline silicon (*c*-Si) is a silicon oxide layer about 13 nm thick. Si-ncs with a mean size of 3.8 ± 0.5 nm and embedded into this material are clearly observed in the image. In Fig. 1(b) a typical scheme of the device structure is presented.

The *I-V* curves (Fig. 2) are quite symmetrical for both polarities in the whole range of dc voltages, which suggests that, (i) leakage current is mainly due to electrons,

0146-9592/11/142617-03$15.00/0 © 2011 Optical Society of America

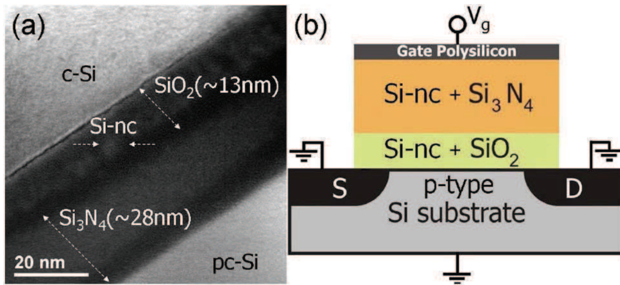

Fig. 1. (Color online) (a) Cross section EFTEM image showing the SRSO/SRSN bilayer and Si-ncs into the SiO_2 layer. (b) Scheme of the light emitting device structure.

and (ii) the current is limited by the active layer and not by the electrode [10], although the dielectric structures are not symmetric. In addition, a strong saturation is observed at high voltages, attributed to the spatial charge formed at the interface between substrate or electrode (depending on the applied voltage) and the active layer, in agreement with previously published works [2]. The inset shows the good concordance of the experimental data, in accumulation and inversion regimes, with two different conduction mechanisms depending on the voltage values. At low voltages, the Poole-Frenkel (PF) mechanism is predominant, whereas at high voltages the space charge-limited current (SCLC) mechanism predominates. By fitting the experimental data to the theoretical expressions corresponding to these mechanisms [10] (see inset of Fig. 2), the average values obtained for the relative permittivity and the drift mobility in accumulation and inversion regime are $\varepsilon_r = 7.2$ and $\mu = 1.42 \times 10^{-5}\ \mathrm{cm^2/V{\cdot}s}$. According to effective medium theory, the value of ε_r can vary between 3.9 and 7.5, depending on the SiO_2 and Si_3N_4 permittivities, respectively. Therefore, this suggests that the ε_r-value deduced in the present work is physically correct. Likewise, the value of μ in our SRSO/SRSN bilayer is 1 order of magnitude lower than the value ($10^{-4}\ \mathrm{cm^2/V{\cdot}s}$) observed in the SRSN layer by Warga *et al.* [2], and 3 orders of magnitude higher than the value ($10^{-8}\ \mathrm{cm^2/V{\cdot}s}$) in the SRSO layer reported by Ryabchikov *et al.* [11]. This fact suggests the existence of a trade-off between the drift mobility values of the SRSN and SRSO layers, which indicates that the μ-value obtained is physically acceptable. Consequently, the electron mobility into the bilayer used in the present work will be mostly limited by the SRSN layer.

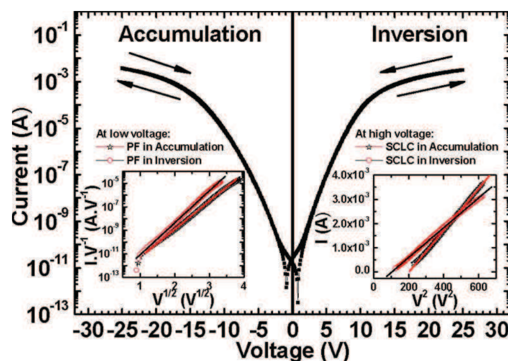

Fig. 2. (Color online) *I-V* characteristic in accumulation and inversion. The inset shows the PF and SCLC fits in both regimes at low and high voltages, respectively.

An interesting switching effect is observed in Fig. 3, not reported before for MNOSLED based on SRSN/SRSO bilayer structure. By changing the dc voltage sign applied to the gate, the line-shape varies completely, thus leading to a switchable EL from a blue–green spectrum at positive dc voltage (inversion regime) to a near-IR spectrum at negative dc voltage (accumulation regime).

This difference can be understood by considering the radiative recombination processes taking place in each of the SRSN and SRSO single layers in both cases. At negative dc voltages, electrons are injected from gate to substrate through the bilayer following a PF conduction mechanism and, simultaneously, holes injection from the Si substrate into the few nanometer SRSO layer occurs [12]. (As mentioned above, no transport of holes is observed). Thus, the electrons find positively charged Si-ncs embedded into SiO_2, due to hole injection and the creation of excitons takes place (see left inset of the Fig. 4). Therefore, bipolar injection by direct tunneling in the SRSO leads to the near-IR light emission around 800 nm reported in the Fig. 3, in accordance with previous results [2,3], whereas the little blue–green peak (~535 nm) in the same spectrum is ascribed to defects of the SRSN, such as Si-dangling bonds located in the middle of the Si_3N_4 bandgap, as well as to bonding states of Si—Si units that are close to the valence band edge [4,13], which are optically activated by PF ionization. On the contrary, when a positive dc voltage is applied to the gate, the channel is formed in the *p*-type substrate when both source and drain are grounded, leading electrons to flow from the channel to the gate through Si-nc to Si-nc in the SRSO layer and defect to defect in the SRSN layer (see right inset of the Fig. 4). If voltage is large enough, the defects of the SRSN are optically activated, thus producing solely the blue–green light emission (~515 nm), which is attributed to PF ionization. It implies that the excitation of the Si_3N_4 defects, in this case, dominates over excitation of the Si-ncs into the SiO_2 layer (emission at ~800 nm). This latter fact is only possible in an inversion regime due to the lack of injected holes from the electrode. Time-resolved EL measurements were

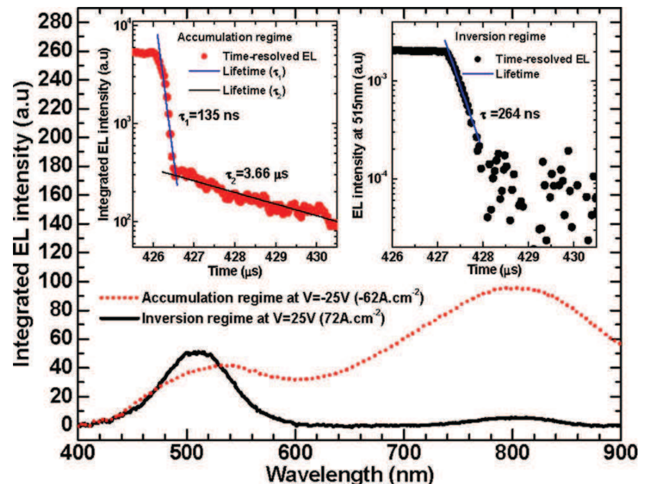

Fig. 3. (Color online) EL spectra for both gate polarities. Inversion regime (black solid line) and accumulation regime (red dot line). The inset shows the lifetimes of each luminescent species in both gate polarities.

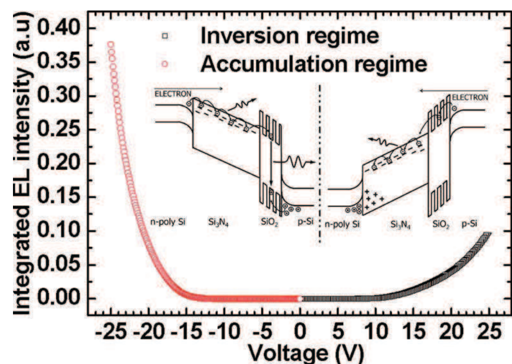

Fig. 4. (Color online) Integrated EL intensity versus voltage in accumulation and inversion regimes. The inset depicts the band diagram for both cases.

performed in both gate polarities using square pulses of 1 kHz. Two lifetimes (135 ns and 3.66 μs) were measured in accumulation (see left inset Fig. 3) ascribed to Si nitride related defects and excitonic recombination inside the Si-ncs, respectively. Whilst, in an inversion regime, solely a fastest lifetime was detected (see right inset Fig. 3), thus confirming the previous analysis. Moreover, in a typical Arrhenius plot (graph not shown) the activation energy of the traps (Si nitride related defects) drops as the driving voltage increases. This observation is consistent with a PF-type mechanism, where the thermal ionization is assisted by the applied electric field. The activation energy value found was 0.32 eV at 5 MeV/cm, which closely agrees with the value reported by Sze (0.64 eV at the same electric field) [10] for a single silicon nitride films. Si-based light emitters using an Eu-implanted SiO_2 single layer have been previously reported [6], where two colors were generated considering the two different transition energies of the Eu^{2+} (~2 eV) and Eu^{3+} (2.5 eV–3 eV), respectively. However, very large operating voltages (>105 V) are needed to excite either Eu^{2+} or Eu^{3+}, whereas a similar effect is obtained here with voltages five times lower (reducible by decreasing insulator thickness) and without rare-earth ion doping.

Finally, Fig. 4 depicts the integrated EL intensity versus voltage in accumulation and inversion regimes. Observe that the EL intensity increases with the applied voltage for both gate polarities. However, for accumulation it is larger than for inversion at ±25 V, which implies that the devices in accumulation are more effective in terms of optical power. This phenomenon suggests that by electrical pumping, Si-ncs in SiO_2 act as better luminescent centers than the Si nitride related defects (see Fig. 3).

In conclusion, a blue–green to near-IR switching EL has been demonstrated from an SRSO/SRSN bilayer structure by changing the gate dc voltage polarity in MNOSLED. The EL emission peaks in each spectrum were ascribed to Si-ncs into SiO_2 and defects in Si_3N_4. These results suggest that this structure allows the activation of two kinds of luminescent species due to the injection and transport properties of the whole bilayer. This work opens interesting perspectives on Si-based full-color microdisplays.

This work was supported by the Spanish Ministry of Science and Innovation (projects ICTS-NGG-31, TEC2009-08359, MAT2010-16407 and CSD2009-00013).

References

1. R. J. Walters, G. I. Bourianoff, and H. A. Atwater, Nat. Mater. **4**, 143 (2005).
2. J. Warga, R. Li, S. N. Basu, and L. Dal Negro, Appl. Phys. Lett. **93**, 151116 (2008).
3. M. Perálvarez, J. Barreto, J. Carreras, A. Morales, D. Navarro-Urrios, Y. Lebour, C. Domínguez, and B. Garrido, Nanotechnology **20**, 405201 (2009).
4. Z. H. Cen, T. P. Chen, Z. Liu, Y. Liu, L. Ding, M. Yang, J. I. Wong, S. F. Yu, and W. P. Goh, Opt. Express **18**, 20439 (2010).
5. A. Irrera, D. Pacifici, M. Miritello, G. Franzò, F. Priolo, F. Iacona, D. Sanfilippo, G. D. Stefano, and P. G. Fallica, Appl. Phys. Lett. **81**, 1866 (2002).
6. S. Prucnal, J. M. Sun, W. Skorupa, and M. Helm, Appl. Phys. Lett. **90**, 181121 (2007).
7. J. Barreto, M. Perálvarez, A. Morales, B. Garrido, J. Montserrat, and C. Domínguez, J. Mater. Res. **23**, 1513 (2008).
8. J. M. Sun, W. Skorupa, T. Dekorsy, M. Helm, L. Rebohle, and T. Gebel, Appl. Phys. Lett. **85**, 3387 (2004).
9. R. Huang, H. Dong, D. Wang, K. Chen, H. Ding, X. Wang, W. Li, J. Xu, and Z. Ma, Appl. Phys. Lett. **92**, 181106 (2008).
10. S. M. Sze, *Physics of Semiconductor Devices*, 2nd ed. (Wiley, 1981).
11. Yu. V. Ryabchikov, P. A. Forsh, E. A. Lebedev, V. Yu. Timoshenko, P. K. Kashkarov, B. V. Kamenev, and L. Tsybeskov, Semiconductor **40**, 1052 (2006).
12. M. V. Fischetti, D. J. DiMaria, S. D. Brorson, T. N. Theis, and J. R. Kirtley, Phys. Rev. B **31**, 8124 (1985).
13. J. Robertson and M. J. Powell, Appl. Phys. Lett. **44**, 415 (1984).

PAPER VI

Correlation between charge transport and electroluminescence properties of Si-rich oxide/nitride/oxide-based light emitting capacitors

Y. Berencén,[1,a)] J. M. Ramírez,[1] O. Jambois,[1] C. Domínguez,[2] J. A. Rodríguez,[3] and B. Garrido[1]

[1]*MIND-IN2UB, Dept. Electrònica, Universitat de Barcelona, Martí i Fanquès 1, 08028 Barcelona, Spain*
[2]*Instituto de Microelectrónica de Barcelona (IMB-CNM, CSIC), Bellaterra, 08193 Barcelona, Spain*
[3]*Physics Faculty, University of Havana, San Lázaro y L, Vedado, 10400 Havana, Cuba*

(Received 28 April 2012; accepted 5 July 2012; published online 14 August 2012)

The electrical and electroluminescence (EL) properties at room and high temperatures of oxide/nitride/oxide (ONO)-based light emitting capacitors are studied. The ONO multidielectric layer is enriched with silicon by means of ion implantation. The exceeding silicon distribution follows a Gaussian profile with a maximum of 19%, centered close to the lower oxide/nitride interface. The electrical measurements performed at room and high temperatures allowed to unambiguously identify variable range hopping (VRH) as the dominant electrical conduction mechanism at low voltages, whereas at moderate and high voltages, a hybrid conduction formed by means of variable range hopping and space charge-limited current enhanced by Poole-Frenkel effect predominates. The EL spectra at different temperatures are also recorded, and the correlation between charge transport mechanisms and EL properties is discussed. © *2012 American Institute of Physics*. [http://dx.doi.org/10.1063/1.4742054]

I. INTRODUCTION

Over the past years, intensive investigations have been devoted to the development of efficient silicon-based optically active materials that would permit the photonics and electronics integration in the same chip.[1–10] Silicon-rich silicon nitride (SRSN) and silicon-rich silicon oxide (SRSO) materials have mostly been considered due to their good emission properties (under optical and electrical excitation) and compatibility with the mainstream complementary metal oxide semiconductor (CMOS) technology.[1–8] Much effort has been dedicated to improve the electroluminescence (EL) intensity as well as the efficiency of the light-emitting devices.[1–4] Published works span from those centering the attention on the material optimization in terms of the different fabrication processes,[6,7] to those that mostly focus on the electrical and EL properties.[8–10] Efficient light-emitting devices have already been demonstrated using either SRSN or SRSO films.[2,4]

In former papers, we have reported the development of metal-nitride-oxide-semiconductor light-emitting devices that we called MNOSLEDs.[9,10] A typical structure of metal-oxide-semiconductor field effect transistor (MOSFET), where the gate oxide was substituted by an oxide/nitride (ON, bi-layer) or oxide/nitride/oxide (ONO, tri-layer) gate stack was used. The photometric analysis conducted in these layers represented a proof of concept for the development of silicon-based solid state lighting.[9] Until that time, no report on the use of silicon ONO-structure in electroluminescent devices had previously been published.

Two well defined bands in the EL spectra were reported in those papers: one in the near-infrared, attributed to excitonic recombination in silicon nanocrystals (Si-ncs) embedded in the tunnel SiO_2 layer and the other in the blue-green, ascribed to Si-related defects in Si_3N_4 film. Moreover, a preliminary analysis of the charge transport mechanism as well as a correlation with the electroluminescent properties was accomplished. However, neither study of the electrical conduction nor EL dependence with temperature was reported in Ref. 9 or in Ref. 10 for the ONO-based devices to firmly confirm the proposed assertions. To gain more in-depth into the physics of these mechanisms, in this paper we present a detailed study of the charge transport and electroluminescent mechanisms as a function of temperature. The MNOSLEDs studied are driven as capacitors (light-emitting capacitors), which are simpler devices than transistors from the technological and electrical viewpoint. They are based on ONO multidielectric stack. Details of the device structure as well as of the experimental measurements are given in Sec. II. The experimental results and the analysis of the electrical and electro-optical properties are discussed in Sec. III.

II. EXPERIMENTAL DETAILS

The ONO multidielectric structures were fabricated by plasma-enhanced chemical vapor deposition (PECVD) technique on B-doped p-type ⟨100⟩ Si wafer. The layer thicknesses were measured with a Gaertner L117 ellipsometer (incident He-Ne laser wavelength of 632.8 nm). The results achieved for the ONO stack are (4.2 ± 1.6)nm (top SiO_2), (29.1 ± 3.4)nm (Si_3N_4), and (7.4 ± 2.2)nm (bottom SiO_2), respectively. A silicon excess of 19% was introduced by means of ion implantation at 30 KeV and a Si dose of 4×10^{16} atoms/cm^2, after transport of ions in matter (TRIM) simulations.[11] To lower the potential barrier height and favor the hole injection from substrate into ONO active layers, the maximum of Si ions profile is centered near the lower oxide/

[a)]Author to whom correspondence should be addressed. Electronic mail: yberencen@el.ub.es. Tel.: +34 93 4039175. Fax: +34 93 4021148.

 © 2012 American Institute of Physics

nitride interface (see inset of Fig. 1(a)). Subsequently, an annealing treatment at 1000 °C for 1 h was performed to recover dielectric matrices from implantation induced defects and produces a phase separation with precipitation on Si-ncs. A semitransparent polycrystalline silicon gate electrode of 100 nm thick was deposited by low-pressure chemical vapor deposition (LPCVD) at 630 °C and highly doped with $POCl_3$ at 950 °C. The ohmic contact to the lower surface of the silicon substrate was obtained by depositing 600 nm of aluminium and subsequently annealing it at 450 °C in forming gas. The device-to-device isolation was achieved by means of shallow trench isolation (STI) technique and growing a thermal oxide of 400 nm thick in the trench. The overall process sequence used follows the standard MOS procedures, which results in the final capacitor structure, as illustrated in the inset of Fig. 1(a). The device area is 5×10^{-5} cm^2.

Light emission coming from the polysilicon region was collected with a Seiwa 888 L microscope coupled to a probe station and driven through an internal system of lens to the sensitive area of detector. EL spectra were recorded with a cryogenically cooled Princeton Instruments Spec-10-100B/LN charge-coupled device and an Acton 2300i grating spectrometer. Decay EL trace was obtained with a digital GHz oscilloscope connected to a photomultiplier (R928) and a photon counter (SR430) synchronously triggered by an Agilent 8114 A pulse generator. Spectra were corrected with the optical response of the system. The electrical characterization of the devices was accomplished with a semiconductor device analyser (Agilent B1500) and a probe station (Cascade Microtech Summit 11000) with a thermal chuck system and a Faraday cage (microchamber). All the electrical and electro-optical measurements were conducted at room temperature and at different temperatures ranging from 25 °C to 300 °C.

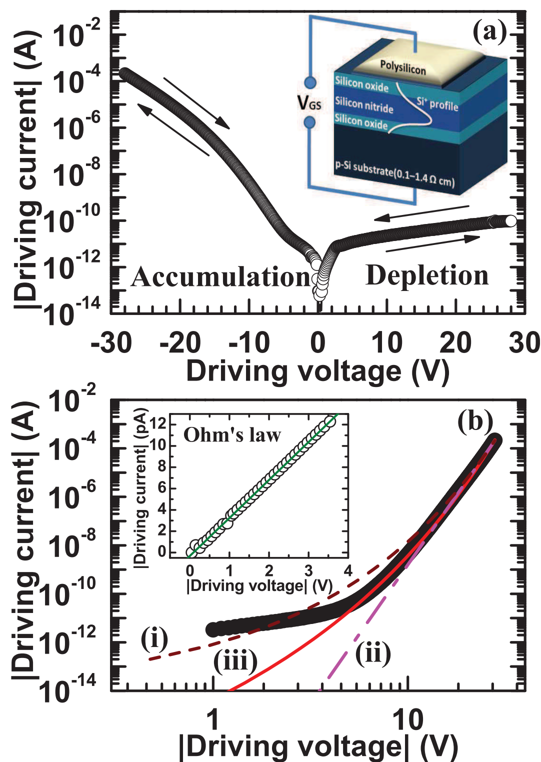

FIG. 1. (a) Typical $I(V)$ curve for light emitting capacitors based on Si-rich ONO gate stack. Inset shows a cross-sectional view and bias scheme of the devices. (b) Experimental data of $I(V)$ curve in accumulation fitted according to the different electrical conduction models listed in Table I. Schottky emission (dashed line), SCLC (dashed dotted line), and SCLC enhanced by PF effect (solid line). Inset shows the ohmic behavior at low voltages regime.

III. RESULTS AND DISCUSSION

Current-voltage characteristics $I(V)$ were first recorded at room temperature between −28 V (accumulation of the substrate, forward bias, negative voltage applied to gate) and +28 V (depletion of the substrate). A typical $I(V)$ curve is shown in Fig. 1(a). A notable rectifying behavior is seen for the devices, i.e., a very low driven current is seen in depletion regime. This feature is because of the low supply of minority carriers by the inverted substrate (electrons). It has to be also mentioned that such a depletion effect (and thus rectifying behavior) did not occur in the MNOSLED transistor structures[10] since the minority carriers can be supplied from the highly doped source and drain regions of the transistor. In the accumulation regime, a good conductivity at low and high voltages is observed. Accordingly, different conduction mechanisms (both electrode- and bulk-limited current models) were studied in detail for the $I(V)$ curves in accumulation.

Figure 1(b) shows $I(V)$ experimental data in the accumulation regime and the theoretical curves corresponding to the mechanisms and expressions listed in Table I. An ohmic dependence is observed in the inset of Fig. 1(b) for $V < \sim 3.5$ V (absolute values will be used here after). This fact could be associated with a variable range hopping-type (VRH) conduction through the localized states related with the Si-ncs.[12] The resistivity at room temperature is about 2.4×10^{16} Ω.cm at $V = 3.5$ V ($F = 0.8$ MeV/cm) which is of the same order of magnitude as that of the typical insulators.[13] Furthermore, the Schottky emission and space charge-limited current (SCLC) models are fitted to the expressions listed in Table I ranging from 3.5 V up to device breakdown (see Fig. 1(b) curves (i) and (ii), respectively). However, for this voltage range (3.5 V–28 V), the best fit is achieved with a space charge-limited current enhanced by Poole-Frenkel (PF) effect mechanism (Fig. 1(b), curve (iii)). Therefore, in this wide voltage range, the conduction is governed by a bulk-limited mechanism involving the presence of trap levels in the gap.

To confirm this assertion, before discussing the two models proposed (VRH at low voltages and SCLC enhanced by PF effect at moderate and high voltages) in more details, an Arrhenius plot has been done in accumulation regime for

TABLE I. Mechanisms of electrical conduction in insulators usually studied, and their expected current-voltage dependences.

Type of conduction	Current-voltage relation
(i) Schottky emission[14]	$I \sim \exp(aV^{1/2}/kT)$
(ii) SCLC[15]	$I \sim V$ (low fields) $I \sim V^n$ ($n > 1$, high fields)
(iii) Space charge-limited currents enhanced by Poole-Frenkel effect[16]	$I \sim V^2\exp(aV^{1/2}/kT)$

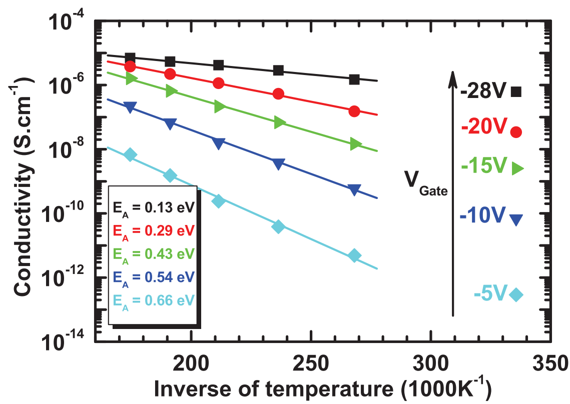

FIG. 2. Dependence between conductivity and temperature in an Arrhenius plot at different driving voltages.

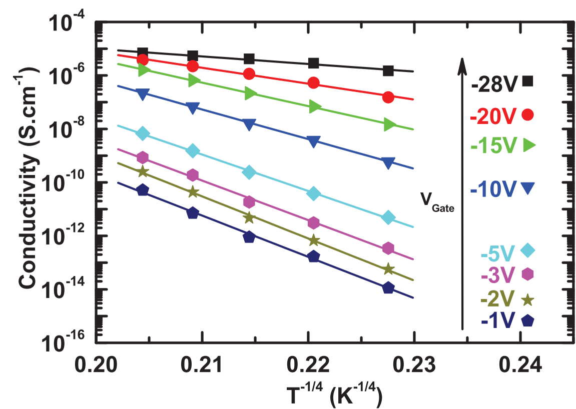

FIG. 3. Temperature dependence of the conductivity in a Mott's law plot at different driving voltages.

various driving voltages (see Fig. 2). The linear dependence observed at moderate and high voltages suggests that the existence of a thermally activated conduction mechanism (e.g., Poole-Frenkel conduction), whose average activation energy (E_A) is around 0.41 eV. This value is in close agreement with that one reported by Sze (0.64 eV) for a single stoichiometric Si_3N_4 layer.[13] In addition, further analysis of Fig. 2 shows that the activation energy decreases as the driving voltage increases. This behavior is physically acceptable as long as we consider the existence of a trap level, whose energy barrier for carrier excitation is gradually lowered by the electric field. Therefore, the activation energy E_A can be interpreted as the minimum carrier energy required to surmount the potential barrier existing between occupied and unoccupied sites.

A. Low voltages: Variable range hopping

As the conduction mechanism for silicon nitride and other dielectrics with a significant concentration of traps is mostly bulk-limited and thermally activated, we will consider the existence of a hopping-type conduction at the Fermi level located below the conduction band (at about 0.41 eV within the band gap). Thus, a VRH conduction would take place, as was originally described by Mott and Davies.[17] In such a regime, conforming to the Mott's law the conductivity is expected to vary with the temperature (T) according to exp $(-BT^{-1/4})$, where $B = 2.06(\alpha^3/kN_F)^{1/4}$, k is the Boltzmann constant in eV, N_F is the density of states at Fermi level, and α^{-1} is the localization length characterizing the decay of the wave-function at a site. Consequently, Fig. 2 has been recalculated in a $T^{-1/4}$ representation including the low voltage range values and the resulting plot is depicted in Fig. 3. The linear behavior obtained demonstrates that the temperature dependence of the conductivity can be explained by the Mott's principle. The average value of the slope found for various driving voltages was $B = 195\mathrm{K}^{1/4}$. Thus, if we take $\alpha = 2$ nm, which is the mean radius of our Si-ncs,[10] we find that $N_F \cong 1.12 \times 10^{18}\,\mathrm{cm}^{-3}.\mathrm{eV}^{-1}$. Moreover, considering that the hopping distance R and the width of the defect band ω in the VRH conduction mechanism are given by

$$R = \left(\frac{9}{8\pi\alpha N_F kT}\right)^{1/4} \quad \text{and} \quad \omega = \frac{3}{4\pi N_F R^3},$$

respectively,[17,18] we find that $R \cong 8$ nm at 300 K and $\omega = 0.42$ eV. This latter value is in agreement with the value of 0.41 eV of the Fermi level located below the conduction band. Hence, the temperature dependence of the conductivity with $\sim\exp(-BT^{-1/4})$ obtained, clearly demonstrates a pure VRH mechanism at low voltages, which is mediated by the localized states associated with the Si-ncs and/or traps distributed along the ONO multidielectric structure. By this way, we also prove the initial assumption concerning to the origin of the ohmic component. In addition, from Fig. 3, we want to stress the fact that the VRH conduction mechanism is also present at moderate and high voltages. Therefore, there will be a hybrid conduction coming from VRH and SCLC enhanced by PF effect mechanisms.

B. Moderate and high voltages: Variable range hopping + space charge-limited current enhanced by Poole-Frenkel effect

The space charge-limited current theory assumes that the trap barrier height is constant for any applied field. However, Murgatroyd[16] demonstrated that at high electric fields, the trap barrier height is lowered due to the Poole-Frenkel effect. This reduction in the barrier height increases the current level higher than that predicted by the standard space charge-limited current theory.[16,19] As can be seen in Fig. 1(b) (curve (iii)) at moderate and high voltages, the $I(V)$ curves depart from the ohmic behavior (linear) at low voltages and enter in a regime where the ratio I/V^2 proportionally raises with the square root of the voltage. Such electrical conduction feature in insulators is generally ascribed to space charge-limited current enhanced by Poole-Frenkel effect as was initially described by Murgatroyd.[16] The $I(V)$ relationship for SCLC enhanced by PF effect mechanism is given by the following expression:

$$I = \frac{9}{8}\mu\varepsilon_0\varepsilon_r S\frac{V^2}{d^3}\theta\exp\left\{\frac{0.891}{kT}\left(\frac{e^3V}{\pi\varepsilon_0\varepsilon_r d}\right)^{1/2}\right\},$$

where $\theta = N_c/N_t\,\exp(-E_A/kT)$ is the ratio of free to trapped electron concentration, N_c is the effective density of states in the conduction band, N_t is the density of traps, kT is the

thermal energy, S is the area of gate electrode, e is the electron charge, μ is the drift mobility, ε_0 is the vacuum permittivity, and ε_r is the relative permittivity of the insulator; while the factor 0.891 is derived from a numerical solution of the continuity equation. Assuming a relative permittivity of 7 and a drift mobility value of $1.25 \times 10^{-5} cm^2/(V \cdot s)$, which were previously reported in similar structures,[9] we have found from fit a value of $\theta = 8.62 \times 10^{-12}$. Therefore, by using the former expression relating this parameter (θ) with N_c, N_t, E_A, and kT we are able to estimate the value of density of traps (N_t) in our Si-rich ONO multidielectric structures. Taking the typical value of $N_c \cong 10^{19} cm^{-3}$ (e.g., for Si, $N_c = 2.8 \times 10^{19} cm^{-3}$), $E_A = 0.41$ eV and $kT = 0.025$ eV we find $N_t \cong 10^{22} cm^{-3}$. This value is three orders of magnitude higher than for the Si non-implanted ONO structures reported by Maruyama and Shirota,[20] which suggests that the Si-ions implantation increases the density of traps in the layers irrespective of the post-annealing process. This result demonstrates and put in perspective the fact that Si-ncs could act as charge trapping centers. Obviously, the probability of occupancy of the traps depends on the Fermi-Dirac distribution function.

Summarizing the results obtained in Secs. III A and III B, we conclude that VRH is purely present at low voltages, whereas at moderate and high voltages a hybrid conduction formed by means of VRH and SCLC enhanced by PF predominates.

C. EL properties and correlation with charge transport mechanisms

Figure 4 depicts the evolution of the EL spectra as a function of temperature. It is observed that the whole visible range and part of the near-infrared are covered. Two peaks are exhibited, one centered at 1.5 eV and other broad one spanning from 2.0 eV to 3.0 eV with the maximum at 2.2 eV. The combination gives rise to a quasi-white light emission extending over the near-infrared region. The line-shape of EL spectra does not change with temperature but EL intensity for both peaks drops as the temperature increases, thus suggesting an increase of non-radiative recombination. In addition, inset of Fig. 4 shows two EL decay lifetimes (290 ns and 8.33 μs). These values were extracted from time-resolved EL measurements at room temperature by applying step-like voltage pulses to the gate with a period of 1 ms ranging from −28 V to 0 V. Moreover, both EL trace decays were well-fitted by means of a single exponential function. These lifetime values are in accordance with those recently reported by us for MNOSLED transistor structures.[10] As a result, the fastest lifetime is attributed to Si-related defects or traps present in silicon nitride matrix, likely reinforced by Si-ion implantation, whereas the lowest component corresponds to excitonic recombination due to quantum confinement effects in Si-ncs embedded into SiO_2 bottom layer.

We have also plotted the EL spectra as a function of the driving current, as can be seen in Fig. 5. It has to be noticed that both EL peaks increase with the driving current and there are not remarkable spectral changes. This fact suggests that all luminescence species (defects and Si-ncs) are being simultaneously excited. Moreover, the inset of Fig. 5 shows a power law between the integrated EL intensity and the driving current, whose dependence is linear ($\Gamma = 1$). This observed linearity between the integrated EL and the driving current in combination with the absence of EL spectral changes suggests a univocal correlation between the injected carriers and the excited ones (i.e., Si-related defects in Si_3N_4 matrix and Si-ncs embedded into SiO_2, respectively).

The precedent results allow correlating the charge transport with the EL properties of our devices. Indeed, since the threshold voltage to get EL is around 11 V, the EL emission takes place in the range 11 V–28 V, where the electrical conduction is fully dominated by VRH and SCLC enhanced by PF effect mechanisms. Thus, electrons flow from the gate electrode through the traps present in the ONO multidielectric structures via VRH conduction and simultaneously, the trap filling process starts. This former phenomenon occurs in the voltage range from 3.5 V to 11 V before the EL emission begins. Therefore, when the electric field is strong enough ($F > 3$ MeV/cm ($V > 11$ V)) to induce the lowering of the trap barrier height, the EL emission at 2.2 eV takes place. This emission band is correlated with the PF-type ionization of the Si-related traps in Si_3N_4 matrix.[9,10] Meanwhile, the

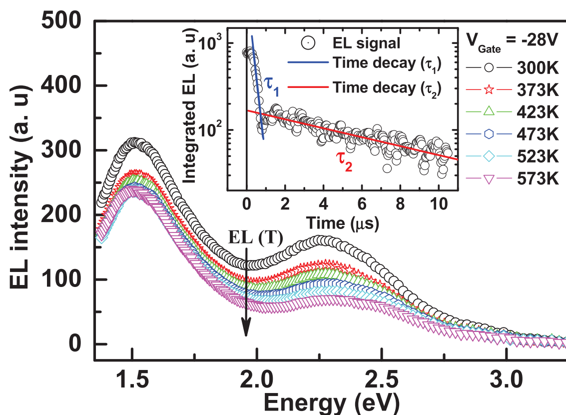

FIG. 4. Typical EL spectra for Si-rich ONO-based light emitting capacitors and their evolution as a function of the temperature. The inset shows both EL lifetimes at room temperature corresponding to Si-related defects or traps in Si_3N_4 ($\tau_1 = 290$ ns) and excitonic recombination onto Si-ncs in SiO_2 ($\tau_2 = 8.33$ μs), respectively.

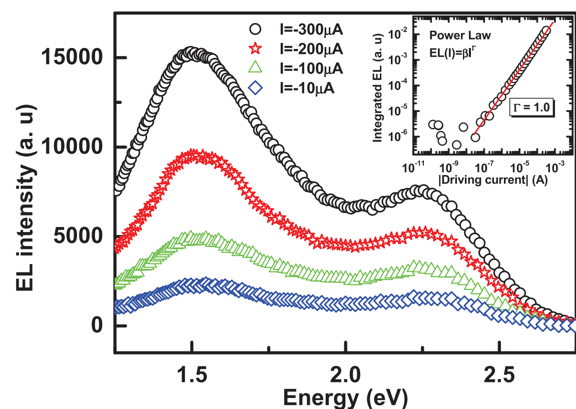

FIG. 5. EL spectra at different driving currents. Inset shows linear dependence between integrated EL intensity and driving current.

emission peak at 1.5 eV appears due to the excitonic recombination, thanks to the holes injected from the substrate into the Si-ncs embedded in the bottom layer of SiO_2,[10,21] which are recombined with the electrons injected from the gate electrode (i.e., bipolar injection).

The most distinctive difference observed between Si-rich ONO-based light emitting capacitors presented here and MNOSLEDs transistor structures previously studied lies on the electrical properties due to presence of the drain and source currents in the MNOSLEDS. As a consequence, the integrated EL intensity is higher in the transistors than the capacitors although the two EL bands are equally exhibited on both devices in accumulation regime. Nevertheless, the advantage of using MNOS capacitors instead of MNOS transistors rests on its simple structure and simple fabrication process, as well as its simplicity of analysis from the electrical and EL properties viewpoint.

IV. CONCLUSION

In summary, we have studied and correlated the charge transport and electroluminescence properties of Si-rich ONO-based light emitting capacitors from their temperature dependence. Two electrical mechanisms govern the conduction in the devices. In particular, they are variable range hopping at low voltages and variable range hopping with space charge-limited currents enhanced by Poole-Frenkel effect at moderate and high voltages, respectively. With the conduction model (VRH) at low voltages we found that the electrical conduction takes place at the Fermi level located at around 0.42 eV within the band gap, whose density of states is about $1.18 \times 10^{18}\,cm^{-3}.eV^{-1}$. Whereas at moderate and high voltages, from the SCLC enhanced by PF effect conduction model, we found that the density of the traps (N_t) is about $10^{22}\,cm^{-3}$. In addition, two EL peaks at 1.5 eV and 2.2 eV were simultaneously observed in the VRH with SCLC enhanced by PF effect conduction mechanism and correlated with the two different lifetimes noticed in the time-resolved EL measurements. Furthermore, each lifetime (290 ns and 8.33 μs) was ascribed to a PF ionization of the Si-related traps in Si_3N_4 and to an electron-hole recombination in the Si-ncs embedded in SiO_2 bottom layer, respectively. Therefore, the predominant EL excitation mechanism proceeds through the VRH and SCLC enhanced by PF effect at moderate and high voltages in which holes and electrons recombine in the Si-ncs embedded in SiO_2 bottom layer, simultaneously with the Si-related trap EL emission in the Si_3N_4 layer.

ACKNOWLEDGMENTS

The authors acknowledge funding from the Ministry of Science and Innovation (MICINN) for sample fabrication in the Integrated Nano and Microelectronics Clean Room at IMB-CNM through the ICTS access program (Project No. ICTS-NGG-31). Y.B. acknowledges financial support from the Subprograma de Formación de Personal Investigador FPI-MICINN (TEC2009-08359).

[1] J. Warga, R. Li, S. N. Basu, and L. Dal Negro, Appl. Phys. Lett. **93**, 151116 (2008).
[2] A. Marconi, A. Anopchenko, M. Wang, G. Pucker, P. Bellutti, and L. Pavesi, Appl. Phys. Lett. **94**, 221110 (2009).
[3] Z. H. Cen, T. P. Chen, Z. Liu, Y. Liu, L. Ding, M. Yang, J. I. Wong, S. F. Yu, and W. P. Goh, Opt. Express **18**, 20439 (2010).
[4] M. Perálvarez, J. Carreras, J. Barreto, A. Morales, C. Domínguez, and B. Garrido, Appl. Phys. Lett. **92**, 241104 (2008).
[5] D. Li, J. Huang, and D. Yang, Physica E **41**, 920 (2009).
[6] A. López-Suárez, J. Fandiño, B. M. Monroy, G. Santana, and J. C. Alonso, Physica E **40**, 3141 (2008).
[7] B. Shankar Sahu, F. Delachat, A. Slaoui, M. Carrada, G. Ferblantier, and D. Muller, Nanoscale Res. Lett. **6**, 178 (2011).
[8] A. A. González-Fernández, J. Juvert, A. Morales-Sánchez, J. Barreto, M. Aceves-Mijares, and C. Domínguez, J. Appl. Phys. **111**, 053109 (2012).
[9] Y. Berencén, J. Carreras, O. Jambois, J. M. Ramírez, J. A. Rodríguez, C. Domínguez, C. E. Hunt, and B. Garrido, Opt. Express **19**, A234 (2011).
[10] Y. Berencén, O. Jambois, J. M. Ramírez, J. M. Rebled, S. Estradé, F. Peiró, C. Domínguez, J. A. Rodríguez, and B. Garrido, Opt. Lett. **36**, 2617 (2011).
[11] J. F. Ziegler, J. P. Biersack, and U. Littmark, *The Stopping and Range of Ions in Solids* (Pergamon, New York, 1985).
[12] J. J. Van Hapert, Ph.D. dissertation, University of Utrecht, the Netherlands, 2002.
[13] S. M. Sze, *Physics of Semiconductor Devices*, 2nd ed. (Wiley, New York, 1981).
[14] J. O'Dwyer, *The Theory of Electrical Conduction and Breakdown in Solid Dielectrics* (Clarendon, Oxford, 1973).
[15] M. A. Lampert and P. Mark, *Current Injection in Solids* (Academic, New York, 1970).
[16] N. Murgatroyd, J. Phys. D: Appl. Phys. **3**, 151 (1970).
[17] N. F. Mott and E. A. Davies, *Electronic Processes in Non-Crystalline Materials* (Clarendon, Oxford, 1971).
[18] B. Massarani, J. C. Bourgoin, and R. M. Chrenko, Phys. Rev. B **17**, 1758 (1978).
[19] D. F. Barbe, J. Phys. D: Appl. Phys. **4**, 1812 (1971).
[20] T. Maruyama and R. Shirota, J. Appl. Phys. **78**, 3912 (1995).
[21] M. V. Fischetti, D. J. DiMaria, S. D. Brorson, T. N. Theis, and J. R. Kirtley, Phys. Rev. B **31**, 8124 (1985).

Erratum: "Correlation between charge transport and electroluminescence properties of Si-rich oxide/nitride/oxide-based light emitting capacitors" [J. Appl. Phys. 112, 033114 (2012)]

Y. Berencén,[1,a)] J. M. Ramírez,[1] O. Jambois,[1] C. Domínguez,[2] J. A. Rodríguez,[3] and B. Garrido[1]
[1]*MIND-IN2UB, Dept. Electrònica, Universitat de Barcelona, Martí i Fanquès 1, 08028 Barcelona, Spain*
[2]*Instituto de Microelectrónica de Barcelona (IMB-CNM, CSIC), Bellaterra, 08193 Barcelona, Spain*
[3]*Physics Faculty, University of Havana, San Lázaro y L, Vedado, 10400 Havana, Cuba*

(Received 25 October 2012; accepted 1 November 2012; published online 20 November 2012)

[http://dx.doi.org/10.1063/1.4768249]

We have recently noticed a typographical mistake in the x-axis numbers of the Fig. 2.[1] This typo does not affect the results (activation energy values shown in the figure), discussion neither scientific conclusions. The authors regret for the error made in the x-axis numbers. The correct x-axis numbers of Fig. 2 are shown below.

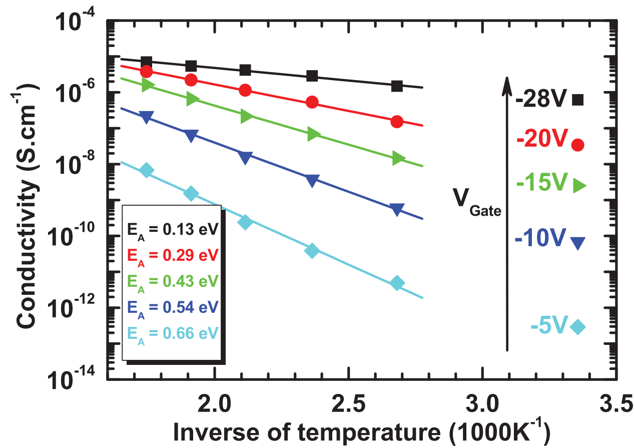

FIG. 2.

[1]Y. Berencén, J. M. Ramírez, O. Jambois, C. Domínguez, J. A. Rodríguez, and B. Garrido, J. Appl. Phys. **112**, 033114 (2012).

[a)]Author to whom correspondence should be addressed. Electronic mail: yberencen@el.ub.es. Tel.: +34 93 4039175. Fax: +34 93 4021148.

 © 2012 American Institute of Physics

[This article is copyrighted as indicated in the abstract. Reuse of AIP content is subject to the terms at: http://scitation.aip.org/termsconditions. Downloaded to] IP: 161.116.96.2 On: Fri, 25 Oct 2013 11:57:34

PAPER VII

Intense green-yellow electroluminescence from Tb^+-implanted silicon-rich silicon nitride/oxide light emitting devices

Y. Berencén,[1,a)] R. Wutzler,[2] L. Rebohle,[2] D. Hiller,[3] J. M. Ramírez,[1] J. A. Rodríguez,[4] W. Skorupa,[2] and B. Garrido[1]

[1]*MIND-IN2UB, Dept. Electrònica, Universitat de Barcelona, Martí i Fanquès 1, 08028 Barcelona, Spain*
[2]*Institute of Ion Beam Physics and Materials Research, Helmholtz-Zentrum Dresden-Rossendorf, P.O. Box 510119, 01314 Dresden, Germany*
[3]*IMTEK, Faculty of Engineering, Albert-Ludwigs-University Freiburg, Georges-Köhler-Allee 103, 79110 Freiburg, Germany*
[4]*Physics Faculty, University of Havana, San Lázaro y L, Vedado, 10400 Havana, Cuba*

(Received 21 June 2013; accepted 26 August 2013; published online 9 September 2013)

High optical power density of 0.5 mW/cm^2, external quantum efficiency of 0.1%, and population inversion of 7% are reported from Tb^+-implanted silicon-rich silicon nitride/oxide light emitting devices. Electrical and electroluminescence mechanisms in these devices were investigated. The excitation cross section for the 543 nm Tb^{3+} emission was estimated under electrical pumping, resulting in a value of 8.2×10^{-14} cm^2, which is one order of magnitude larger than one reported for Tb^{3+}:SiO_2 light emitting devices. These results demonstrate the potentiality of Tb^+-implanted silicon nitride material for the development of integrated light sources compatible with Si technology. *© 2013 AIP Publishing LLC*. [http://dx.doi.org/10.1063/1.4820836]

The incorporation of rare earth (RE) ions in a silicon dioxide (SiO_2) matrix sparked the race toward recent routes for developing efficient Si-based light sources compatible with complementary metal-oxide-semiconductor (CMOS) technology. Such light emitters seem an appealing solution to circumvent the microelectronic bottleneck nowadays, for instance, heat dissipation and interconnection problems.[1] Other promising approaches toward this aim are Si-nanocrystals (Si-ncs) embedded in a SiO_2 matrix (SiO_x)[2] and also co-doped with RE ions.[3] Published works run from those covering the visible range with RE ions, such as Ce^{3+},[4] Eu^{3+},[5] and Tb^{3+},[6] to those only focusing on the near infrared region with Nd^{3+} (Ref. 7) and Er^{3+} (Ref. 3) ions. However, little attention has been paid to the electroluminescence (EL) properties of those RE ions embedded either in silicon nitride (Si_3N_4) or silicon-rich silicon nitride (SiN_x) dielectrics. In fact, SiN_x-based materials offer considerable advantages over SiO_x-based active ones: (i) lower carrier injection barrier at the Si/Si_3N_4 interface, giving rise to the fabrication of low-voltage light emitting devices (LEDs),[8] (ii) better electrical stability with direct impact on the device operation lifetimes,[9] and (iii) higher effective refractive index for making high quality resonant cavities.[10] Also, we have recently demonstrated the suitability of SiN_x, in combination with SiO_2 tunnel layers, as promising candidate for the silicon-solid state lighting.[11] Thus, an encouraging scenario toward RE-doped SiN_x LEDs is envisaged. We are only aware of Er-doped SiN_x electroluminescent devices, where the potentiality of this material for the engineering of light emitters at 1.5 μm was reported.[12] Therefore, SiN_x co-doped with RE ions, whose radiative electronic transitions are in the visible range, remains practically unexploited from the electroluminescent viewpoint. Particularly, the most efficient RE ion,[13] namely, Tb^{3+}, is an unexplored candidate embedded in SiN_x for evaluating its electro-optical properties aimed for the realization of integrated, electrically driven Si-based light emitters.

In the present work, the investigation on the nature of electrical and EL mechanisms in Tb^{3+}:SiN_x/SiO_2 LEDs is reported. We demonstrate high optical power density as high as 0.5 mW/cm^2 and we estimate the effective Tb^{3+} excitation cross section as well as the fraction of inverted Tb^{3+} ions. The possibility to obtain integrated Si-based light sources by introducing Tb^{3+} ions in a SiN_x matrix is established.

30 nm-thick SiO_2 and 40 nm-thick SiN_x layers were deposited on highly doped *n*-type Si (100) substrates with resistivity of 1–5 mΩ cm using plasma enhanced chemical vapor deposition (PECVD). An annealing treatment at 1000 °C for 60 min to create the Si-ncs in the silicon nitride layer with 12% of Si excess was performed. The incorporation of Si-ncs was conceived to improve the conductivity and the device operation lifetime.[9] Subsequently, the silicon-rich silicon nitride layer was implanted with Tb^+ ions, whose implantation energy (75 keV) and dose (1.9×10^{15} atoms/cm^2) were adjusted to generate a concentration of nearly 1.5% in the depth range of 20–25 nm. The implantation was followed by post annealing procedure at 900 °C for 30 min in N_2 atmosphere to mitigate defects caused by implantation. On a reference sample, with identical structure and technological parameters but introducing Er^{3+} (a somewhat similar ion in terms of their atomic radii and diffusivity coefficients) instead of Tb^{3+} ions, around 93% of the total ions quantity was determined by secondary ion mass spectroscopy profile into the SiN_x layer. Likewise, no Er^{3+} clusters were detected by energy-filtered transmission electron microscopy images. The preferred gate electrode was a 100 nm transparent indium-tin-oxide (ITO) layer (*n*-type) deposited by rf sputtering. Different circular areas with sizes ranging from 100 μm to 1200 μm diameter were defined by conventional lithography and fabricated. A cross section scheme of the

[a)]Electronic mail: yberencen@el.ub.edu

 © 2013 AIP Publishing LLC

obtained devices is shown in Fig. 1(a). Quasi-static current-voltage characteristics (*I-V*) were measured using a semiconductor device analyzer (Agilent B1500A) connected to a probe station (Cascade Microtech Summit 11000) with a Faraday cage. The EL spectra were collected from the top of the devices using a cryogenically cooled Princeton Instruments Spec-10-100B/LN charge-coupled device attached to an Acton 2300i grating spectrometer. Time-resolved EL experiments were conducted using an Agilent 8114A pulse generator, whereas the decay EL traces were recorded with a digital GHz oscilloscope connected to a calibrated photomultiplier (R928). A 1 kΩ resistance in serial connection to back contact of our devices was used for measuring the current passing through it. Both *I-V* and EL measurements were acquired at room temperature by positively biasing the *n*-type ITO electrode, as sketched in Fig. 1(a).

Fig. 1(b) shows the evolution of the current density (J) with the applied voltage (V) ramped at a constant rate of 50 mV/s from 0 V up to just before device breakdown, which occurs at around 41 V. The constant-current density zone of the curve constitutes a measure of the capacitance of the structure $C = J_d S(dV/dt)^{-1}$, which is around 45 pF, where J_d is the displacement current density and S is the electrode area. The *J-V* curve also shows a good concordance with two well-defined conduction mechanisms depending on the voltage values, after the threshold for real current density injection (i.e., for current density typically $>J_d$, $V \sim 21$ V). At moderate voltages, the Poole-Frenkel (PF) mechanism[14] governs the conduction (red solid line), whereas at high voltages the trap-assisted tunneling[15] (TAT) one is predominant

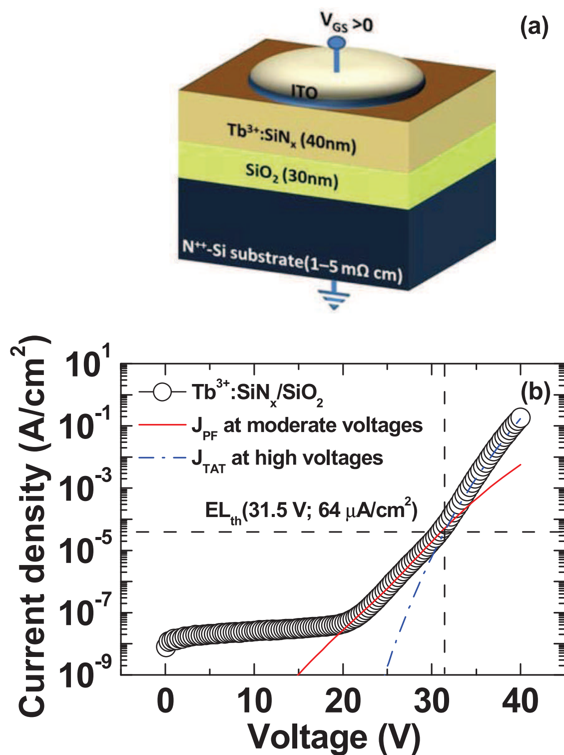

FIG. 1. (a) Cross section scheme of the Tb^{3+}:SiN_x/SiO_2 light emitting device. (b) J-V characteristic of the device showing both fitting models related with Poole-Frenkel and trap-assisted tunneling conduction mechanisms at moderate and high voltages, respectively.

(blue dashed dotted line). Hereafter, we will only pay attention to this latter mechanism because the Tb^{3+} emission takes place solely under this regime, concretely the EL turn on point is at (31.5 V; 64 μA/cm^2) as can be seen in Fig. 1(b). This fact also suggests that the Tb^{3+} excitation is primarily generated by impact ionization by hot electrons in the conduction band, rather than, for instance, by energy transfer from Si-ncs to Tb^{3+} ions.[3] Thus, the electron injection is exclusively limited by the energetic level of the traps situated at the SiO_2 band gap close to the Si/SiO_2 interface. In particular, the trap is energetically placed at around $\Phi_t = (2.0 \pm 0.3)$ eV below the oxide conduction band edge, that is in good agreement with TAT formalism.[15] This value was extracted from the experimental data fitting to the TAT relationship given by $J_{TAT} \propto \exp(-4d_{ox}\sqrt{2m^*}\Phi_t^{3/2}/3q\hbar V_{ox})$, where d_{ox} is the SiO_2 thickness, m^* is the effective electron mass, Φ_t is the trap energy (in eV) below the oxide conduction band edge, q is the electron charge, $\hbar$ is the reduced Planck's constant, and V_{ox} is the voltage drops in the SiO_2 layer. The V_{ox} relationship with the applied voltage (V) is given by $V_{ox} = Vd_{ox}/[d_{ox} + (\varepsilon_{ox}/\varepsilon_{SiN_x})d_{SiN_x}]$, where d_{SiNx} is the SiN_x thickness, as well as $\varepsilon_{ox} = 3.9$ and $\varepsilon_{SiNx} = 7.5$ are the relative permittivity of the SiO_2 and SiN_x, respectively. This conduction mechanism is related to the intrinsic traps created close to the SiO_2/Si-substrate interface due to electric stress generated by effects of high electric field.[15] The introduction of the SiO_2 layer was *ad hoc* conceived for boosting the Tb^{3+} EL by hot electrons. Indeed, this SiO_2 layer introduces a potential energy step of ~1.3 eV at the interface between the SiO_2 and the Si_3N_4 due to the difference in electron affinities (i.e., $SiO_2 = 0.8$ eV and $Si_3N_4 = 2.1$ eV) which offers the possibility of hot electrons injection into the Tb^{3+}:SiN_x active layer. In addition, the SiN_x/SiO_2 bilayer stack was envisaged for achieving a trade-off between EL efficiency and electrical stability of the devices.

Four emission bands in the visible range under direct current pumping were observed. These bands are related to the radiative electronic transitions of Tb^{3+} from $^5D_4$ to $^7F_6$, $^7F_5$, $^7F_4$, and $^7F_3$ energetic states,[13] respectively, as shown in Fig. 2(a). The line-shape of the measured spectra for different constant current values does also not change (i.e., the emission lines preserve their relative intensities). Moreover, a broad EL band peaking at 465 nm from non-implanted Tb^+ reference device was detected. In former published works, this emission was ascribed to Si-related defects in silicon nitride.[16] However, this electroluminescence was not clearly observed in the studied devices due to the overlapping with the intense Tb^{3+} emission. Fig. 2(b) depicts a linear dependence of the optical power density with respect to the injected current density. An optical power density as high as 0.5 mW/cm^2 is reached at the highest current density, where a light saturation is clearly observed on the graph. This is the largest optical power density value ever reported for Tb^+-implanted SiN_x LEDs. Moreover, an external quantum efficiency (EQE) of 0.1% is obtained. This EQE value is also the highest ever reported for RE in SiN_x matrices, that is comparable with the one obtained for Er^{3+}:SRO LEDs.[17] Strong green-yellow emission coming from the top of the devices is observed to naked eye under daylight conditions as well as very stable over hours. This green-yellow light is

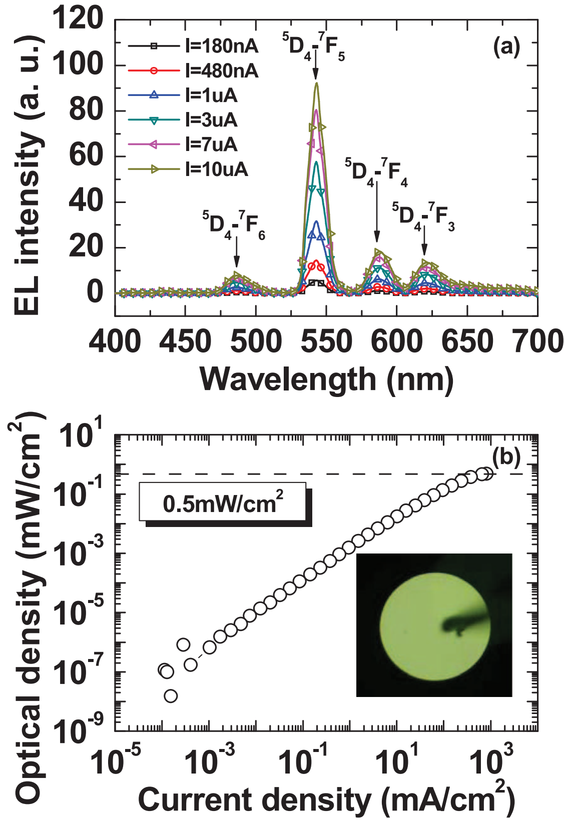

FIG. 2. (a) Electroluminescence spectra at different constant current values and several Tb^{3+} electronic transitions from $^5D_4$ to $^7F_6$, $^7F_5$, $^7F_4$, and $^7F_3$, respectively. (b) Optical power density versus current density. Inset shows green-yellow emission at naked eyes.

ascribed to the main Tb^{3+} radiative electronic transition ($^5D_4$-$^7F_5$) at 543 nm, which is responsible of the 58% of the overall emission in our devices. In the inset of Fig. 2(b), a photograph collected from the emission area of the device by a commercial digital camera demonstrates this latter fact. This emission line is also close to the wavelength of 555 nm, where the human eye sensitivity is maximal.[18] Therefore, taking advantage of the high optical power density at the most suitable wavelength, an encouraging scenario can be envisaged for the development of silicon-based solid state lighting. A detailed photometric study, including color quality, color rendering, and luminous efficacy of radiation, is currently in progress in this materials platform.

Under alternate current pumping, the electrical excitation cross section (σ) of the Tb^{3+} at 543 nm was calculated by measuring the EL rise time (τ_{rise}) at different excitation square pulses. Fig. 3 shows that the EL decay time (τ_{decay}) remains constant with respect to the charge flux (ϕ), whereas the EL rise time drops as the charge flux increases. This behavior is consistent with a two-level system at low fluxes, where σ does not depend of the injected electron flux.[19] Hence, using the expression $1/\tau_{rise} = \sigma\phi + 1/\tau_{decay}$, we can deduce the electrical cross section of the Tb^{3+} 543 nm emission by a linear fit.[12] Prior to that, both EL rise and decay times were well-fitted by a single exponential function. The EL rise time values at different charge fluxes range from 0.5 ms to 0.7 ms, whereas the EL decay time was found to be 0.5 ms, which is close to the one measured under optical

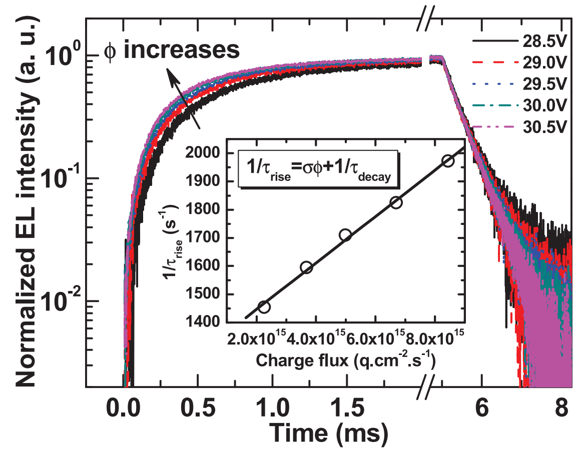

FIG. 3. Normalized EL intensity as a function of time excited by different square voltage pulses. Inset: Linear relationship of the inverse rise time ($1/\tau_{rise}$) of the EL at 543 nm with respect to charge flux (ϕ) considering a two-level system at low flux regime.

pumping in Tb^{3+}:SiO_2 films.[20] The inset of Fig. 3 depicts the linear relationship between the inverse rise time and charge flux. The charge flux was calculated taking into account the measured current through 1 kΩ resistance in serial connection to back contact of our devices instead of using the injected current deduced from the applied voltage. Therefore, the Tb^{3+} excitation cross section at 543 nm was found to be $(8.2 \pm 0.5) \times 10^{-14}$ cm^2, that is one order of magnitude larger than one reported for Tb^+-implanted SiO_2 light emitting devices under electrical pumping.[6] As a consequence, the probability of Tb^{3+} excitation in silicon nitride is higher than the silicon dioxide matrix.

In order to estimate the fraction of inverted Tb^{3+} ions (N_2) in the main radiative electronic transition ($^5D_4$-$^7F_5$) at 543 nm, we used the following formula:[17] $N_2 = D_{opt} \cdot \tau_{rad} / \hbar\varpi \cdot d$, where D_{opt} is the emitted optical power density, τ_{rad} is the Tb^{3+} radiative lifetime, and $\hbar\varpi$ is the photon energy. Therefore, the maximum emitted optical power density can be calculated considering the following circumstances: (i) the number of introduced Tb^{3+} ions is 4.8×10^{20} at/cm^3, which corresponds to a maximum power density value of 4.8×10^{20} photons/cm^3 and (ii) a Tb^{3+} radiative lifetime of 3.5 ms. This Tb^{3+} radiative lifetime value was chosen taking into account that had been reported for two different host matrices,[21,22] which suggests to be not strongly sensitive to the matrix-type. Taking the measured EL decay time value of 0.5 ms would neglect all Tb^{3+} ions that are excited, but will relax in a non-radiative way. Then, the total internal emitted power density is 0.2 W/cm^2. However, the fraction of emitted light able to escape from electrode and collected by our microscope objective with 0.4 of numerical aperture was found to be 4%. The collection angle (23.5°) related with the numerical aperture of the used microscope objective is lesser than the critical angle (30°) associated to the total internal reflection phenomena inside the active layer. Additionally, 91% of the emitted light is transmitted at 543 nm through the 100 nm ITO electrode. Therefore, the out-coupling efficiency is around 3.6%. Hence, taking into account these corrections the external optical power density is 7.2 mW/cm^2. Now, comparing this latter value with the

maximum measured optical power density (0.5 mW/cm^2) from our device, we get an optical power density ratio of about 7%, which corresponds to the fraction of inverted Tb^{3+} ions at steady state. This value is still far from 50% that is the minimum required to achieve lasing action. The precedent calculation had not been reported before for Tb^+-implanted SiN_x/SiO_2 light emitting devices, even though the results are still lower than those previously published for Er^{3+}:SRO-based devices, where 20% of inverted Er^{3+} ions was reported.[17]

In conclusion, Tb^+-implanted SiN_x/SiO_2 light emitting devices with optical power density as high as 0.5 mW/cm^2 and EQE of 0.1% were fabricated. The EL mechanism of the devices can be ascribed to impact ionization of the Tb^{3+} luminescent centers by hot electrons with cross section of 8.2×10^{-14} cm^2. A Tb^{3+} population inversion of 7% under electrical pumping was estimated. The suitability of this materials platform for the realization of integrated Si-based light emitters fully compatible with CMOS technology was demonstrated.

This work was financially supported by the Spanish Ministry of Science and Innovation (Project No. TEC2009-08359). Y.B. acknowledges the financial support from Grant No. EEBB-I-2012-04552 during his research stay at *Helmholtz-Zentrum Dresden-Rossendorf* in Germany. The authors also thank the Rossendorf implantation and clean room facility group for ion implantation and clean room preparations, respectively.

[1]L. C. Kimerling, L. Dal Negro, S. Saini, Y. Yi, D. Ahn, S. Akiyama, D. Cannon, J. Liu, J. G. Sandland, D. Sparacin, J. Michel, K. Wada, and M. R. Watts, in *Silicon Photonics*, edited by L. Pavesi and D. J. Lockwood (Springer, New York, 2004).
[2]C.-H. Cheng, Y.-C. Lien, C.-L. Wu, and G.-R. Lin, Opt. Express **21**, 391 (2013).
[3]J. M. Ramírez, F. Ferrarese Lupi, O. Jambois, Y. Berencén, D. Navarro-Urrios, A. Anopchenko, A. Marconi, N. Prtljaga, A. Tengattini, L. Pavesi, J. P. Colonna, J. M. Fedeli, and B. Garrido, Nanotechnology **23**, 125203 (2012).
[4]J. M. Sun, S. Prucnal, W. Skorupa, M. Helm, L. Rebohle, and T. Gebel, Appl. Phys. Lett. **89**, 091908 (2006).
[5]S. Prucnal, J. M. Sun, W. Skorupa, and M. Helm, Appl. Phys. Lett. **90**, 181121 (2007).
[6]J. M. Sun, W. Skorupa, T. Dekorsy, M. Helm, L. Rebohle, and T. Gebel, J. Appl. Phys. **97**, 123513 (2005).
[7]O. Debieu, J. Cardin, X. Portier, and F. Gourbilleau, Nanoscale Res. Lett. **6**, 161 (2011).
[8]R. Huang, K. Chen, H. Dong, D. Wang, H. Dong, W. Li, J. Xu, Z. Ma, and L. Xu, Appl. Phys. Lett. **91**, 111104 (2007).
[9]Y. Berencén, J. M. Ramírez, and B. Garrido, in Proceedings of the 2013 Spanish Conference on Electron Devices, CDE 2013, (IEEE Xplore, Valladolid, 2013).
[10]M. Makarova, V. Sih, J. Warga, R. Li, L. Dal Negro, and J. Vuckovic, Appl. Phys. Lett. **92**, 161107 (2008).
[11]Y. Berencén, J. Carreras, O. Jambois, J. M. Ramírez, J. A. Rodríguez, C. Domínguez, C. E. Hunt, and B. Garrido, Opt. Express **19**, A234 (2011).
[12]S. Yerci, R. Li, and L. Dal Negro, Appl. Phys. Lett. **97**, 081109 (2010).
[13]L. Rebohle and W. Skorupa, *Rare-Earth Implanted MOS Devices for Silicon Photonics* (Springer, Heidelberg, 2010).
[14]O. Jambois, Y. Berencén, K. Hijazi, M. Wojdak, A. J. Kenyon, F. Gourbilleau, R. Rizk, and B. Garrido, J. Appl. Phys. **106**, 063526 (2009).
[15]M. P. Houng, Y. H. Wang, and W. J. Chang, J. Appl. Phys. **86**, 1488 (1999).
[16]Z. H. Cen, T. P. Chen, L. Ding, Y. Liu, J. I. Wong, M. Yang, Z. Liu, W. P. Goh, F. R. Zhu, and S. Fung, Appl. Phys. Lett. **94**, 041102 (2009).
[17]O. Jambois, F. Gourbilleau, A. J. Kenyon, J. Montserrat, R. Rizk, and B. Garrido, Opt. Express **18**, 2230 (2010).
[18]E. Fred Schubert, *Light Emitting Diodes*, 2nd ed. (Cambridge University Press, New York, 2006).
[19]S. Wang, A. Eckau, E. Neufeld, R. Carius, and Ch. Buchal, Appl. Phys. Lett. **71**, 2824 (1997).
[20]A. Podhorodecki, G. Zatryb, J. Misiewicz, J. Wojcik, P. R. J. Wilson, and P. Mascher, Nanotechnology **23**, 475707 (2012).
[21]D. K. Sardar, K. L. Nash, R. M. Yow, J. B. Gruber, U. V. Valiev, and E. P. Kokanyan, J. Appl. Phys. **100**, 083108 (2006).
[22]W. Di, X. Wang, B. Chen, S. Lu, and X. Zhao, J. Phys. Chem. B **109**, 13154 (2005).